Islanded Operation of Parallel Inverter-interfaced Microgrids with Photovoltaic Systems

ISLANDED OPERATION OF PARALLEL INVERTER-INTERFACED MICROGRIDS WITH PHOTOVOLTAIC SYSTEMS

MOHAMMAD IMRAN AZIM

A thesis submitted in fulfilment of the requirements of the degree of

Master of Engineering (Research)

Supervisor:
A/Prof. Hemanshu Roy Pota

School of Engineering and Information Technology
The University of New South Wales
Canberra, Australia

March 2017

Abstract

This thesis presents autonomous droop-based control schemes to share power proportionally in inverter-connected islanded microgrids; in which different microgrid structures such as inductive (L-type), resistive (R-type), and resistive-inductive (RL-type) are considered. The main aim of designing new controllers in this dissertation is to distribute the load change among intermittent distributed generators according to their power ratings.

A linearized model of microgrids is used to evaluate the change in powers (real-reactive) of the distributed generators due to the load change, but it is noticed that the linearized modeling of microgrids depends on the distribution line parameters. Thus, proportional power sharing cannot be maintained. Improved droop-based algorithms are developed to share power based on droop gains by including a voltage control law; in which the reference values of the generator voltages are kept the same.

A compensation-based droop control is provided by adding a power offset to the real power for balancing the inverter output power during the variation in the output of distributed generation. A derivative term is also included in droop algorithms for damping the oscillatory modes of the controllers so that improved dynamic performance can be ensured.

This thesis contains eigenvalue analysis to predict the stability of microgrids. However, it is anticipated that this method may not provide satisfactory results in large inverter-dominated systems as it is based on the quasi-static approximation. In order to overcome this shortcoming, an extended dynamic phasors analysis is described in this dissertation in details to find out a suitable stability range of droop gains for the proposed controllers.

Finally, the performance of the designed droop-based power sharing controller is verified on a multi photovoltaic source-based islanded test microgrid and superior dynamic performance is obtained compared with the conventional RL-type droop controller.

Acknowledgements

First of All, I want to thank my creator Almighty Allah for giving me intelligence, strength, and perseverance to pursue the journey towards masters.

I would like to express my sincere thanks to my supervisor, A/Prof. Hemanshu Roy Pota, and co-supervisor, A/Prof. Jahangir Hossain, for their excellent supervision, continuous support with technical and editorial advice, and encouragement throughout my candidature. Despite their busy schedule, they always managed time for me to squeeze in a meeting when needed. Their motivational activities made easy for me to conduct research on microgrids. They also instructed me how to write good technical papers. During two years of study, I found them as open-minded and inspiring people that helped me enrich my growth as a student. It was really an honor for me to pursue my higher education under their supervision.

My appreciation goes to the University of New South Wales (UNSW) for their financial support in my research work. I am also grateful to the entire UNSW Canberra school office members, staff, research group mates, and other postgraduate students for their co-operations in making my research journey enjoyable.

Personally, I offer thanks to my parents, Mohammad Anwar Azim and Tasmina Haque Joardar, and my younger brother, Md Farhan Azim, for their constant sacrifice, love, encouragement, prayers, and guidance. Sincere gratefulness goes to my local guardians, Mohammed Imroz Sohel, Nazneen Nowsher, Setaur Rahman, and Ziaur Rahman, for their wonderful family supports which really motivated me to study precisely.

Dedicated to my parents,

Mohammad Anwar Azim and Tasmina Haque Joardar

List of Publications

Refereed Journal Papers

1. **M. I. Azim**, M. J. Hossain, and H. R. Pota, "Design of Droop-based Control for Power Management in Islanded RL-type Microgrids," *International Journal of Emerging Electric Power Systems*, De Gruyter. (Accepted)
2. **M. I. Azim**, and H. R. Pota, "Design of a Dynamic Phasors-based Droop Controller for PV-based Islanded Microgrids," *IEEE Systems Journal*, IEEE. (Under Review)
3. **M. I. Azim**, A. O. M. Haruni, and H. R. Pota, "An Improved Droop-based Control Strategy for Proportional Real Power Sharing in Resistive Islanded Microgrids with Dynamic Phasors Modeling," *Journal of Modern Power Systems and Clean Energy*, Springer. (Under Review)

Refereed Conference Papers

1. **M. I. Azim**, M. A. Hossain, S. M. Mohiuddin, M. J. Hossain, and H. R. Pota, "Proportional Reactive Power Sharing for Islanded Microgrids," *11th IEEE Conference on Industrial Electronics and Applications*, Hefei, China, June 5-7, 2016.
2. **M. I. Azim**, M. J. Hossain, and H. R. Pota, "Design of a Controller for Active Power Sharing in a Highly-Resistive Microgrid," *9th IFAC Symposium on Control of Power and Energy Systems*, New Delhi, India, pp. 288-293, December 9-11, 2015.

3. **M. I. Azim**, M. J. Hossain, F. H. M. Rafi, and H. R. Pota, "An Improved Droop Control Scheme for Islanded Microgrids," *5th Australian Control Conference*, Gold Coast, Australia, pp. 225-229, November 5-6, 2015.
4. **M. I. Azim**, M. A. Hossain, M. J. Hossain, and H. R. Pota, "Effective Power Sharing Approach for Islanded Microgrids," *IEEE PES ISGT Asia*, Bangkok, Thailand, pp. 1-4, November 4-6, 2015.
5. **M. I. Azim**, M. J. Hossain, and H. R. Pota, "Design of a General Droop Controller for Islanded Microgrids," *25th Australasian Universities Power Engineering Conference*, Wollongong, Australia, pp. 1-5, September 27-30, 2015.
6. **M. I. Azim**, M. A. Hossain, M. J. Hossain, and H. R. Pota, "Droop Control for Islanded Microgrids with Compensating Approach," *25th Australasian Universities Power Engineering Conference*, Wollongong, Australia, pp. 1-6, September 27-30, 2015.

Group Papers

1. M. A. Hossain, **M. I. Azim**, M. A. Mahmud, and H. R. Pota, "Active Power Control in an Islanded Microgrid using DC Link Voltage Status," *IEEE PES ISGT Asia*, Bangkok, Thailand, pp. 1-6, November 4-6, 2015.
2. M. A. Hossain, **M. I. Azim**, M. A. Mahmud, and H. R. Pota, "Primary Voltage Control of a Single Phase Inverter using Linear Quadratic Regulator with Integrator," *25th Australasian Universities Power Engineering Conference*, Wollongong, Australia, pp. 1-6, September 27-30, 2015.

Contents

List of Tables

List of Figures

Abbreviations and Acronyms

PV	Photovoltaic
RES	Renewable Energy Source
DG	Distributed Generators
EPS	Electric Power System
MG	Microgrid
VSC	Voltage-Source Converter
PWM	Pulse-Width Modulation
SPWM	Sinusoidal Pulse-Width Modulation
LV	Low-Voltage
R-type	Resistive
L-type	Inductive
RL-type	Resistive-Inductive
FDC	Forward Droop Control
DDC	Derivative Droop Control
RDC	Reverse Droop Control
GDC	Generalized Droop Control
LF	Load-Flow
DPM	Dynamic Phasors Modeling
KVL	Kirchhoff's Voltage Law
KCL	Kirchhoff's Current Law

Chapter 1

Introduction

1.1 Background

Presently, fossil fuels are the main source of energy. However, some environmental concerns are raised by their use [1]. With a view to keeping the environment clean, these fossil fuels are now being replaced by the renewable energy sources (RESs) such as solar, wind, geothermal, hydro and so on. These renewable sources are mostly available as distributed-generation (DG) units [2]. Compared to conventional centralized generators, DG units are responsible for providing more reliable local services in terms of voltage regulation, power quality, and power factor correction [2]. In the present world, RES-based DG technology is gaining popularity to generate electric power. This is because of the fact that a variety of dispersed energy can be used here [3]. DG technology offers numerous technical, environmental, and economical benefits [4] such as reliable and effective power supply with higher energy efficiency, low transmission and distribution losses with flexible installation, less environmental pollution, and low operating costs [5].

DG units, with energy storage and control devices, are generally connected to the distributed load-side by means of dc/ac converters such as inverters [6], [7], and the overall system is widely known as a microgrid (MG) [8], [9]. Modern inverters are fast acting devices and power balance is obtained by them very quickly. Thus, it is meaningful to implement them during the operation of microgrids [10]. Microgrids

are becoming popular throughout the world nowadays as they are small-scale, self-contained, medium/low-voltage electric power systems (EPS) [11]. They also ensure the effective use of renewable energies with proper capital investments, reduction of the system losses, maintenance of adequate power flow and voltage profile [12]-[14]. There are two modes of operations in microgrids: grid-connected and islanded [15]. The standalone mode of operation is more challenging as the power flow and the voltage profile are maintained locally with proper voltage and frequency control [16]. In this dissertation, islanded microgrids are modeled as parallel inverter-interfaced networks integrated with renewable generation, i.e., PV, and connected to a shared load.

However, the available inverter-connected microgrids do not have the rotating inertia [16] and they cannot distribute power among DG units during frequent load change, which is a very common phenomenon in islanded microgrids [17]. Hence, the planning and the operation of electrical networks are affected [18]. Their performance can further be deteriorated by the co-existence of multiple DG units [19]. Moreover, automatic power sharing among parallel-operated inverters may not be possible without accurate control strategies [20]. In general, microgrids are controllable networks [21]. In recent times, various control approaches (mostly local independent control strategies [22]) have been developed with or without the help of communication [23], [24] for the desired operation of microgrids [25]. Centralized control of microgrids, based on communication, has been reported in [26], but in some cases it has been shown to be impractical in remote areas with long distance connection among inverters. The distribution of dynamic signals characterized by high-bandwidth is also expensive [26]. In addition, this control scheme might be affected by the reliability issues in few circumstances due to lack of clear communication [27]. A signal injection-based load sharing mechanism is investigated in

[27], but the complexity of signal injection has made this method far from being practical. On account of these reasons, decentralized or automatic control strategies are utilized by the microgrid operators [28].

1.2 Literature Review on Droop-based Control

A well-established primary level of hierarchical control scheme for inverter-based microgrids is droop-based control [29], [30], which emulates the characteristic of synchronous machines [28] and protects the system from instability without the need for any communication [31]. Forward droop control (FDC) is so described that the reactive power depends on the voltage magnitude, whereas the real power is controlled by the frequency [32]-[35]. Within an interconnected microgrid, inverters and loads are certainly designed to operate at a rated frequency. However, frequency droop causes the frequency to change from its nominal value, resulting in frequency imbalance. Consequently, another controller needs to be implemented for bringing the frequency back to its rated value. This drawback can be eliminated by representing frequency droop control as a rate-of-change of angle droop control [36]. In simulation modeling, most droop controllers are designed by assuming instantaneous change in the output power of DG units owing to the change in the renewable generation, but in reality this cannot be guaranteed rather a delay is noticed [37]-[39]. In order to eradicate this problem, a buffer (such as capacitor) can be used in the modeling to supply or absorb the difference in the inverter output power and the generated power. However, this process may not be fruitful if the buffer fails to operate swiftly. Thus, existing droop control should be modified to cope with the change in the renewable generation.

Although a derivative term is included in conventional FDC to control the start-up transients in [40]-[43], the classical $P/\dot{\delta}$ and Q/V droop controllers are designed

only for inductive (L-type) distribution line-based microgrids. Hence, they perform poorly in low-voltage (LV) microgrids dominated by the resistances [44]. A virtual output inductance-based control method has been used in [40], [45] to overcome the effect of high resistance on the performance of microgrids, but it does not work well in plug-and-play feature-based systems where DG units and loads are connected at any points without any error [46]. In [46], an improved control scheme is given but it requires fast communication and is proved to be expensive as well [47]. Another control scheme, known as robust servo-mechanism, is proposed in [48]. However, it cannot operate in a system; in which there exists more than one DG units. This is because of the inapplicability of the control algorithms in multi-source systems. To address the above limitations, P/V and $Q/\dot{\delta}$ droop controllers are studied in [34], [44], [49]. Although this control approach shows excellent performance in highly-resistive (R-type) microgrids, it cannot stabilize inductive microgrids. As a result, two different droop algorithms are required depending on the microgrid structures that may be inconvenient for microgrid operators [50]. In order to ensure a generalized islanded microgrid control, the authors in [43], [50]-[52] proposed a more realistic droop-based control that can operate both in resistive and inductive (RL-type) microgrids and can provide a simultaneous control in system's voltage and frequency. However, power sharing quality of these controllers needs to be verified.

Effective power sharing is an important reason for which microgrids are controlled [28]. This is because when the load changes from its initial condition, the change has to be divided among DG units according to their capacity. In droop-controlled inductive microgrids, the real power can be shared proportionally based on the rate-of-change of voltage phase angle [28], [36], [53], but proportional reactive power sharing based on the terminal voltage is not possible [54]. That is why; a linearized model-based reactive power sharing strategy is used in [28], [36], [37], [53]. In

linearized model-based microgrid power sharing, the change in the power of DG units is calculated (caused by the load change) [36]. However, it is found that the linearized modeling of microgrids relies on the distribution line parameters. Thus, proportional power sharing cannot be ensured after the change in the load [55], [56]. Proportional power sharing is recommended in microgrids because it enables DG units to supply power to the load based on their power ratings [36]. A hierarchical droop control with proportional power sharing feature is presented in [57], [58], but this approach needs a sequence of synchronization events though communication network, which increases the complexity of the system. Integral argument-based power sharing strategy of microgrids is provided in [54]. However, the applicability of this method in different types of microgrids is not clear. Moreover, it is required to fix a suitable droop gain selection procedure for this method.

It is worth noting that proper gain selection of droop-based controllers is necessary for maintaining the system stability and ensuring expected power sharing. In literatures [46], [59]-[62], the complete small-signal model of microgrids is developed with a view to predicting the system response during the change in parameters. Although this analysis is helpful to predict the system stability and dynamics, more computational efforts are required in large inverter-dominated systems [63]. Furthermore, on account of the quasi-static nature of small-signal analysis [64], the dynamics of the power network elements are neglected [65]. This method is appropriate for slow-acting inverters but provides questionable results in the presence of inverters with low-inertia and fast-acting qualities. Moreover, this model is no longer useful when it is required to consider high-gain values [66]. As a consequence, dynamic phasors modeling (DPM) is proposed in [64]-[67] to select the control parameters. Dynamic phasors are time-varying phasors. They consider the dynamics

of the power network circuit elements to predict the transient response and to determine the stability limits accurately [64], [68]. The method by which they are used is known as dynamic phasors modeling (DPM) [67], [68]. However, the challenging task is to include droop-based control algorithms with this method with a view to determining the precise stability margins for various microgrid controllers.

1.3 Motivations for Current Research

- The available droop-based controllers cannot guarantee proportional reactive power sharing in inductive microgrids, proportional real power sharing in resistive microgrids, and proportional real-reactive power sharing in inductive-resistive microgrids. Proportional power sharing is recommended to distribute the change in the load and in the renewable generation among distributed generators based on their power ratings. Hence, it is essential to develop new types of droop-based algorithms in order to ensure proportional power sharing in all types of microgrids.
- The challenging task is to extend the existing dynamic phasors modeling by including the droop-based control algorithms with it so that the control parameters can be determined.

1.4 Underlying Research Questions

- How the algorithms of the conventional droop-based controllers can be modified to ensure proportional power sharing in different types of microgrids?
- How droop-based control algorithms can be included with the existing dynamic phasors models to determine the control parameters?

1.5 Thesis Contributions

- New types of droop-based control algorithms are developed to share power proportionally in different types of microgrids such as inductive, resistive, and inductive-resistive microgrids. The focus of this research is proportional power sharing so that the change in the load among distributed generators can be distributed depending on their power ratings. The controllers are designed by including a voltage control law in droop-based control algorithms. In steady-state the developed control algorithms guarantee that the power is shared inversely proportional to the droop gains (Provided in **Chapter 2**).
- A compensation-based droop controller is designed to balance the inverter output power during the change in the renewable generation. Power balance is ensured by adding a power offset to the real power output and this power offset is expressed as a function of the variation in the renewable generation (Provided in **Chapter 2**).
- The existing dynamic phasors modeling is extended by including the developed control algorithms with it. The characteristic equations of the closed-loop systems are calculated and then the stability margins for the designed controllers are determined (Provided in **Chapter 3**).
- A new type of droop-based control algorithm is developed for Photovoltaic (PV) systems that can share power proportionally during the load change and also can balance power if PV generation varies (Provided in **Chapter 4**).

1.6 Thesis Outline

This thesis begins with an introduction of decentralized control algorithms for proportional power sharing in islanded microgrids in **Chapter 2**. These algorithms are proposed for different microgrid structures such as L-type, R-type, and generalized

(RL-type), and are developed to distribute the change in the load among parallel inverter-connected DG units based on their capacity without any communication. Algorithms are also improved to ensure well-damped system responses and to provide protection against the change in the dc-bus voltage.

In **Chapter 3**, the gain selection methodologies of the proposed controllers are provided. The linear modal analysis is carried out due to the fact of obtaining control gains. Successive approximation is done to get the eigenvalues by ensuring that no values have got any positive real parts. However, the dynamics of the power circuit elements are ignored in linear modal approach. For this reason, there exists an anticipation of evaluating the accurate stability limit in power electronics-based large microgrids. Therefore, this chapter also describes a more feasible gain selection method, known as dynamic phasors modeling, to overcome the shortcomings of eigenvalue analysis in determining the range of the control parameters for the designed controllers.

Chapter 4 contains the combined algorithms of the proposed droop-based power sharing controller and the performance of this controller is evaluated on a photovoltaic (PV)-based islanded microgrid by means of MATLAB simulation. Diverse case studies are considered such as the load change in R-type, L-type, and RL-type microgrids, and the variation in the PV generation. In all cases, the performance of the designed controller is compared with the existing RL-type droop controller and the simulation results show that the proposed control scheme is more accurate than the conventional one in terms of damping aspect.

Conclusions and directions for further research are given in **Chapter 5**.

The results, obtained from the research carried out in this thesis, have been published in different referred international conference proceedings and journals (some are accepted or submitted). A list of these publications are presented at the beginning of this dissertation.

Chapter 2

Decentralized Control for Proportional Power Sharing in Islanded Microgrids

2.1 Chapter Purposes

This chapter develops a compensation-based droop control algorithm to distribute the change in the load and in the renewable generation proportionally. A derivative droop control is provided to ensure well-damped dynamic performance of the DG units. A current-based droop control scheme is proposed to protect the microgrid against short-circuit phenomenon that may occur at the distributed lines. A linearized model-based power sharing analysis is described to share real power in resistive (R-type) microgrids, reactive power in inductive (L-type) microgrids, and real-reactive powers in inductive-resistive (RL-type) microgrids. Finally, new types of droop-based controllers are designed to share power proportionally among DG units based on droop gains only (without relying on the distribution line parameters).

2.2 Literature Review

Droop-based control schemes emulate the characteristic of synchronous machines [28] and operate without communication [31]. Forward droop control (FDC) is a popular control method for L-type microgrids; in which frequency is varied depending on the change in the real power [32]-[35]. Since frequency has to be at its rated value, an additional controller is required to use for frequency adjustment. In

[36], it is reported that modern inverters can change the phase angle of the output voltage. That is why; frequency droop control is illustrated by the rate-of-change of voltage angle droop control. Modified FDC algorithms is provided in [36], [55], [56] to distribute the change in the reactive power, due to the load change, among inverter-connected DG units based on their power ratings. However, the change in the renewable generation is neglected in most literatures of droop control [37]. A feedback control strategy is introduced in this chapter which enhances the feasibility of FDC in microgrids if either load or renewable generation varies.

It is shown in [44] that forward droop control lacks accuracy in highly-resistive microgrids, and reverse droop control (RDC) is presented by the authors in [34], [49]. With reverse droop control method, reactive power can be shared easily but real power sharing is complicated. For this reason, linearized model-based real power sharing approach is demonstrated in this chapter. However, this strategy depends on the distribution line parameters. Therefore, an improved reverse droop control control algorithm is also developed for proportional real power sharing.

As RDC is inapplicable to L-type microgrids [50], a more realistic control scheme regarded as generalized droop control (GDC) is proposed in [43], [51], [52]. GDC can operate in any types of microgrids. However, power sharing with this control approach is very complicated. This chapter discusses how GDC can be used to share power via linearized model analysis of microgrids. Because of the constraint of linearized model method, improved GDC is also proposed to share real-reactive power proportionally among inverter-interfaced DG units.

2.3 Chapter Outline

The rest of the chapter is structured as follows: Section 2.4 derives power-flow equations for the microgrid system. Section 2.5 contains the existing droop-based

control algorithms with modifications. In Section 2.6, power sharing features of the existing controllers are given. New types of droop-based controllers are proposed for proportional power sharing in Section 2.7. Section 2.8 outlines the chapter summary.

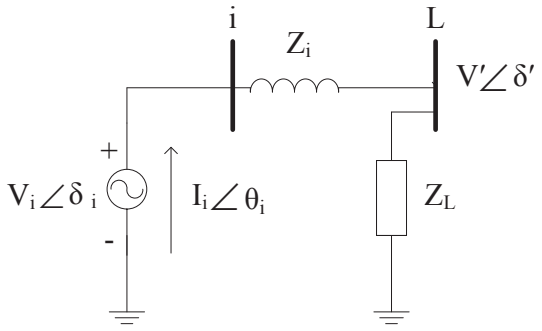

Figure 2.1. Basic single-line diagram of a simple microgrid.

2.4 Microgrid Power-flow Equations

Majority of renewable sources are connected to microgrids by means of voltage-source converter (VSC) such as inverters. Inverter-interfaced renewable generation can be modeled as a voltage-source; in which the voltage magnitude and phase angle are controlled [36]. Fig. 2.2 shows a two voltage-source microgrid with one load. Analysis of a two-source microgirds is enough to understand the basic operation a microgrid and its research problems. In this figure, distributed generator bus is denoted by i-bus where i stands for the ith generator and load is connected at L-bus. The voltage magnitude and phase angle of sources and the load are represented by $V_i\angle\delta_i$ and $V^{'}\angle\delta^{'}$ respectively.

The apparent power (S) flowing from sources to the load is [51]:

$$\bar{S}_i = P_i + jQ_i = \bar{V}_i\bar{I}_i^* = \bar{V}_i(\frac{\bar{V}_i - \bar{V}^{'}}{\bar{Z}_i})^* \tag{2.1}$$

where, $\bar{V}_i = V_i \angle \delta_i$, $\bar{V}' = V' \angle \delta'$, and $\bar{Z}_i = Z \angle \phi_i$ (ϕ_i=line impedance angle).

Let assume, $\delta_i = 0$ and $\delta' = -\Delta\delta_i$.

Eqn. (2.1) can be written as:

$$\bar{S}_i = P_i + jQ_i = \frac{V_i^2}{Z_i e^{-j\phi_i}} - \frac{V_i V' e^{j\Delta\delta_i}}{Z_i e^{-j\phi_i}} = \frac{V_i^2}{Z_i} e^{j\phi_i} - \frac{V_i V'}{Z_i} e^{j(\phi_i + \Delta\delta_i)} \tag{2.2}$$

From Euler's formula, real power (P) and reactive power (Q):

$$P_i = \frac{V_i^2}{Z_i} \cos\phi_i - \frac{V_i V'}{Z_i} \cos(\phi_i + \Delta\delta_i) \tag{2.3}$$

$$Q_i = \frac{V_i^2}{Z_i} \sin\phi_i - \frac{V_i V'}{Z_i} \sin(\phi_i + \Delta\delta_i) \tag{2.4}$$

Let consider, line impedance (Z_i)=line resistance (R_i)+j $\times$ line reactance (X_i),

$\cos(\phi_i + \Delta\delta_i) = \cos\phi_i \cos\Delta\delta_i - \sin\phi_i \sin\Delta\delta_i$,

$\sin(\phi_i + \Delta\delta_i) = \sin\phi_i \cos\Delta\delta_i + \cos\phi_i \sin\Delta\delta_i$.

Therefore, Eqns. (2.3) and (2.4) become:

$$P_i = \frac{V_i}{R_i^2 + X_i^2}(R_i V_i - R_i V' \cos\Delta\delta_i + X_i V' \sin\Delta\delta_i) \tag{2.5}$$

$$Q_i = \frac{V_i}{R_i^2 + X_i^2}(X_i V_i - X_i V' \cos\Delta\delta_i - R_i V' \sin\Delta\delta_i) \tag{2.6}$$

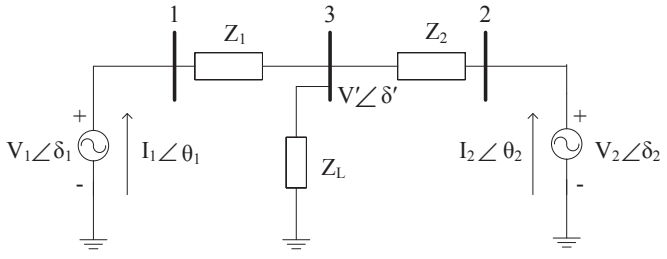

Figure 2.2. Single-line diagram of a two-source microgrid.

The relation between bus currents and bus voltages in the microgrid is [36, 37]:

$$Y_{\text{bus}}\, V_{\text{bus}} = I_{\text{bus}} \tag{2.7}$$

$$Y_{\text{bus}} = \begin{bmatrix} \frac{1}{Z_1} & 0 & -\frac{1}{Z_1} \\ 0 & \frac{1}{Z_2} & -\frac{1}{Z_2} \\ -\frac{1}{Z_1} & -\frac{1}{Z_2} & \frac{1}{Z_1}+\frac{1}{Z_2}+\frac{1}{Z_{\text{L}}} \end{bmatrix} \tag{2.8}$$

$$V_{\text{bus}} = \begin{bmatrix} V_1\angle\delta_1 \\ V_2\angle\delta_2 \\ V_3\angle\delta_3 \end{bmatrix} ;\ I_{\text{bus}} = \begin{bmatrix} I_1\angle\theta_1 \\ I_2\angle\theta_2 \\ I_3\angle\theta_3 \end{bmatrix} \tag{2.9}$$

Let, the distribution line parameters are: $Z_1 = \text{j}0.25$ pu, and $Z_2 = \text{j}0.05$ pu.

Load-flow analysis is carried out to determine the initial set values of different bus parameters. It is assumed that bus-1 is a generator bus, bus-2 is a slack or reference bus, and bus-3 is a load bus. Considered initial set values: $P_1^0 = 0.5$ pu, $V_1^0 = 1$ pu, $V_2^0 = 1$ pu, $\delta_2^0 = 0^0$, and load resistor, Z_{L}^0=1 pu.

Load-flow solution gives the initial set values of δ_1,V_3, and δ_3; these are: $\delta_1^0 = 5.7663^0$, $V_3^0 = 0.9984$ pu, $\delta_3^0 = -1.4258^0$. Using Eqn. (2.7), $I_1^0 = 0.5014$ pu, $\theta_1^0 = 1.4544^0$, I_2^0 $= 0.4983$ pu, $\theta_2^0 = -4.3241^0$, $P_2^0 = 0.4969$ pu, $P_3^0 = P_{Z_{\text{L}}}^0 = 0.9969$ pu, $Q_1^0 = 0.0377$ pu, and $Q_2^0 = 0.0376$ pu (θ_i=current phase angle).

In order to see the impact of load change, the load impedance, Z_{L}, is changed from 1 pu to 0.5 pu. It is assumed that the voltage magnitudes and the phase angles of voltage-sources are at the pre-changed values. From these values, the real power and the reactive power provided by the voltage-sources are: $P_1 = 0.6616$ pu, $P_2 = 1.3190$ pu, $Q_1 = 0.0740$ pu, and $Q_2 = 0.1247$ pu.

Now, ΔP_1=P_1-P_1^0=0.1616 pu and ΔP_2=P_2-P_2^0=0.8221 pu; from these values it is noticed that the two voltage-sources are unable to share the extra load evenly. For sound operation of microgrids, it is recommended to divide the extra load among DG units in accordance with their ratings [36].

Therefore, a method is required for maintaining this automatic load distribution and droop-based control strategies are deployed in this chapter.

2.5 Existing Droop-based Control Algorithms

In this section, various microgrid control algorithms are introduced with a view to ascertaining system stability under diverse microgrid structures. For example, forward droop control (FDC) for inductive (L-type) microgrids is discussed in Subsection 2.5.1. The following sub-section contains reverse droop control (RDC) for resistive (R-type) microgrids, and Sub-section 2.5.3 provides generalized droop control (GDC) for inductive-resistive (RL-type) microgrids.

2.5.1 Forward Droop Control (FDC) Algorithm with Modifications

This sub-section presents droop control scheme for L-type microgrids ($Z_1 = \text{j}0.25$ pu, and $Z_2 = \text{j}0.05$ pu). The voltage phase angle in distributed generation can be changed based on a control law, and this strategy can be regarded as a droop [36, 55]. For instance, voltage phase angle is increased if DG-units supply less than the connected load and vice-verse.

Let the change in phase angles, $\Delta\delta_i$, is small such that $\sin\Delta\delta_i \approx \Delta\delta_i$ and $\cos\Delta\delta_i \approx 1$. Eqns. (2.5) and (2.6) then become:

$$\Delta\delta_i = \frac{X_i P_i}{V_i V'} \tag{2.10}$$

$$V_i - V' = \Delta V_i = \frac{X_i Q_i}{V_i} \tag{2.11}$$

Motivated by these relations, the droop equations can be written as [36], [37], [53], [68], [69] ($i = 1, 2$):

$$\Delta\dot{\delta}_i = -k_{\text{f}_i}(P_{\text{m}_i} - P_i^0) \tag{2.12}$$

$$\Delta V_i = -k_{\text{v}_i}(Q_{\text{m}_i} - Q_i^0) \tag{2.13}$$

where, subscript m stands for measured values, δ_i represents the phase angle of inverter-connected DG sources, and ΔV_i denotes the voltage difference between the instant voltage and the initial voltage. P_i^0 and Q_i^0 are reference active and reactive powers. P_i and Q_i indicate instant real and reactive powers. P_{m_i} and Q_{m_i} are measured powers. Besides, k_{f_i} and k_{v_i} are the control parameters. In this chapter, the control gain values chosen for simulation are: $k_{\mathrm{f}_1} = 1$, $k_{\mathrm{f}_2} = 5$, $k_{\mathrm{v}_1} = 0.001$, and $k_{\mathrm{v}_2} = 0.005$. The selection procedures of control gains are provided in **Chapter 3**.

Let assume that measurement sensors of real-reactive powers possess a first-order dynamics and their transfer functions can be expressed as [36] ($i = 1, 2$):

$$\frac{P_{\mathrm{m}_i}(s)}{P_i(s)} = \frac{w_{\mathrm{f}}}{s + w_{\mathrm{f}}}; \frac{Q_{\mathrm{m}_i}(s)}{Q_i(s)} = \frac{w_{\mathrm{f}}}{s + w_{\mathrm{f}}} \tag{2.14}$$

where, w_{f} is the time constant whose value is defined as $12\,\mathrm{rad\,s^{-1}}$.

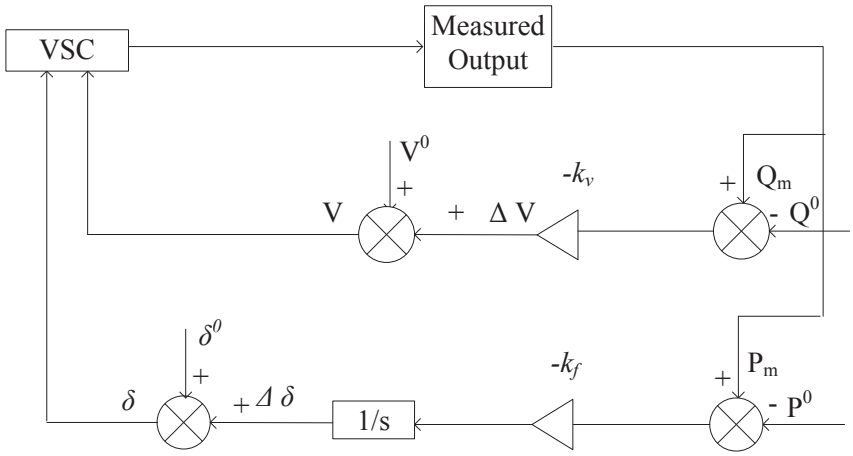

Figure 2.3. Schematic block diagram of FDC.

Fig. 2.3 shows the droop control strategy; in which if the load changes, the variation between original load and measured load is multiplied by the droop gains and the controller controls it in a way that angle difference, voltages, real powers

and reactive powers of the system remain stable. The droop control equations are denoted in this diagram by means of summations and gains.

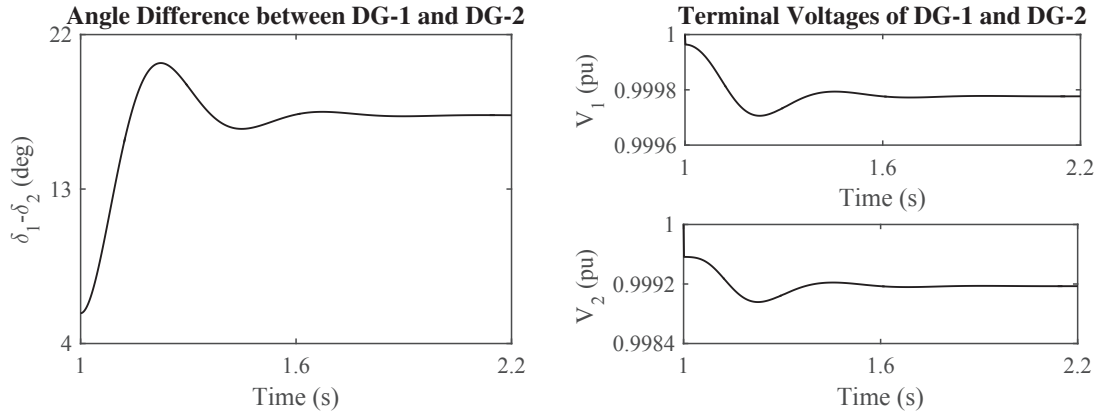

(a) Angle Difference. (b) Voltages.

Figure 2.4. L-type microgrids- angle difference and voltages by FDC.

Let consider, there is a 50 percent reduction in the load impedance at 1 second. It increases active power and droop control decreases the rate-of-change of phase angle of both DG sources to significant amounts. As a result, the angle difference of the islanded microgrid increases. Since it is of fixed value (17.3010^0), as seen from Fig. 2.4(a), the rate-of-change of angles (frequencies) are the same and a stable operation is maintained throughout the system. Fig. 2.4(b) depicts the terminal voltages of DG units. Their values decrease from initial value of 1 pu due to the reduction in the load impedance.

2.5.1.1 Developed Compensation-based FDC Algorithm

The traditional droop control strategy is modified in this thesis and represented as droop control with compensation. This is because of ascertaining the balance in the real power output of the microgrid by changing it according to the change in the dc-bus voltage of the power sources (V_{dc_i}). For this purpose, power offset (added to the output real power) is expressed as a function of the variation in the dc-link

voltage [37]-[39]. The proposed droop equations are ($i = 1, 2$):

$$P^0_{\mathrm{ft}_i} = k_{\mathrm{dc}_i}(V^0_{\mathrm{dc}_i} - V_{\mathrm{dc}_i}) \tag{2.15}$$

$$\Delta\dot{\delta}_i = -k_{\mathrm{f}_i}(P_{\mathrm{m}_i} + P^0_{\mathrm{ft}_i} - P^0_i);\ \Delta V_i = -k_{\mathrm{v}_i}(Q_{\mathrm{m}_i} - Q^0_i) \tag{2.16}$$

where, $P^0_{\mathrm{ft}_i}$ is the offset power. $V^0_{\mathrm{dc}_i}$ and V_{dc_i} are initial and actual values of the renewable generation. Proportional control keeps $(V^0_{\mathrm{dc}_i} - V_{\mathrm{dc}_i})$ to a constant. The value of dc control gain, k_{dc_i}, is selected 1 for simulation in this dissertation.

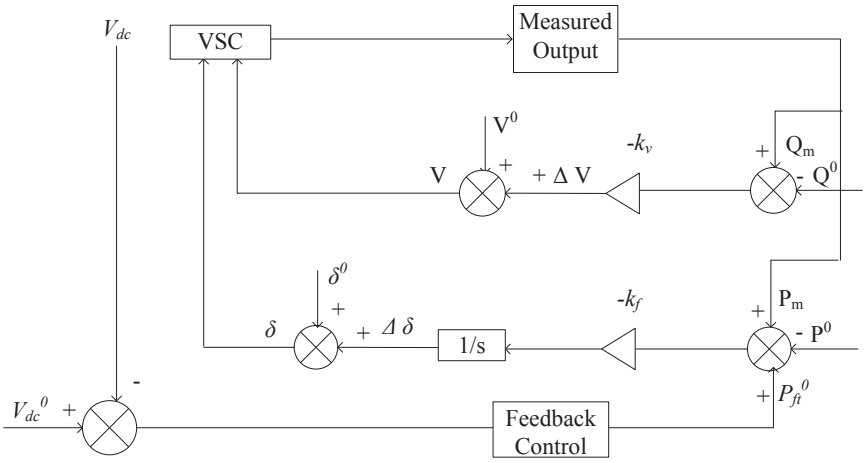

Figure 2.5. Schematic block diagram of FDC with compensation.

In Fig. 2.5, a feedback controller is added with the existing droop controller in order to control the voltage magnitude and the phase angle of a dc/ac converter-interfaced voltage-source (connected in an islanded microgrid) when either renewable generation, load or both vary.

Let assume a situation where a sudden change occurs in the generation of dc micro-sources. Consequently, V_{dc_i} changes from its set value of 1 pu. Now, the proposed feedback control strategy changes the output power of the microgrid in

accordance with the change in V_{dc_i}. This will allow the microgrid to obtain a natural balancing.

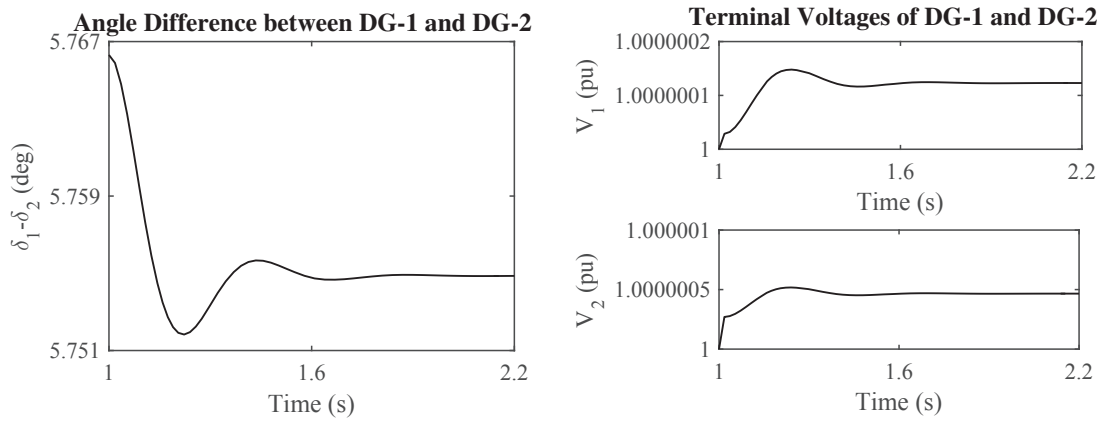

(a) Angle Difference. (b) Voltages.

Figure 2.6. L-type microgrids- angle difference and voltages by FDC with compensation.

When there is a sudden reduction (say 10 percent) in the dc generation at 1 second, transients are found in the wave-shapes of angle difference and voltages of L-type microgrids. The designed control returns the system to a steady-state within 2 seconds that can be noticed from Fig. 2.6(a) and Fig. 2.6(b), indicating stable operation after transients.

2.5.1.2 Derivative FDC Algorithm

A derivative term is added in conventional droop equations to improve the controller performance. Derivative term ensures that a sudden load demand will be picked by the DG units at a same rate. Thus, the rate-of-change in output power of DG units can be restricted [40]-[43]. The derivative droop control (DDC) equations are $(i = 1, 2)$:

$$\Delta\dot{\delta}_i = -k_{\mathrm{f}_i}(P_{\mathrm{m}_i} - P_i^0) - k_{\mathrm{fd}_i}(\frac{dP_{\mathrm{m}_i} - P_i^0}{dt}) \tag{2.17}$$

$$\Delta V_i = -k_{\mathrm{v}_i}(Q_{\mathrm{m}_i} - Q_i^0) - k_{\mathrm{vd}_i}(\frac{dQ_{\mathrm{m}_i} - Q_i^0}{dt}) \tag{2.18}$$

where, k_{fd_i} and k_{vd_i} are derivative gains whose values are chosen as follows: $k_{\mathrm{fd}_1} = 0.1$, $k_{\mathrm{fd}_2} = 0.5$, $k_{\mathrm{vd}_1} = 0.1$, and $k_{\mathrm{vd}_2} = 0.5$.

In Fig. 2.7, the operation of the proposed derivative droop controller is demonstrated. The controller works like a droop such that if the measured active power is greater than the initial reference value, it decreases the phase angle. Similarly, voltage is decreased when the measured reactive power is more than the initial reference value. Derivative terms maintain well-damped responses of angle difference, voltages, and powers within the L-type microgrid.

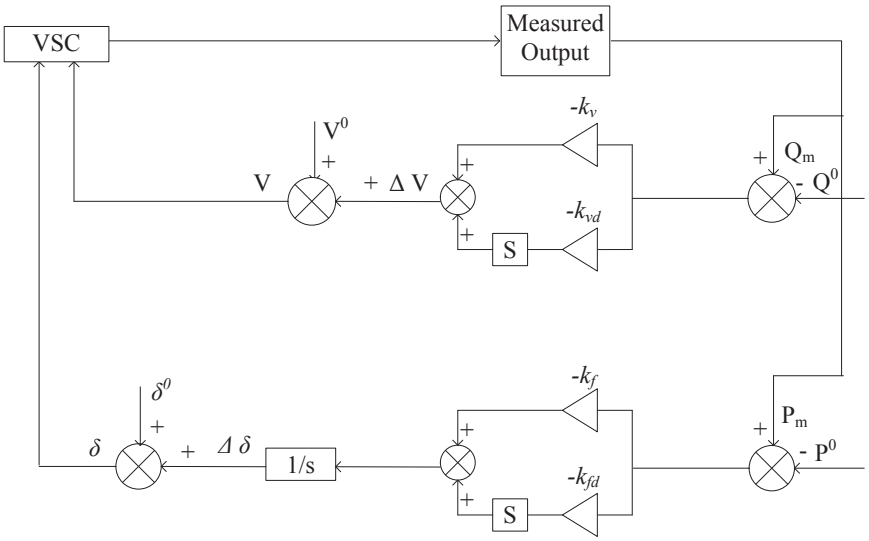

Figure 2.7. Schematic block diagram of DDC.

The designed controller is able to keep the angle difference between two DG units at a constant value, which can be seen from Fig. 2.8(a). Consequently, the rate-of-change of angles (frequencies) are equal and the system is stable. Fig. 2.8(b) represents the responses of terminal voltages at buses-1 and 2. The steady-state values of them are achieved within 4 seconds. All these figures highlight the utility

of the derivative droop controller in providing well-damped dynamic performance for each DG units.

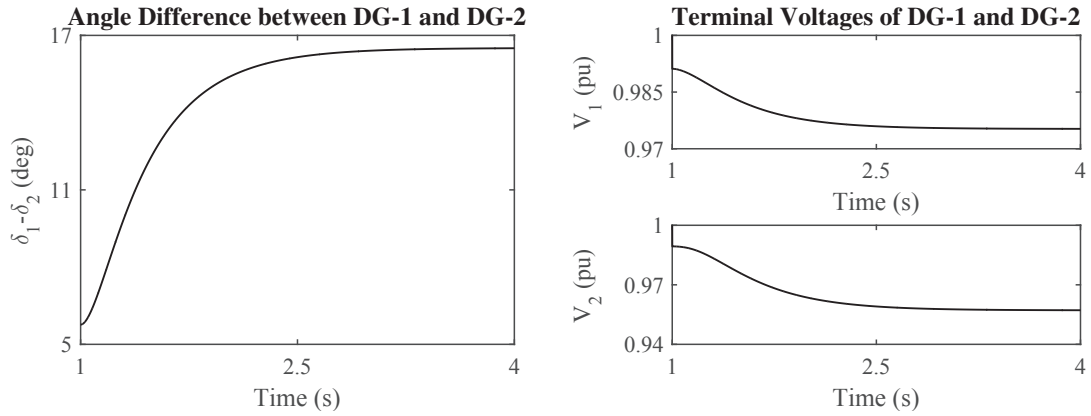

(a) Angle Difference. (b) Voltages.

Figure 2.8. L-type microgrids- angle difference and voltages by DDC.

2.5.1.3 Developed Current-based FDC Algorithm

When a short-circuit occurs at the distribution lines, the droop Eqns. (2.12) and (2.13) would cause infinitely high currents. To avoid this situation and to control the currents of DG units, current-based droop control is proposed in this thesis. Since the currents of DG units can be expressed by the ratio of power and voltage, Eqns. (2.10) and (2.11) can be modified as ($i = 1, 2$):

$$\Delta\delta_i = X_i I_{\mathrm{p}_i} \tag{2.19}$$

$$V_i - V^{'} = \Delta V_i = X_i I_{\mathrm{q}_i} \tag{2.20}$$

where, I_{p_i} and I_{q_i} are real and reactive currents of DG units ($i = 1, 2$). Current-based droop control equations can be derived as ($i = 1, 2$):

$$\Delta\dot{\delta}_i = -k_{\mathrm{f}_i}(I_{\mathrm{p}_{\mathrm{m}_i}} - I^0_{\mathrm{p}_i}) \tag{2.21}$$

$$\Delta V_i = -k_{\mathrm{v}_i}(I_{\mathrm{q}_{\mathrm{m}_i}} - I^0_{\mathrm{q}_i}) \tag{2.22}$$

where, $I^0_{\mathrm{p}_i}$ and $I^0_{\mathrm{q}_i}$ are reference active and reactive currents, and $I_{\mathrm{p}_{\mathrm{m}_i}}$ and $I_{\mathrm{q}_{\mathrm{m}_i}}$ are measured currents.

The current-based controller ensures stable responses of both real and reactive current components of two DG units. Their responses are simulated in Fig. 2.9.

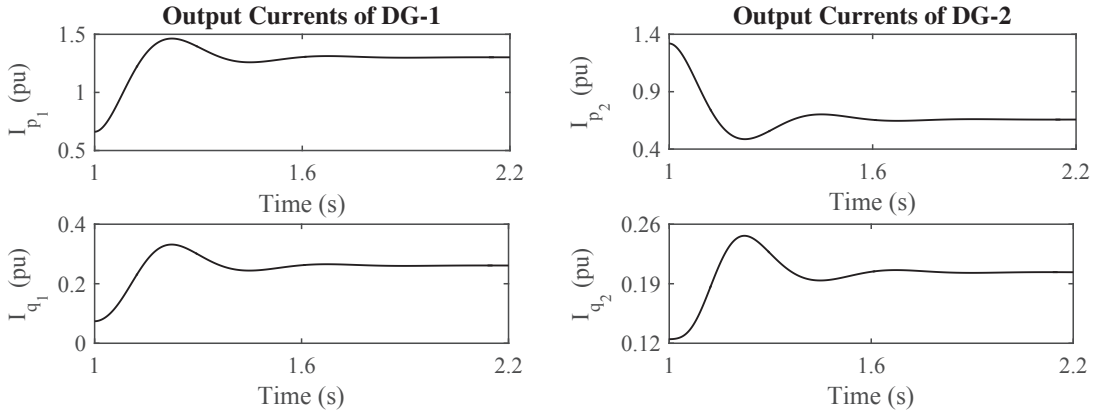

(a) Currents (DG-1). (b) Currents (DG-2).

Figure 2.9. L-type microgrids- real and reactive currents.

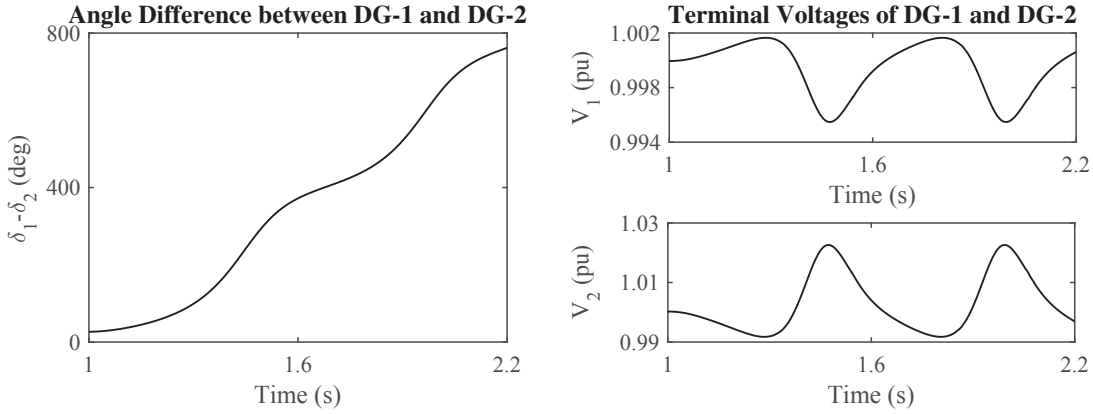

(a) Angle Difference. (b) Voltages.

Figure 2.10. R-type microgrids- angle difference and voltages by FDC.

2.5.1.4 FDC Algorithm in R-type Microgrids

In this sub-section, the FDC algorithm is applied on highly-resistive (R-type) microgrids to see its feasibility in this kind of microgrids; in which the distribution line

impedances are considered as: $Z_1 = 0.25$ pu, and $Z_2 = 0.05$ pu (inductive elements are neglected).

However, it is observed from Fig. 2.10 that this algorithm cannot ensure the system stability due to the high resistances of the distribution lines.

2.5.2 Reverse Droop Control (RDC) Algorithm

The perception of reverse droop control (RDC) arises for ensuring reliable and stable operation of R-type microgrids. For highly-resistive microgrids, $R_i >> X_i$. This means that X_i can be ignored as it is smaller than R_i [52]. If the change in phase angles ($\Delta\delta_i$) is small, then $\sin\Delta\delta_i \approx \Delta\delta_i$ and $\cos\Delta\delta_i \approx 1$. Eqns. (2.5) and (2.6) can now be reduced as ($i = 1, 2$):

$$\Delta\delta_i = -\frac{R_i Q_i}{V_i V'} \tag{2.23}$$

$$V_i - V' = \Delta V_i = \frac{P_i R_i}{V_i} \tag{2.24}$$

Eqns. (2.23) and (2.24) show a strong linkage between the reactive power and the phase angle of the inverter-interfaced DG units, as well as between the real power and the voltage magnitude of DG units. Thus, the proposed reverse droop equations are [41], [44] ($i = 1, 2$):

$$\Delta\dot{\delta}_i = k_{\mathrm{f}_i}(Q_{\mathrm{m}_i} - Q_i^0) \tag{2.25}$$

$$\Delta V_i = -k_{\mathrm{v}_i}(P_{\mathrm{m}_i} - P_i^0) \tag{2.26}$$

The operation of the proposed control is illustrated in Fig. 2.11. When the load changes from a fixed value, the controller starts operating to share powers between two DG units. It controls the voltage of a VSC-connected R-type microgrid by

multiplying the change in the real power with k_{v}, while the voltage phase angle is controlled by the change in the reactive power multiplied by k_{f}.

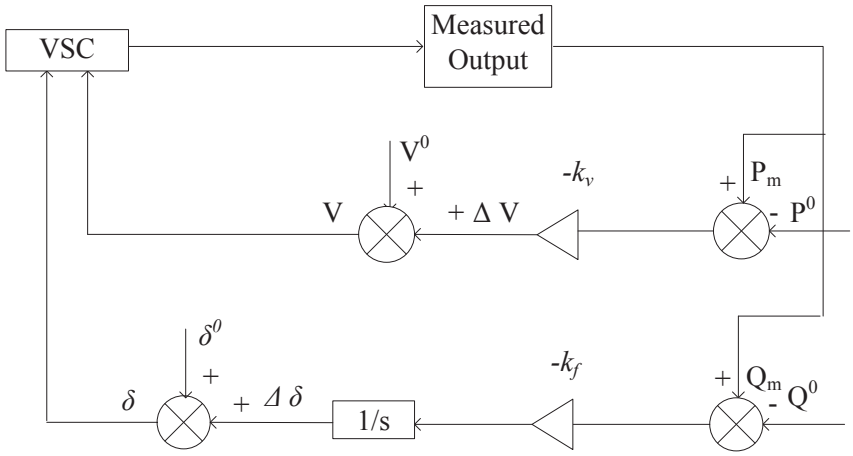

Figure 2.11. Schematic block diagram of RDC.

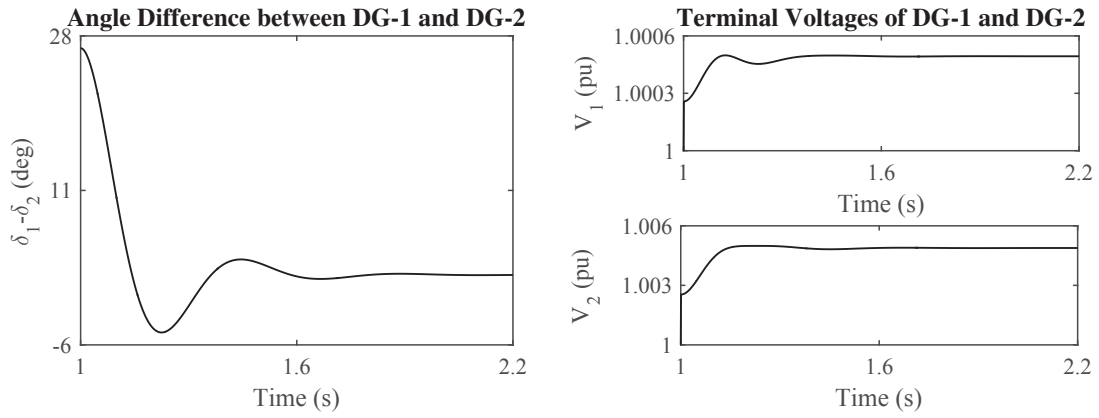

(a) Angle Difference. (b) Voltages.

Figure 2.12. R-type microgrids- angle difference and voltages by RDC.

The main objective of P/V droop control is to ascertain the stability in low-voltage (LV) microgrids with the maintenance of power balance during load variations. It is seen from Fig. 2.12(a) that the implementation of RDC (when the

load impedance changes from 1 pu to 0.5j pu) causes the microgrid angle difference to approach a constant value of 1.695^0, hence maintaining a stable operation. The responses of the terminal voltages of DG units are shown in Fig. 2.12(b). The steady-state values for them are obtained within 1 second of controller operation.

RDC Algorithm in L-type Microgrids

As is observed from Fig. 2.13 that RDC performs poorly in L-type microgrids, although it provides satisfactory results in highly-resistive networks. This feature of RDC urges the necessity of implementing two various types of control algorithms depending upon the particular structure of microgrids. With a view to ensuring generalized microgrid (L-type, R-type, and RL-type) control, a generalized droop control (GDC) is presented in Sub-section 2.5.3.

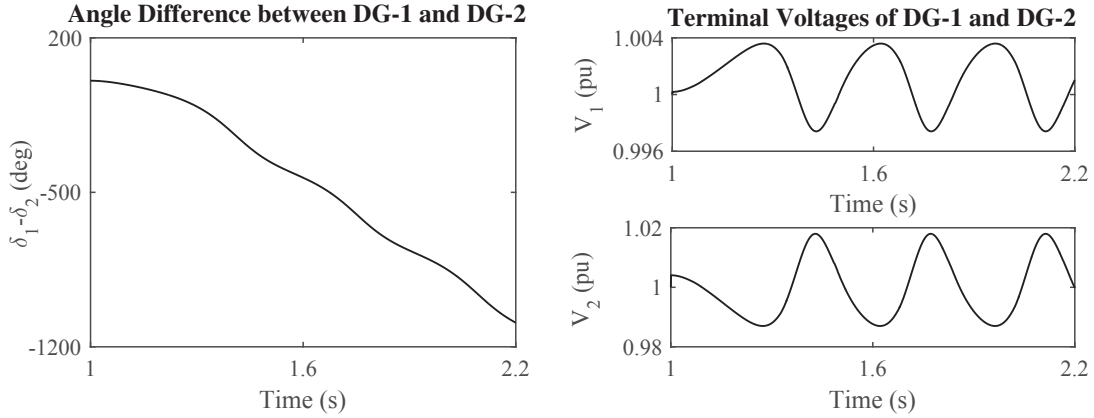

(a) Angle Difference. (b) Voltages.

Figure 2.13. L-type microgrids- angle difference and voltages by RDC.

2.5.3 Generalized Droop Control (GDC) Algorithm

This sub-section describes GDC strategy, which has the feature of controlling both resistive and inductive islanded microgrids. As a consequence, this control scheme is more effective. Let derive GDC equations. If the change in phase angles, $\Delta\delta_i$, is small. That means $\sin\Delta\delta_i \approx \Delta\delta_i$ and $\cos\Delta\delta_i \approx 1$. Eqns. (2.5) and (2.6) become:

$$P_i = \frac{V_i}{R_i^2 + X_i^2}[R_i V_i - R_i V^{'} + X_i V^{'} \Delta\delta_i] \tag{2.27}$$

$$Q_i = \frac{V_i}{R_i^2 + X_i^2}[X_i V_i - X_i V^{'} \Delta\delta_i - R_i V^{'} \Delta\delta_i] \tag{2.28}$$

Eqns. (2.27) and (2.28) show that not only the real power but also the reactive power depend on the distribution line parameters, the voltage magnitude, and the phase angle. According to these relations, the generalized droop equations can be expressed as [50] ($i = 1, 2$):

$$\Delta\dot{\delta}_i = -k_{\mathrm{f}_i}\frac{X_i}{|Z_i|}(P_{\mathrm{m}_i} - P_i^0) + k_{\mathrm{f}_i}\frac{R_i}{|Z_i|}(Q_{\mathrm{m}_i} - Q_i^0) \tag{2.29}$$

$$\Delta V_i = -k_{\mathrm{v}_i}\frac{R_i}{|Z_i|}(P_{\mathrm{m}_i} - P_i^0) - k_{\mathrm{v}_i}\frac{X_i}{|Z_i|}(Q_{\mathrm{m}_i} - Q_i^0) \tag{2.30}$$

where, R_i, X_i, and Z_i are distribution line resistances, inductances and impedances; in which $|Z_i| = \sqrt{R_i^2 + X_i^2}$.

Real power and reactive power measurement sensors are believed to have a first-order dynamics and their transfer functions are [46] ($i = 1, 2$):

$$\frac{P^{'}_{\mathrm{m}_i}(s)}{P^{'}_i(s)} = \frac{w_{\mathrm{f}}}{s + w_{\mathrm{f}}};\ \frac{Q^{'}_{\mathrm{m}_i}(s)}{Q^{'}_i(s)} = \frac{w_{\mathrm{f}}}{s + w_{\mathrm{f}}} \tag{2.31}$$

where, $P^{'}_{\mathrm{m}_i} = \frac{X_i}{|Z_i|}P_{\mathrm{m}_i} - \frac{R_i}{|Z_i|}Q_{\mathrm{m}_i}$, $Q^{'}_{\mathrm{m}_i} = \frac{R_i}{|Z_i|}P_{\mathrm{m}_i} + \frac{X_i}{|Z_i|}Q_{\mathrm{m}_i}$,
$P^{'}_i = \frac{X_i}{|Z_i|}P_i - \frac{R_i}{|Z_i|}Q_i$, $Q^{'}_i = \frac{R_i}{|Z_i|}P_i + \frac{X_i}{|Z_i|}Q_i$.

The overall control operation is shown in Fig. 2.14, which reveals that the controller operates as a droop and adjusts both the voltage magnitude and the rate-of-change of voltage angle when the load value changes from its reference one. In the diagram, $k_1 = k_{\mathrm{v}_i}\frac{R_i}{|Z_i|}$, $k_2 = k_{\mathrm{v}_i}\frac{X_i}{|Z_i|}$, $k_3 = k_{\mathrm{f}_i}\frac{R_i}{|Z_i|}$, and $k_4 = k_{\mathrm{f}_i}\frac{X_i}{|Z_i|}$.

The system parameters with this control approach are: $Z_1 = 0.25$+j0.25 pu, and $Z_2 = 0.05$+j0.05 pu.

Let there is a 50 percent change in the load impedance (0.5 pu) at 1 second. Fig. 2.15(a) depicts that the angle difference increases to 21.2024^0 after slight initial

oscillations due to the sensor dynamics. The voltages of DG-buses are also decreased because of reducing the load impedance. This can be noticed from Fig. 2.15(b).

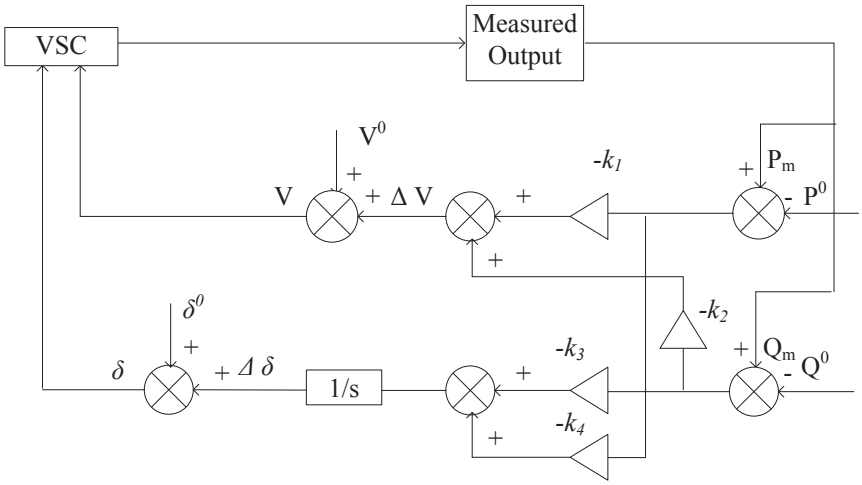

Figure 2.14. Schematic block diagram of GDC.

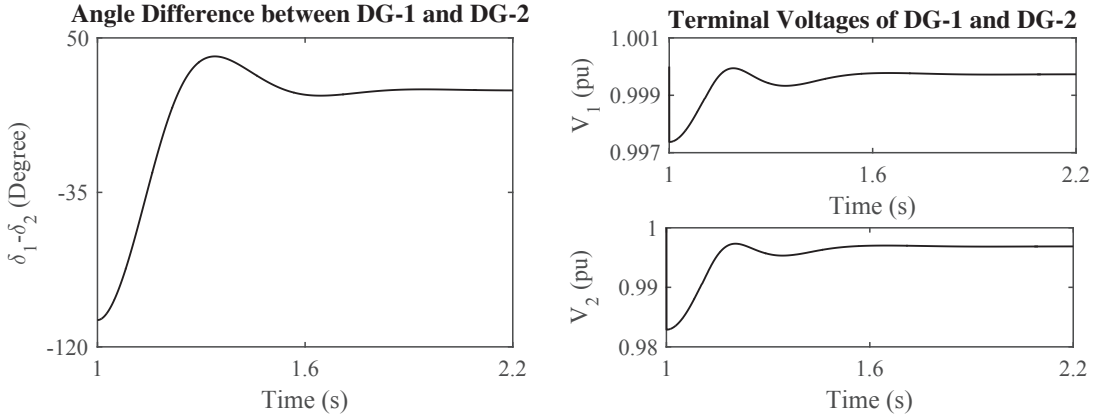

(a) Angle Difference. (b) Voltages.

Figure 2.15. RL-type microgrids- angle difference and voltages by GDC.

2.6 Power Sharing with Existing Controllers

Power sharing qualities of conventional droop-based algorithms are discussed in this section. Linearized model-based power sharing approaches are also provided, where

proportional power sharing is not possible.

2.6.1 Power Sharing based on FDC Algorithm

This sub-section deals with the real-reactive power sharing capability of forward droop-based controllers. It has been found that the reactive power sharing with FDC is complicated.

2.6.1.1 Real Power Sharing

For stable operation of microgrids, frequencies of each inverter output should be the same, i.e., $\dot{\delta_1} = \dot{\delta_2}$ [36].

Define $\Delta P_i = P_{\mathrm{m}_i} - P_i^0$ $(i = 1, 2)$; and from Eqn. (2.12),

$$\Delta P_1 = \frac{k_{\mathrm{f}_2}}{k_{\mathrm{f}_1}} \Delta P_2 = 5\Delta P_2 \quad [k_{\mathrm{f}_1} = 1, k_{\mathrm{f}_2} = 5] \tag{2.32}$$

The steady-state values of real power of both the inverter-connected voltage-sources are: P_1=1.3017 pu, and P_2=0.6567 pu. Now, ΔP_1=P_1-P_1^0=0.8017 pu and ΔP_2=P_2-P_2^0=0.1598 pu, giving $\Delta P_1 \cong 5\Delta P_2$. This indicates that the control analysis resembles the stability criteria and the real power is shared at real-droop gain ratio.

2.6.1.2 Reactive Power Sharing

If $\Delta V_1 = \Delta V_2$, from Eqn. (2.13),

$$\Delta Q_1 = \frac{k_{\mathrm{v}_2}}{k_{\mathrm{v}_1}} \Delta Q_2 = 5\Delta Q_2 \quad [k_{\mathrm{v}_1} = 0.001, k_{\mathrm{v}_2} = 0.005] \tag{2.33}$$

The steady-state reactive powers are: Q_1=0.2611 pu, and Q_2=0.2034 pu. Therefore, ΔQ_1=Q_1-Q_1^0=0.2234 pu and ΔQ_2=Q_2-Q_2^0=0.1658 pu. However, it is noticed that FDC cannot share reactive power in accordance with the reactive power ratings of DG units.

Fig. 2.16 shows how real powers are shared between two DG units by FDC methodology.

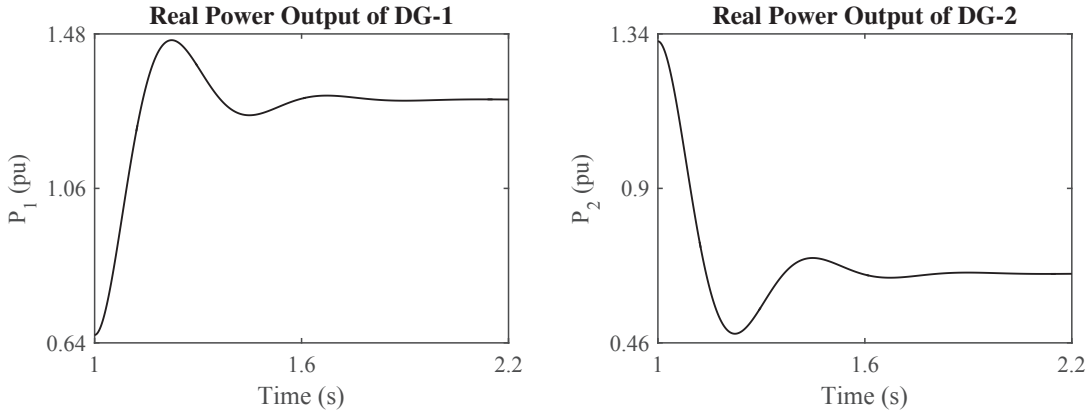

(a) Real Power (DG-1). (b) Real Power (DG-2).

Figure 2.16. L-type microgrids- real powers by FDC.

2.6.1.3 Linearized Model-based Reactive Power Sharing

In order to share the reactive power accurately, a linearized model-based analysis is provided in [36], [37]; in which the change in reactive powers is evaluated after the load change so that the sharing ratio can be obtained.

The reactive power-flow of a 3-bus microgrid, demonstrated in Fig. 2.2, can be expressed as $(i = 1, 2, 3;\ j \neq i)$ [37]:

$$Q_i = \sum_{j=1}^{3} V_i V_j (G_{ij}\ \sin\delta_{ij} - B_{ij}\ \cos\delta_{ij}) \tag{2.34}$$

where, G_{ij} and B_{ij} are the line conductance and susceptance respectively.
For negligible G_{ij}, it can be written as $(i = 1, 2)$:

$$Q_i = -V_i V_3 B_{i3}\ \cos\delta_{i3} - V_i^2 B_{ii} \tag{2.35}$$

Let the reactive power at node-3 of Fig. 2.2 changes owing to the load change, and reactive powers at node-1 and node-2 become:

$$\Delta Q_1 = k_{\mathrm{v}_1}\Delta Q_1 V_3^0 B_{13}\cos\delta_{13}^0 - V_1^0|\Delta V_3|B_{13}\cos\delta_{13}^0 + V_1^0 V_3^0 B_{13}\sin\delta_{13}^0 + 2k_{\mathrm{v}_1}\Delta Q_1 V_1^0 B_{11} \tag{2.36}$$

$$\Delta Q_2 = k_{\mathrm{v}_2}\Delta Q_2 V_3^0 B_{23}\cos\delta_{23}^0 - V_2^0|\Delta V_3|B_{23}\cos\delta_{23}^0 + V_2^0 V_3^0 B_{23}\sin\delta_{23}^0 + 2k_{\mathrm{v}_2}\Delta Q_2 V_2^0 B_{22} \tag{2.37}$$

The simplified forms of Eqns. (2.36) and (2.37) are:

$$\Delta Q_1 = \frac{-V_1^0|\Delta V_3|B_{13}\ \cos\delta_{13}^0 + V_1^0 V_3^0 B_{13}\ \sin\delta_{13}^0}{1 - k_{\mathrm{v}_1}V_3^0 B_{13}\ \cos\delta_{13}^0 - 2k_{\mathrm{v}_1}V_1^0 B_{11}} \tag{2.38}$$

$$\Delta Q_2 = \frac{-V_2^0|\Delta V_3|B_{23}\ \cos\delta_{23}^0 + V_2^0 V_3^0 B_{23}\ \sin\delta_{23}^0}{1 - k_{\mathrm{v}_2}V_3^0 B_{23}\ \cos\delta_{23}^0 - 2k_{\mathrm{v}_2}V_2^0 B_{22}} \tag{2.39}$$

where, $|\Delta V_3| = V_3^0\sqrt{(\cos\delta_3)^2 + (-\sin\delta_3)^2} = V_3^0$.

It is prominent from Eqns. (2.38) and (2.39) that the ratio of change in ΔQ_1 and ΔQ_2, due to the change in ΔQ_3, using the forward droop control strategy gives the reactive power sharing ratio.

2.6.2 Power Sharing based on RDC Algorithm

2.6.2.1 Real Power Sharing

Let consider, $\Delta V_1 = \Delta V_2$. It can be written from Eqn. (2.26),

$$\Delta P_1 = \frac{k_{\mathrm{v}_2}}{k_{\mathrm{v}_1}}\Delta P_2 = 5\Delta P_2 \quad [k_{\mathrm{v}_1} = 0.001, k_{\mathrm{v}_2} = 0.005] \tag{2.40}$$

The steady-state values of real powers are: P_1=0.0063 pu and P_2=0.1635 pu. Now, ΔP_1=P_1-P_1^0=0.4937 pu, and ΔP_2=P_2-P_2^0=-0.9765 pu. Thus, RDC is unable to share the real power based on the real power ratings of DG units.

2.6.2.2 Developed Linearized Model-based Real Power Sharing

The real power-flow of a 3-bus microgrid system, shown in Fig. 2.2, is [44] ($i = 1, 2, 3;\ j \neq i$):

$$P_i = \sum_{j=1}^{3} V_i V_j (G_{ij}\ \cos\delta_{ij} + B_{ij}\ \sin\delta_{ij}) \tag{2.41}$$

For negligible B_{ij}, Eqn. (2.41) can be written as ($i = 1, 2$):

$$P_i = V_i V_3 G_{i3} \cos\delta_{i3} + V_i^2 G_{ii} \tag{2.42}$$

A variation in the real power at node-3 of Fig. 2.2 occurs owing to the load impedance change, and it can be written using Eqn. (2.26) as:

$$\Delta P_1 = -k_{\mathrm{v}_1}\Delta P_1 V_3^0 G_{13}\cos\delta_{13}^0 + V_1^0|\Delta V_3|G_{13}\cos\delta_{13}^0 - V_1^0 V_3^0 G_{13}\sin\delta_{13}^0 - 2k_{\mathrm{v}_1}\Delta P_1 V_1^0 G_{11} \tag{2.43}$$

$$\Delta P_2 = -k_{\mathrm{v}_2}\Delta P_2 V_3^0 G_{23}\cos\delta_{23}^0 + V_2^0|\Delta V_3|G_{23}\cos\delta_{23}^0 - V_2^0 V_3^0 G_{23}\sin\delta_{23}^0 - 2k_{\mathrm{v}_2}\Delta P_2 V_1^0 G_{22} \tag{2.44}$$

The simplified form of Eqn. (2.43) is:

$$\Delta P_1 = \frac{V_1^0|\Delta V_3|G_{13}\cos\delta_{13}^0 - V_1^0 V_3^0 G_{13}\sin\delta_{13}^0}{1 + k_{\mathrm{v}_1} V_3^0 G_{13}\cos\delta_{13}^0 + 2k_{\mathrm{v}_1} V_1^0 G_{11}} \tag{2.45}$$

Similarly, Eqn. (2.44) can be expressed as:

$$\Delta P_2 = \frac{V_2^0|\Delta V_3|G_{23}\cos\delta_{23}^0 - V_2^0 V_3^0 G_{23}\sin\delta_{23}^0}{1 + k_{\mathrm{v}_2} V_3^0 G_{23}\cos\delta_{23}^0 + 2k_{\mathrm{v}_2} V_2^0 G_{22}} \tag{2.46}$$

Eqns. (2.45) and (2.46) suggest that the ratio of change in ΔP_1 and ΔP_2 with the help of a reverse droop control scheme is the ratio of conductances. That is why; real power sharing becomes dependent on the distribution line parameters, which hampers the desired sharing of real powers based on real-droop gains.

2.6.2.3 Reactive Power Sharing

The system will be in steady-state when Eqn. 2.47 is held [36].

$$\dot{\delta}_1 = \dot{\delta}_2 \tag{2.47}$$

Define $\Delta Q_i = Q_{\mathrm{m}_i} - Q_i^0$ where $i = 1, 2$; and using Eqn. (2.25), $\Delta Q_1 = \frac{k_{\mathrm{f}_2}}{k_{\mathrm{f}_1}}\Delta Q_2$. The steady-state values of the reactive power of inverter-interfaced voltage-sources are: Q_1=0.234 pu and Q_2=1.7685 pu. Now, ΔQ_1=Q_1-Q_1^0=1.6694 pu, and ΔQ_2=Q_2-Q_2^0=0.3331 pu, providing ΔQ_1=5ΔQ_2. Again, $\frac{k_{\mathrm{f}_2}}{k_{\mathrm{f}_1}} = 5$. Hence, the proposed reverse

control scheme maintains proportional reactive power sharing (wave-shapes are provided in Fig. 2.17).

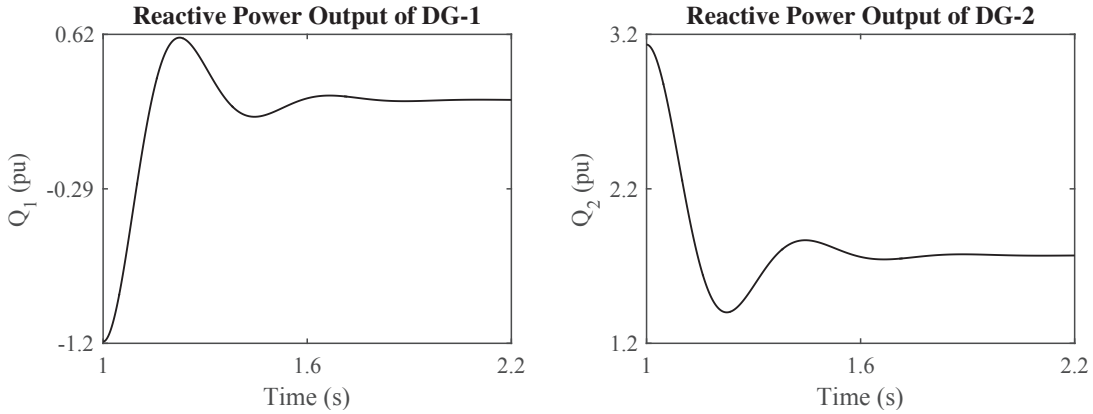

(a) Reactive Power (DG-1). (b) Reactive Power (DG-2).

Figure 2.17. R-type microgrids- reactive powers by RDC.

2.6.3 Power Sharing based on GDC Algorithm

The generalized droop control equations, as observed from Eqns. (2.29) and (2.30), include the distribution line impedances to ensure their feasibility in any types of microgrid structures. Because of this characteristic, GDC algorithm cannot distribute the load change proportionally among distributed generators. For this reason, linearized model-based power sharing approach is used in this dissertation.

2.6.3.1 Developed Linearized Model-based Real Power Sharing

The change in real power outputs, due to the load change, can be expressed as:

$$\begin{aligned}\Delta P_1 = &-k_{\mathrm{v}_1}\left(\frac{R_1}{|Z_1|}\Delta P_1 + \frac{X_1}{|Z_1|}p_1\right)V_3^0 G_{13}\ \cos\delta_{13}^0 + V_1^0|\Delta V_3|G_{13}\ \cos\delta_{13}^0 \\ &- V_1^0 V_3^0 G_{13}\ \sin\delta_{13}^0 - 2k_{\mathrm{v}_1}\left(\frac{R_1}{|Z_1|}\Delta P_1 + \frac{X_1}{|Z_1|}p_1\right)V_1^0 G_{11} \qquad (2.48)\\ \Delta P_2 = &-k_{\mathrm{v}_2}\left(\frac{R_2}{|Z_2|}\Delta P_2 + \frac{X_2}{|Z_2|}p_2\right)V_3^0 G_{23}\ \cos\delta_{23}^0 + V_2^0|\Delta V_3|G_{23}\ \cos\delta_{23}^0 \\ &- V_2^0 V_3^0 G_{23}\ \sin\delta_{23}^0 - 2k_{\mathrm{v}_2}\left(\frac{R_2}{|Z_2|}\Delta P_2 + \frac{X_2}{|Z_2|}p_2\right)V_2^0 G_{22} \qquad (2.49)\end{aligned}$$

where, $p_i = V_i^0 V_3^0 G_{i3} \cos\delta_{i3}^0$ $(i = 1, 2)$.

The ratio of ΔP_1 and ΔP_2 gives the real power sharing ratio.

2.6.3.2 Developed Linearized Model-based Reactive Power Sharing

Similarly, the change in reactive power outputs can be written as:

$$\begin{aligned}\Delta Q_1 = {} & k_{\mathrm{v}_1}\left(\frac{R_1}{|Z_1|}q_1 - \frac{X_1}{|Z_1|}\Delta Q_1\right)V_3^0 B_{13} \cos\delta_{13}^0 - V_1^0|\Delta V_3|B_{13}\cos\delta_{13}^0 \\ & + V_1^0 V_3^0 B_{13} \sin\delta_{13}^0 + 2k_{\mathrm{v}_1}\left(\frac{R_1}{|Z_1|}q_1 - \frac{X_1}{|Z_1|}\Delta Q_1\right)V_1^0 B_{11} \qquad (2.50)\\ \Delta Q_2 = {} & k_{\mathrm{v}_2}\left(\frac{R_2}{|Z_2|}q_2 - \frac{X_2}{|Z_2|}\Delta Q_2\right)V_3^0 B_{23} \cos\delta_{23}^0 - V_2^0|\Delta V_3|B_{23}\cos\delta_{23}^0 \\ & + V_2^0 V_3^0 B_{23} \sin\delta_{23}^0 + 2k_{\mathrm{v}_2}\left(\frac{R_2}{|Z_2|}q_2 - \frac{X_2}{|Z_2|}\Delta Q_2\right)V_2^0 B_{22} \qquad (2.51)\end{aligned}$$

where, $q_i = V_i^0 V_3^0 B_{i3} \cos\delta_{i3}^0$ $(i = 1, 2)$.

The reactive power is shared at ΔQ_1:ΔQ_2.

As linearized model-based analysis of microgrids relies on the specific distribution line parameters, the change in the load cannot be distributed among DG units based on their capacity without proper optimization among parameters [55], [56]. Infact, for an interconnected microgrid system where usually there exists more than one DG units, the selection of accurate values of distribution line parameters would be difficult.

With a view to sharing the change in the load proportionally, modified droop-based algorithm are proposed in Section 2.7.

2.7 Designed Droop-based Controllers for Proportional Power Sharing

This section proposes new types of droop-based controllers to share reactive power in L-type microgrids, real power in R-type microgrids, and real-reactive power in RL-type microgrids.

2.7.1 Proportional Reactive Power sharing with Improved FDC Algorithm

As is observed in Sub-section 2.6.1.2, the conventional FDC lacks the accuracy in reactive power sharing. That is why; this sub-section provides a new type of forward droop-based algorithm.

The droop-voltage control law can be expressed by the Eqn. (2.52) [54], [70].

$$\Delta V_i = k_{\mathrm{p}_i}((V_i^0 - V_{\mathrm{ref}_i}) - V^{'}) + k_{\mathrm{i}_i} \int ((V_i^0 - V_{\mathrm{ref}_i}) - V^{'})\, dt \tag{2.52}$$

$$V_{\mathrm{ref}_i} = D_{\mathrm{v}_i}(Q_{\mathrm{m}_i} - Q_i^0) \tag{2.53}$$

where, $i = 1, 2$.

k_{p_i} indicates the proportional gain ($k_{\mathrm{p}_1} = 0.1, k_{\mathrm{p}_2} = 0.5$), D_{v_i} is the droop gain ($D_{\mathrm{v}_1} = 0.1, D_{\mathrm{v}_2} = 0.5$), and k_{i_i} represents the integral gain ($k_{\mathrm{i}_1} = 1, k_{\mathrm{i}_2} = 1$).

The improved FDC control diagram is shown in Fig. 2.18; in which PI control is added to the traditional FDC control diagram for proportional reactive power sharing.

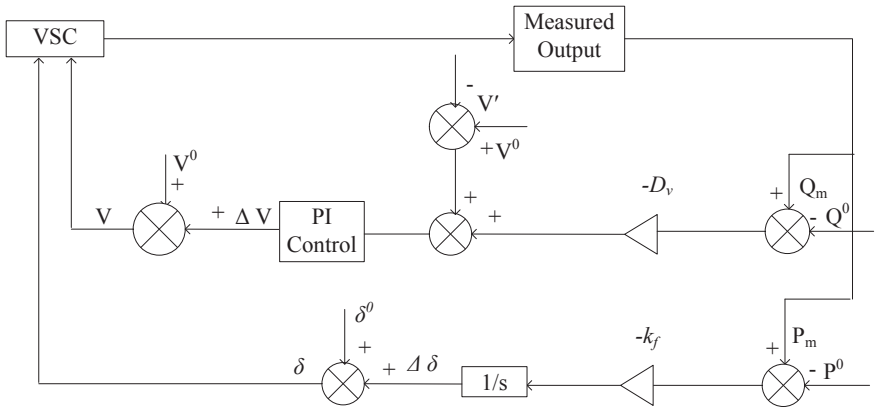

Figure 2.18. Schematic block diagram of improved FDC.

During the stable condition of the system, the integral argument in Eqn. (2.52) should be equal to zero. Therefore,

$$V_i^0 - D_{\mathrm{v}_i}\Delta Q_i - V^{'} = 0 \tag{2.54}$$

where, $\Delta Q_i = Q_{\mathrm{m}_i} - Q_i^0$, $V_1^0 = V_2^0$=1 pu, and
$V^{'}$ is the common load voltage.

From Eqn. (2.54), it can be concluded that if the initial values of the voltages are kept the same, then the controller can share reactive powers inversely proportional to reactive-droop gains.

The performance of the designed controller is simulated in Fig. 2.19. Here, start-up oscillations are found on account of the integral control. These oscillations are eliminated by the controller within 0.8 second of its operation.

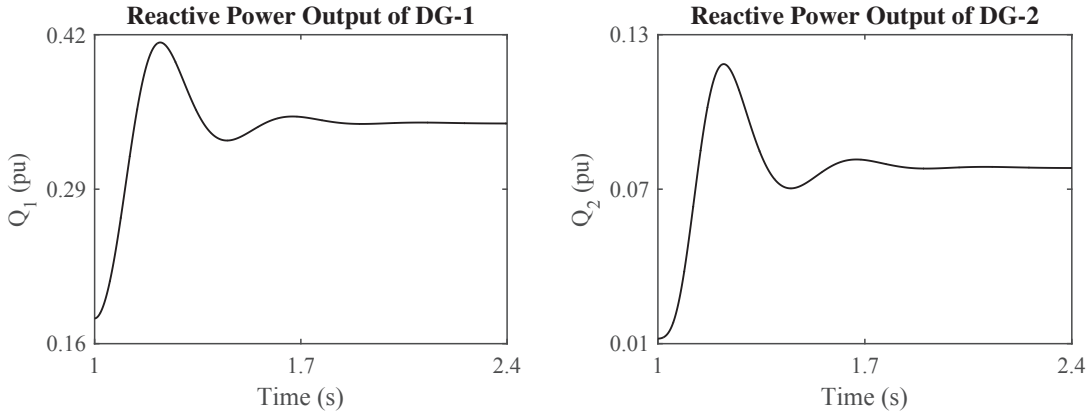

(a) Reactive Power (DG-1). (b) Reactive Power (DG-2).

Figure 2.19. L-type Microgrids- reactive powers by improved FDC.

2.7.2 Proportional Real Power sharing with Developed RDC Algorithm

Since RDC cannot divide the real power among DG units after the load change evenly, an improvement is done in the control algorithm with a view to ascertaining

proportional real power sharing. For RDC, the value of V_{ref_i} is:

$$V_{\mathrm{ref}_i} = D_{\mathrm{v}_i}(P_{\mathrm{m}_i} - P_i^0) \tag{2.55}$$

Fig. 2.20 illustrates the proposed RDC control strategy for proportional power sharing in R-type microgrids, and Fig. 2.21 shows the performance of the designed controller in real power sharing.

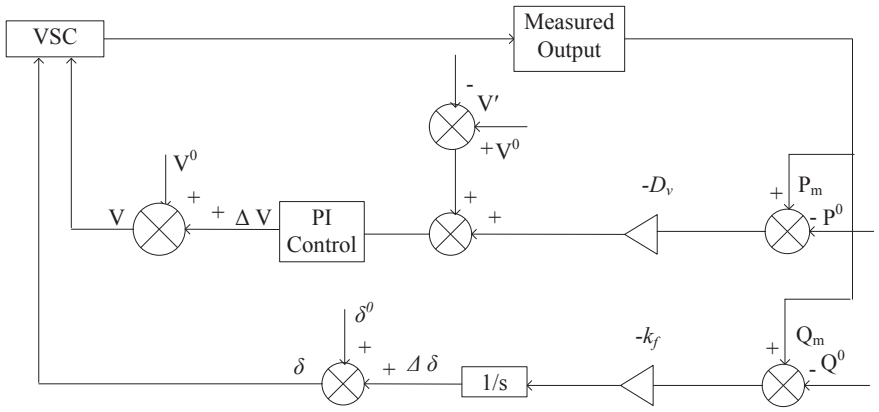

Figure 2.20. Schematic block diagram of proposed RDC.

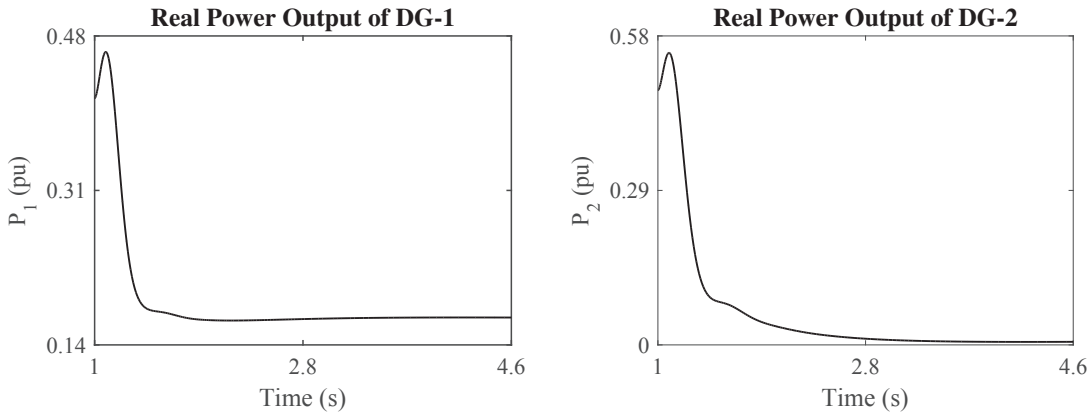

(a) Real Power (DG-1). (b) Real Power (DG-2).

Figure 2.21. R-type microgrids- real powers by proposed RDC.

In the state of stability, the argument of the integral in Eqn. (2.52) becomes zero. Hence,

$$V_i^0 - D_{\mathrm{v}_i}\Delta P_i - V^{'} = 0 \tag{2.56}$$

Eqn. (2.56) suggests that real powers can be shared inversely proportional to real-droop gains if the initial values of the parallel voltage-sources are the same.

2.7.3 Proportional Power sharing with Developed GDC Algorithm

This sub-section discusses improved GDC for sharing power according to the ratings of DG units. Substituting Eqns. (2.55) and (2.53) into Eqn. (2.52), the voltage droop-based modified GDC equations can be written as ($i = 1, 2$):

$$\begin{aligned}\Delta V_i = {} & k_{\mathrm{p}_i}(V_i^0 - D_{\mathrm{v}_i}(P_{\mathrm{m}_i} - P_i^0) - V^{'}) + k_{\mathrm{i}_i}\int (V_i^0 - D_{\mathrm{v}_i}(P_{\mathrm{m}_i} - P_i^0) - V^{'})\, dt \\ & + k_{\mathrm{p}_i}(V_i^0 - D_{\mathrm{v}_i}(Q_{\mathrm{m}_i} - Q_i^0) - V^{'}) + k_{\mathrm{i}_i}\int (V_i^0 - D_{\mathrm{v}_i}(Q_{\mathrm{m}_i} - Q_i^0) - V^{'})\, dt\end{aligned} \tag{2.57}$$

where, integral gain (k_{i_i}) determines the speed of the system response.

For a stable feedback system with control, the argument of the first and second integral in Eqn. (2.57) should be zero. Since V_i^0 are the same and $V^{'}$ is the common point voltage, powers can be shared based on the power-droop gains.

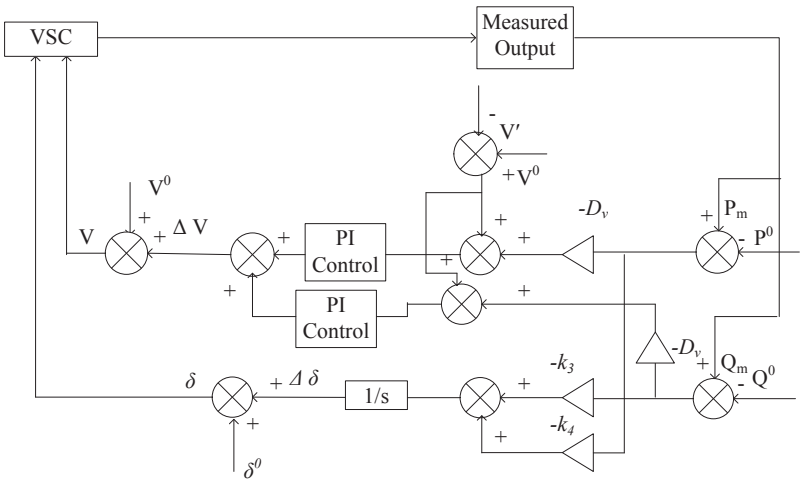

Figure 2.22. Schematic block diagram of proposed GDC.

The proposed GDC control diagram to share real-reactive powers proportionally in RL-type islanded microgrids is depicted in Fig. 2.22. PI control enables the controller to share power effectively. Fig. 2.23 and Fig. 2.24 show the wave-shapes of real and reactive powers, and it has been found that the proposed controller returns the system to stable-state within 2.4 seconds.

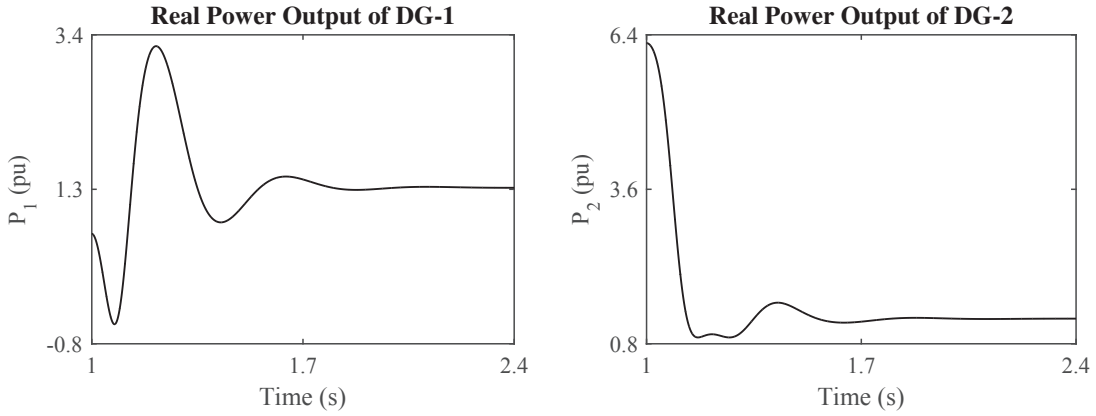

(a) Real Power (DG-1). (b) Real Power (DG-2).

Figure 2.23. RL-type microgrids- real powers by proposed GDC.

2.8 Chapter Summary

In this chapter, the control algorithms in order to distribute the change in the load between two DG units, under diverse microgrid structures (L-type, R-type, and RL-type), are discussed in great details. Algorithms are also modified to reduce the initial oscillations in the system responses, and to control the change in the renewable generation. Power sharing qualities of the existing droop-based controllers are demonstrated by means of load-flow analysis, and linearized model-based power sharing method of microgrids is used to determine the change in powers because of the load change.

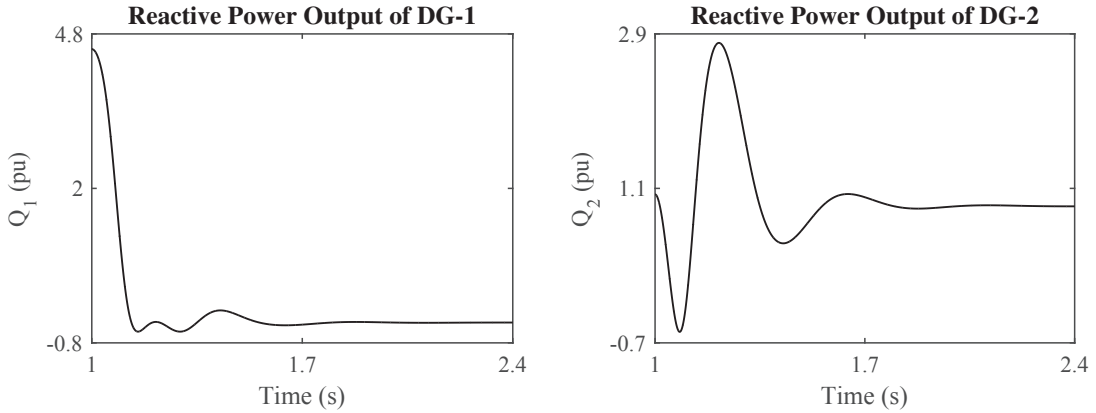

(a) Reactive Power (DG-1). (b) Reactive Power (DG-2).

Figure 2.24. RL-type microgrids- reactive powers by proposed GDC.

More importantly, improved control algorithms are developed for various types of islanded microgrids as linearized model-based power sharing strategies of microgrids rely on the particular distribution line parameters and effective power sharing may not be possible. These algorithms maintain proportional power sharing among common load-based parallel inverter-connected DG units.

A summary of the droop-based algorithms indicating their usage in different types of microgrids is provided in Table 2.1.

Table 2.1. Usage of droop-based algorithms in different microgrids

Algorithms	Usage
Forward droop-based algorithm	Inductive microgrids
Reverse droop-based algorithm	Resistive microgrids
Generalized droop-based algorithm	Inductive-resistive microgrids

The selection methods of the control parameters for these designed controllers are given in the next chapter (**Chapter 3**).

Chapter 3

Gain Selection Methods for the Designed Controllers

3.1 Chapter Objectives

This chapter contains the gain selection processes for the proposed controllers. To begin with, small-signal modeling is discussed in order to get the eigenvalues; from which the stability conditions of the designed controllers in microgrids can be realized. Owing to the vulnerability of this procedure in large inverter-based microgrids, extended dynamic phasors models are proposed in this chapter so that the accurate range of designed droop parameters can be determined.

3.2 Literature Review

The selection of droop-gains has been a challenging task for the utility operators and the researchers usually use small-signal modeling to predict the stability of the system and to choose the control gains [46], [59]-[62]. However, small-signal modeling approach has some demerits. First of all, it is reported in [64], [65], [67] that this method is based on the quasi-static approximation; in which the angular frequency is assumed as static and the dynamics of the power circuit elements are not considered. However, the disturbances occurred because of the dynamic adjustment of magnitude, frequency, and phase angle should be considered in droop-controlled islanded microgrids [65]. In addition, small-signal stability strategy requires more computational analysis in large systems [63], and lacks accuracy in low-inertia and

fast-acting inverter-based systems such as power electronics-connected microgrids [66]. Therefore, advanced gain selection schemes are required to use.

A simple method known as dynamic phasors modeling (DPM) is introduced in [74]-[78] to predict the dynamics and stability limit of the system. As this strategy considers the dynamics of the power circuit elements, it is implemented in fast-acting inverter-dominated microgrids in [67] with a view to predicting the transient response of the system and its stability margin precisely. It is also shown in [67] that DPM can be implemented in large inverter-interfaced systems. However, the inclusion of the improved droop-based controllers in DPM needs to be verified. DPM, with the designed controllers, is described in this chapter in depth in order to determine the stability range of droop gains with higher precision.

3.3 Chapter Outline

The rest of the chapter is organized as follows: in Section 3.4, small-signal analysis is carried out to find out the eigenvalues. Section 3.5 deals with the extended dynamic phasors models for the precise selection of control gains and the chapter summary is drawn in Section 3.6.

3.4 Small-signal Modeling

A small-signal analysis is a widely-used analysis tool by which electromechanical oscillations can be studied and dynamic characteristics of a system (may not be known from time-domain analysis) can be understood [71]. In this method, the equations that represent the system model are linearized about stable or unstable equilibrium points [72]. In general, eigenvalues are evaluated to analyze the small-signal of the system [73]. In this section, microgrids with different structures (L-type, R-type, and RL-type) are linearized and eigenvalues are found out.

3.4.1 System Structure and Linear Modal Analysis

This section depicts the single-line diagram, as seen in Fig. 3.1, of two-source and one load-based islanded microgrid with system linearization.

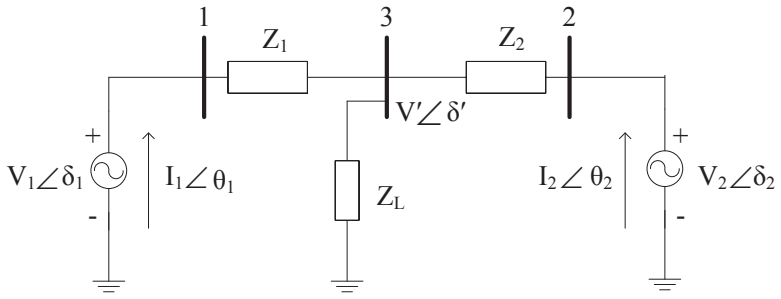

Figure 3.1. Single-line diagram of an islnaded microgrid system.

Linear modal analysis of the non-linear microgrid with the designed controllers is carried out in this chapter with a view to tuning the control parameters and understanding the system dynamics. The complex power can be written as ($i, j = 1, 2\,;\ j \neq i$):

$$S_i = P_i + jQ_i = V_i\angle\delta_i \times I_i\angle -\theta_i \tag{3.1}$$

$$I_i\angle -\theta_i = \sum_{j=1}^{2} Y_{\text{red}_{ij}}\, V_j\angle\delta_j \tag{3.2}$$

where, Y_{red} is the reduced Y_{bus} and it is obtained by grouping voltage-sources and the load as bus '1' and '2' respectively.

Let consider that $Y_{\text{red}_{ij}} = G_{ij} + jB_{ij}$. Putting Eqns. (3.1) and (3.2) together, power equations can be expressed as [36]:

$$P_i = \sum_{j=1}^{2} V_iV_j(G_{ij}\ \cos\delta_{ij} + B_{ij}\ \sin\delta_{ij}) \tag{3.3}$$

$$Q_i = \sum_{j=1}^{2} V_iV_j(G_{ij}\ \sin\delta_{ij} - B_{ij}\ \cos\delta_{ij}) \tag{3.4}$$

where, $\delta_{ij} = \delta_i - \delta_j$. G_{ij} is the line conductance, and B_{ij} is the line susceptance.

The Taylor series expansion for P_i and Q_i can be written as ($i = 1, 2\,;\; j \neq i$):

$$\begin{aligned} P_i &= P_i^0 + \Delta P_i \\ &= P_i^0 + \sum_{j=1}^{2} V_j^0 (G_{ij}\ \cos\delta_{ij}^0 + B_{ij}\ \sin\delta_{ij}^0)\ \Delta V_i \\ &+ \sum_{j=1}^{2} V_i^0 (G_{ij}\ \cos\delta_{ij}^0 + B_{ij}\ \sin\delta_{ij}^0)\ \Delta V_j \\ &+ \sum_{j=1}^{2} V_i^0 V_j^0 (-G_{ij}\ \sin\delta_{ij}^0 + B_{ij}\ \cos\delta_{ij}^0)\ \Delta\delta_{ij} \end{aligned} \tag{3.5}$$

$$\begin{aligned} Q_i &= Q_i^0 + \Delta Q_i \\ &= Q_i^0 + \sum_{j=1}^{2} V_j^0 (G_{ij}\ \sin\delta_{ij}^0 - B_{ij}\ \cos\delta_{ij}^0)\ \Delta V_i \\ &+ \sum_{j=1}^{2} V_i^0 (G_{ij}\ \sin\delta_{ij}^0 - B_{ij}\ \cos\delta_{ij}^0)\ \Delta V_j \\ &+ \sum_{j=1}^{2} V_i^0 V_j^0 (G_{ij}\ \cos\delta_{ij}^0 + B_{ij}\ \sin\delta_{ij}^0)\ \Delta\delta_{ij} \end{aligned} \tag{3.6}$$

where, $\Delta\delta_{ij} = \Delta\delta_i - \Delta\delta_j$ and $\Delta\delta_i = \delta_i - \delta_i^0$.

3.4.2 System Dynamics with Improved Forward Droop Control (FDC)

The equations of improved FDC are [70] ($i = 1, 2$):

$$\Delta\dot{\delta}_i = -k_{\mathrm{f}_i}(P_{\mathrm{m}_i} - P_i^0) \tag{3.7}$$

$$\begin{aligned} \Delta V_i &= k_{\mathrm{p}_i}((V_i^0 - D_{\mathrm{v}_i}(Q_{\mathrm{m}_i} - Q_i^0)) - V^{'}) \\ &\quad + k_{\mathrm{i}_i} \int ((V_i^0 - D_{\mathrm{v}_i}(Q_{\mathrm{m}_i} - Q_i^0)) - V^{'})\, dt \end{aligned} \tag{3.8}$$

$$\frac{P_{\mathrm{m}_i}(s)}{P_i(s)} = \frac{w_{\mathrm{f}}}{s + w_{\mathrm{f}}};\ \frac{Q_{\mathrm{m}_i}(s)}{Q_i(s)} = \frac{w_{\mathrm{f}}}{s + w_{\mathrm{f}}} \tag{3.9}$$

where, V_i^0 is the initial value of the voltages, $V^{'}$ is the common load voltage and m symbolizes measured values.

Let define $\Delta P_{\mathrm{m}_i} = P_{\mathrm{m}_i} - P_i^0$, and $\Delta Q_{\mathrm{m}_i} = Q_{m_i} - Q_i^0$. The system described by the Eqns. (3.7) and (3.9) can now be linearly represented as ($i = 1, 2$):

$$\Delta\dot{\delta}_i = -k_{\mathrm{f}_i}\Delta P_{\mathrm{m}_i} \tag{3.10}$$

$$\Delta\dot{P}_{m_i} = -w_{\mathrm{f}}(\Delta P_{\mathrm{m}_i} - \Delta P_i) = -w_{\mathrm{f}}\Delta P_{\mathrm{m}_i} + w_{\mathrm{f}}\Delta P_i \tag{3.11}$$

$$\Delta\dot{Q}_{\mathrm{m}_i} = -w_{\mathrm{f}}(\Delta Q_{\mathrm{m}_i} - \Delta Q_i) = -w_{\mathrm{f}}\Delta Q_{\mathrm{m}_i} + w_{\mathrm{f}}\Delta Q_i \tag{3.12}$$

where, $i, j = 1, 2$.

$$\Delta P_i = \Delta P^0_{i\delta_j}\Delta\delta_j + \Delta P^0_{iV_j}\Delta V_j \tag{3.13}$$

$$\Delta Q_i = \Delta Q^0_{i\delta_j}\Delta\delta_j + \Delta Q^0_{iV_j}\Delta V_j \tag{3.14}$$

The constants $\Delta P^0_{i\delta_j}$, $\Delta P^0_{iV_j}$, $\Delta Q^0_{i\delta_j}$, and $\Delta Q^0_{iV_j}$ can be obtained from Eqns. (3.5) and (3.6) by letting $\Delta P^0_{i\delta_j} = \frac{\partial P_i}{\partial \delta_j}\mid_{(.)=(.)^0}$, $\Delta P^0_{iV_j} = \frac{\partial P_i}{\partial V_j}\mid_{(.)=(.)^0}$, $\Delta Q^0_{i\delta_j} = \frac{\partial Q_i}{\partial \delta_j}\mid_{(.)=(.)^0}$, and $\Delta Q^0_{iV_j} = \frac{\partial Q_i}{\partial V_j}\mid_{(.)=(.)^0}$.

where, $(.) = (.)^0$ indicates that the equilibrium values of the variables are used to evaluate the function.

Table 3.1. System description of L-type microgrids with improved FDC

Parameter	Value (pu)
Z_1, Z_2	$0.25j$, $0.05j$
V_1^0, V_2^0	1, 1
k_{f_1}, k_{f_2}	1, 5
k_{p_1}, k_{p_2}	0.1, 0.5
D_{v_1}, D_{v_2}	0.1, 0.5
k_{i_1}, k_{i_2}	1, 1
w_{f}	12 (rad/s)

The system description with improved FDC is provided in Table 3.1. The values of k_{f_1}, k_{p_1}, D_{v_1}, k_{i_1}, k_{f_2}, k_{p_2}, D_{v_2}, and k_{i_2} are chosen via repetitive approximation so that the eigenvalues are of negative real parts (with positive or negative complex conjugates). The obtained eigenvalues of the linearized system at the equilibrium point after the change in the load impedance (from 1 pu 0.5 pu) are: -12, -12, -12,

0, -6+j13.763 and -6-j13.763. These values are plotted in Fig. 3.2. Since none of them contains any positive real parts, the system can be regarded as stable.

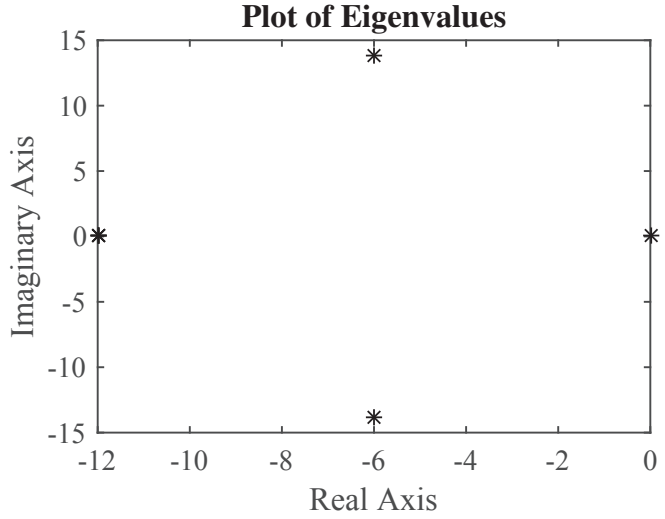

Figure 3.2. Eigenvalues of the closed-loop system with improved FDC.

3.4.3 System Dynamics with Developed Reverse Droop Control (RDC)

The proposed equations of improved RDC can be written as ($i = 1, 2$):

$$\Delta\dot{\delta}_i = k_{\mathrm{f}_i}(Q_{\mathrm{m}_i} - Q_i^0) \tag{3.15}$$

$$\Delta V_i = k_{\mathrm{p}_i}((V_i^0 - D_{\mathrm{v}_i}(P_{\mathrm{m}_i} - P_i^0)) - V^{'}) + k_{\mathrm{i}_i}\int((V_i^0 - D_{\mathrm{v}_i}(P_{\mathrm{m}_i} - P_i^0)) - V^{'})\,dt \tag{3.16}$$

$$\frac{P_{\mathrm{m}_i}(s)}{P_i(s)} = \frac{w_{\mathrm{f}}}{s + w_{\mathrm{f}}};\ \frac{Q_{\mathrm{m}_i}(s)}{Q_i(s)} = \frac{w_{\mathrm{f}}}{s + w_{\mathrm{f}}} \tag{3.17}$$

The linear representation of the microgrid, demonstrated by the Eqns. (3.15) and (3.17), can be expressed as [44] ($i = 1, 2$):

$$\Delta\dot{\delta}_i = k_{\mathrm{f}_i}\Delta Q_{\mathrm{m}_i} \tag{3.18}$$

$$\Delta\dot{P}_{m_i} = -w_{\mathrm{f}}(\Delta P_{\mathrm{m}_i} - \Delta P_i) = -w_{\mathrm{f}}\Delta P_{\mathrm{m}_i} + w_{\mathrm{f}}\Delta P_i \tag{3.19}$$

$$\Delta\dot{Q}_{\mathrm{m}_i} = -w_{\mathrm{f}}(\Delta Q_{\mathrm{m}_i} - \Delta Q_i) = -w_{\mathrm{f}}\Delta Q_{\mathrm{m}_i} + w_{\mathrm{f}}\Delta Q_i \tag{3.20}$$

Table 3.2. System description of R-type microgrids with improved RDC

Parameter	Value (pu)
Z_1, Z_2	0.25, 0.05
V_1^0, V_2^0	1, 1
k_{f_1}, k_{f_2}	1, 5
k_{p_1}, k_{p_2}	0.1, 0.5
D_{v_1}, D_{v_2}	0.1, 0.5
k_{i_1}, k_{i_2}	1, 1
w_{f}	12 (rad/s)

R-type microgrid system with RDC is described in Table 3.2. The eigenvalues of the linearized system at the equilibrium point, after the load impedance changes from 1 pu to 0.5j, are given in Fig. 3.3. As is noticed that there is no positive real parts, meaning the system is stable.

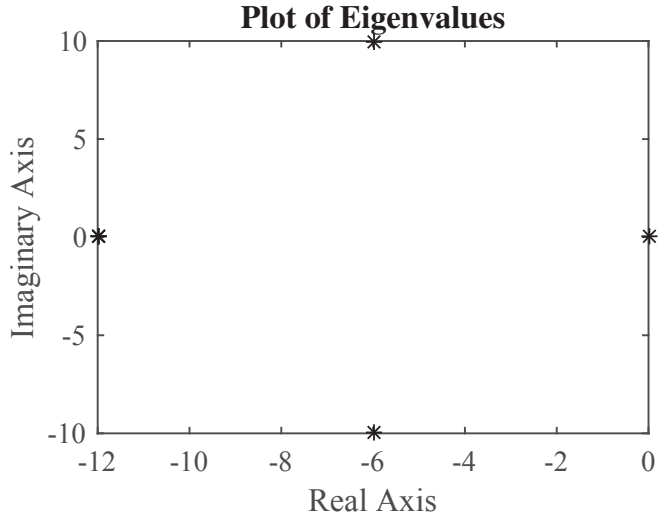

Figure 3.3. Eigenvalues of the closed-loop system with improved RDC.

3.4.4 System Dynamics with Developed Generalized Droop Control (GDC)

The proposed GDC equations are as follows ($i = 1, 2$):

$$\Delta\dot{\delta}_i = -k_{\mathrm{f}_i}\frac{X_i}{|Z_i|}(P_{\mathrm{m}_i} - P_i^0) + k_{\mathrm{f}_i}\frac{R_i}{|Z_i|}(Q_{\mathrm{m}_i} - Q_i^0) \tag{3.21}$$

$$\Delta V_i = k_{\mathrm{p}_i}(V_i^0 - D_{\mathrm{v}_i}(P_{\mathrm{m}_i} - P_i^0) - V^{'}) + k_{\mathrm{i}_i}\int (V_i^0 - D_{\mathrm{v}_i}(P_{\mathrm{m}_i} - P_i^0) - V^{'})\,dt$$
$$+ k_{\mathrm{p}_i}(V_i^0 - D_{\mathrm{v}_i}(Q_{\mathrm{m}_i} - Q_i^0) - V^{'}) + k_{\mathrm{i}_i}\int (V_i^0 - D_{\mathrm{v}_i}(Q_{\mathrm{m}_i} - Q_i^0) - V^{'})\,dt \tag{3.22}$$

$$\frac{P^{'}_{\mathrm{m}_i}(s)}{P^{'}_i(s)} = \frac{w_{\mathrm{f}}}{s + w_{\mathrm{f}}};\ \frac{Q^{'}_{\mathrm{m}_i}(s)}{Q^{'}_i(s)} = \frac{w_{\mathrm{f}}}{s + w_{\mathrm{f}}} \tag{3.23}$$

where, $P^{'}_{\mathrm{m}_i} = \frac{X_i}{|Z_i|}P_{\mathrm{m}_i} - \frac{R_i}{|Z_i|}Q_{\mathrm{m}_i}$,
$Q^{'}_{\mathrm{m}_i} = \frac{R_i}{|Z_i|}P_{\mathrm{m}_i} + \frac{X_i}{|Z_i|}Q_{\mathrm{m}_i}$,
$P^{'}_i = \frac{X_i}{|Z_i|}P_i - \frac{R_i}{|Z_i|}Q_i$,
$Q^{'}_i = \frac{R_i}{|Z_i|}P_i + \frac{X_i}{|Z_i|}Q_i$.

The dynamics of the improved generalized droop-controlled RL-type microgrid (parameters are provided in Table 3.3), depicted by the Eqns. (3.21) and (3.23), can linearly be expressed as [50] ($i = 1, 2$):

$$\Delta\dot{\delta}_i = -\frac{k_{f_i}}{|Z_i|}(X_i\Delta P_{\mathrm{m}_i} - R_i\Delta Q_{\mathrm{m}_i}) \tag{3.24}$$

$$X_i\Delta\dot{P}_{\mathrm{m}_i} - R_{i3}\Delta\dot{Q}_{\mathrm{m}_i} = -w_{\mathrm{f}}(X_i\Delta P_{\mathrm{m}_i} - R_i\Delta Q_{\mathrm{m}_i}) + w_{\mathrm{f}}X_i\Delta P_i - w_{\mathrm{f}}R_i\Delta Q_i \tag{3.25}$$

$$R_i\Delta\dot{P}_{\mathrm{m}_i} + X_i\Delta\dot{Q}_{\mathrm{m}_i} = -w_{\mathrm{f}}(R_i\Delta P_{\mathrm{m}_i} + X_i\Delta Q_{\mathrm{m}_i}) + w_{\mathrm{f}}R_i\Delta P_i + w_{\mathrm{f}}X_i\Delta Q_i \tag{3.26}$$

Table 3.3. System description of RL-type microgrids with improved GDC

Parameter	Value (pu)
Z_1, Z_2	$0.25 + 0.25j$, $0.05 + 0.05j$
V_1^0, V_2^0	1, 1
k_{f_1}, k_{f_2}	1, 5
k_{p_1}, k_{p_2}	0.1, 0.5
D_{v_1}, D_{v_2}	0.1, 0.5
k_{i_1}, k_{i_2}	1, 1
w_{f}	12 (rad/s)

The eigenvalues of the linearized system after the reduction (say 50 percent) in the load impedance are simulated in Fig. 3.4. From this figure, it can be seen that all the values have negative real parts but no positive real parts (both positive and

negative imaginary parts are there on account of the integral terms). Therefore, system stability criteria is fulfilled.

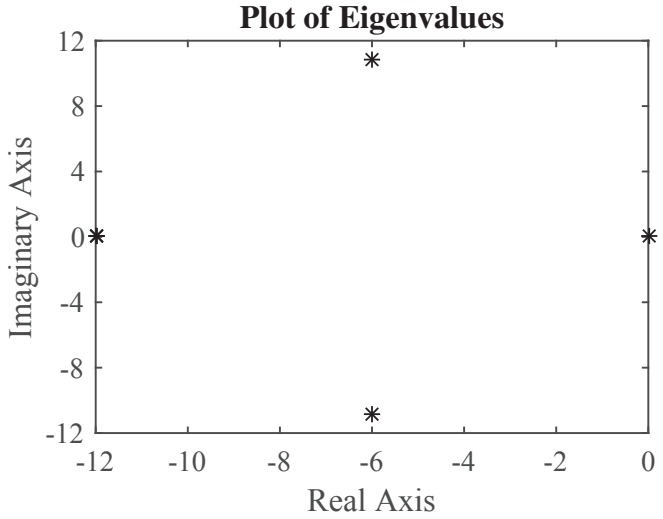

Figure 3.4. Eigenvalues of the closed-loop system with improved GDC.

Small-signal modeling assumes that the angular frequency, w, is constant not the dynamic [67]. This is an inherent limitation of this method. Although satisfactory outcomes are found in the aforementioned analysis of two-source microgrids, sometimes questionable results are obtained while predicting the system stability limit in low inertia-based large microgrids [67]. That is why; in the following section, dynamic phasors-based model is discussed.

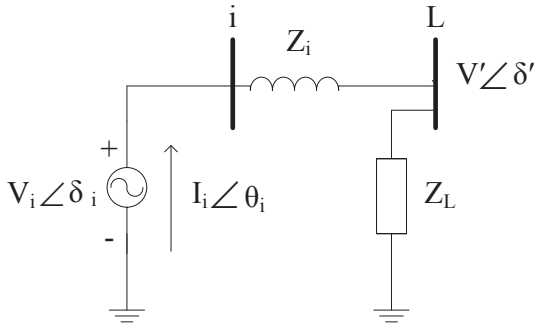

Figure 3.5. Basic single-line diagram of a simple microgrid.

3.5 Dynamic Phasors Modeling (DPM)

The use of dynamic phasors modeling (DPM) in inverter-dominated islanded microgrids has received attention recently as it includes the dynamics of the power circuit elements in the analysis and provides higher precision in predicting the stability limit of the system [67], [68].

Dynamic phasors vary with respect to time. That is why, they are also known as time-varying phasors [64], [65], [68]. In time domain, a single phase time-varying ac signal can be represented as:

$$e(t) = E(t)\ \sin(wt + \delta(t)) \tag{3.27}$$

where, $E(t)$ is the amplitude, w indicates the angular frequency, $\delta(t)$ is the phase anger.

The dynamic phasors $P(e(t))$ of $e(t)$ can be written as [65]:

$$P(e(t)) = \bar{E}(t) = E(t)e^{j\delta} \tag{3.28}$$

where, P represents the transfer from time domain to dynamic phasors and $\bar{E}(t)$ is the dynamic phasors of $e(t)$.

The derivative of $\bar{E}(t)$ can be expressed as:

$$P(\frac{d}{dt}e(t)) = \frac{d}{dt}\bar{E}(t) + jw\bar{E}(t) \tag{3.29}$$

The last term of Eqn. (3.29) is usually ignored in the traditional small-signal modeling. However, as the dynamic adjustment of amplitude and phase angle is required in droop-based parallel systems, it should be included for precise analysis [65].

Let analyze the circuit, described in Fig. 3.5, with DPM approach. Let the line impedance of the circuit is $Z_i = R_i + jwL_i$ (R_i is the line resistance and L_i is the line inductance), where i is the number of inverter-connected DG units and.

The dynamic phasors of the inverter output voltage (based on Fig. 3.5) can be written as [65]:

$$\bar{V}_i(t) - \bar{V}^{'}(t) = (R_i + jwL_i)\bar{I}_i(t) + L_i\frac{d}{dt}\bar{I}_i(t) \tag{3.30}$$

where, $\bar{I}_i(t)$ is the dynamic phasors of the inverter output current.

Solving first order differential Eqn. (3.30), the expression of $\bar{I}_i(t)$ can be written as:

$$\bar{I}_i(t) = \frac{\bar{V}_i(t) - \bar{V}^{'}(t)}{R_i + jwL_i}(1 - e^{-(\frac{R_i+jwL_i}{L_i})t}) \tag{3.31}$$

Now, Eqn. (3.30) can be reorganized using Laplace Transform as:

$$\bar{I}_i = \frac{\bar{V}_i - \bar{V}^{'}}{L_i s + R_i + jwL_i} \tag{3.32}$$

The output power of the single-phase inverter can be written as follows [65]:

$$\bar{S}_i = P_i + jQ_i = \bar{V}_i\bar{I}_i = \frac{\bar{V}_i^2 - \bar{V}_i\bar{V}^{'}}{L_i s + R_i + jwL_i} \tag{3.33}$$

where, $\bar{V}_i = V_i\angle\delta_i$, $\bar{V}^{'} = V^{'}\angle\delta^{'}$.

Let assume, $\delta_i = 0$ and $\delta^{'} = -\Delta\delta_i$. Therefore, $V_i\angle\delta_i = V_i$ and $V^{'}\angle\delta^{'} = V^{'}e^{j\Delta\delta_i}$. From Eqn.(3.33), using Euler's formula, the output real power and reactive power of the single-phase inverter can be expressed as:

$$P_i = \frac{L_i s + R_i}{(L_i s + R_i)^2 + wL_i^2}(V_i^2 - V_iV^{'}\ \cos\Delta\delta_i) + \frac{wL_i}{(L_i s + R_i)^2 + wL_i^2}V_iV^{'}\ \sin\Delta\delta_i \tag{3.34}$$

$$Q_i = \frac{wL_i}{(L_i s + R_i)^2 + wL_i^2}(V_i^2 - V_iV^{'}\ \cos\Delta\delta_i) - \frac{L_i s + R_i}{(L_i s + R_i)^2 + wL_i^2}V_iV^{'}\ \sin\Delta\delta_i \tag{3.35}$$

where, $\Delta\delta_i$ is the change in phase angles. If it is small, then $\sin\Delta\delta_i \approx \Delta\delta_i$ and $\cos\Delta\delta_i \approx 1$. Now, Eqns. (3.34) and (3.35) can be rewritten as:

$$P_i = \frac{L_i s + R_i}{(L_i s + R_i)^2 + wL_i^2}(V_i^2 - V_i V^{'}) + \frac{wL_i}{(L_i s + R_i)^2 + wL_i^2} V_i V^{'} \Delta\delta_i \tag{3.36}$$

$$Q_i = \frac{wL_i}{(L_i s + R_i)^2 + wL_i^2}(V_i^2 - V_i V^{'}) - \frac{L_i s + R_i}{(L_i s + R_i)^2 + wL_i^2} V_i V^{'} \Delta\delta_i \tag{3.37}$$

If there is a small disturbance around the equilibrium points (δ_i, V_i), the linearized equations of real and reactive powers can be written as:

$$\Delta P_i = \frac{\partial P_i}{\partial \delta_i}\Delta\delta_i + \frac{\partial P_i}{\partial V_i}\Delta V_i \tag{3.38}$$

$$\Delta Q_i = \frac{\partial Q_i}{\partial \delta_i}\Delta\delta_i + \frac{\partial Q_i}{\partial V_i}\Delta V_i \tag{3.39}$$

where,

$$\frac{\partial P_i}{\partial \delta_i} = \frac{-L_i s + R_i}{(L_i s + R_i)^2 + wL_i^2} V_i V^{'} \Delta\delta_i + \frac{wL_i}{(L_i s + R_i)^2 + wL_i^2} V_i V^{'} \tag{3.40}$$

$$\frac{\partial P_i}{\partial V_i} = \frac{wL_i}{(L_i s + R_i)^2 + wL_i^2} V^{'} \Delta\delta_i + \frac{L_i s + R_i}{(L_i s + R_i)^2 + wL_i^2}(2V_i - V^{'}) \tag{3.41}$$

$$\frac{\partial Q_i}{\partial \delta_i} = \frac{wL_i}{(L_i s + R_i)^2 + wL_i^2} V_i V^{'} \Delta\delta_i + \frac{-L_i s + R_i}{(L_i s + R_i)^2 + wL_i^2} V_i V^{'} \tag{3.42}$$

$$\frac{\partial Q_i}{\partial V_i} = \frac{-L_i s + R_i}{(L_i s + R_i)^2 + wL_i^2} V^{'} \Delta\delta_i + \frac{wL_i}{(L_i s + R_i)^2 + wL_i^2}(2V_i - V^{'}) \tag{3.43}$$

Let $k_{\mathrm{p}\delta_i} = \frac{\partial P_i}{\partial \delta_i}$, $k_{\mathrm{pv}_i} = \frac{\partial P_i}{\partial V_i}$, $k_{\mathrm{q}\delta_i} = \frac{\partial Q_i}{\partial \delta_i}$, and $k_{\mathrm{qv}_i} = \frac{\partial Q_i}{\partial V_i}$.

In the following sub-sections, extended DPM method is provided to select the range of droop parameters for the proposed controllers.

3.5.1 DPM with Designed Forward droop Controller

This sub-section deals with the implementation of an improved FDC-based controller in DPM analysis. In FDC method, it is assumed that the line inductance is greater than the line resistance and the term R_i is neglected. Hence, Eqns. (3.40), (3.41), (3.42), and (3.43) can be rewritten as:

$$k_{\mathrm{p}\delta_i} = \frac{-L_i s}{(L_i s)^2 + wL_i^2} V_i V^{'} \Delta\delta_i + \frac{wL_i}{(L_i s)^2 + wL_i^2} V_i V^{'} \tag{3.44}$$

$$k_{\mathrm{pv}_i} = \frac{wL_i}{(L_i s)^2 + wL_i^2} V^{'} \Delta\delta_i + \frac{L_i s}{(L_i s)^2 + wL_i^2} (2V_i - V^{'}) \tag{3.45}$$

$$k_{\mathrm{q}\delta_i} = \frac{wL_i}{(L_i s)^2 + wL_i^2} V_i V^{'} \Delta\delta_i + \frac{-L_i s}{(L_i s)^2 + wL_i^2} V_i V^{'} \tag{3.46}$$

$$k_{\mathrm{qv}_i} = \frac{-L_i s}{(L_i s)^2 + wL_i^2} V^{'} \Delta\delta_i + \frac{wL_i}{(L_i s)^2 + wL_i^2} (2V_i - V^{'}) \tag{3.47}$$

Solving Eqns. (3.7), (3.8), (3.9), (3.38), and (3.39), the characteristic equation of the closed-loop system with improved forward droop controller via DPM analysis can be derived as:

$$a_0 s^3 + a_1 s^2 + a_2 s + a_3 = 0 \tag{3.48}$$

The closed-loop system stability can be determined from the coefficients of Eqn. (3.48). From Routh's stability criteria, the condition that all roots have negative real parts are:

$$a_0 a_3 < a_1 a_2; \qquad a_3 > 0 \tag{3.49}$$

If $a_3 > 0$; from the value of a_3, it can be derived as: $k_{f_i} > 0$.

If $a_0 a_3 < a_1 a_2$, the range of D_{v_i} can be written as:

$$D_{\mathrm{v}_i}^2 a^{'} + D_{\mathrm{v}_i} a^{''} + a^{'''} < 0 \tag{3.50}$$

The solution of Eqn. (3.50) is: $D_{\mathrm{v}_i} < \frac{-a^{''} \pm \sqrt{4a^{'} a^{'''}}}{2a^{'}}$.

The solutions coefficients (a_0, a_1, a_2, a_3, $a^{'}$, $a^{''}$, $a^{'''}$ etc) are provided in the appendix. Therefore, one droop gain (k_{f_i}) should always be positive and another droop gain (D_{v_i}) depends on other gains, initial voltages of DG units and common load voltage.

3.5.2 DPM with Designed Reverse Droop Controller

In this sub-section, DPM method with improved reverse droop controller is discussed. Extended DPM is used to evaluate the range of both frequency (rate-of-change of angle) droop gain and voltage droop gain. It is known that RDC works in a system; in which the line resistance is larger than the line inductance. Therefore, Eqns. (3.40), (3.41), (3.42), and (3.43) become:

$$k_{\mathrm{p}\delta_i} = \frac{1}{R_i} V_i V^{'} \Delta\delta_i \tag{3.51}$$

$$k_{\mathrm{pv}_i} = \frac{1}{R_i} (2V_i - V^{'}) \tag{3.52}$$

$$k_{\mathrm{q}\delta_i} = \frac{1}{R_i} V_i V^{'} \tag{3.53}$$

$$k_{\mathrm{qv}_i} = \frac{1}{R_i} V^{'} \Delta\delta_i \tag{3.54}$$

The characteristic equation (obtained by solving Eqns. (3.15), (3.16), (3.17), (3.38), and (3.39)) of the DPM-based system with improved reverse droop controller is:

$$b_0 s^3 + b_1 s^2 + b_2 s + b_3 = 0 \tag{3.55}$$

The coefficients of Eqn. (3.55) can be used to determine the stability range of R-type microgrids. Based on Routh's stability criteria, the condition that all roots have negative real parts are:

$$b_0 b_3 < b_1 b_2; \qquad b_3 > 0 \tag{3.56}$$

If $b_3 > 0$, it can be derived as: $k_{f_i} > 0$, and if $b_0 b_3 < b_1 b_2$, the range of D_{v_i} can be represented as:

$$D_{\mathrm{v}_i}^2 b^{'} + D_{\mathrm{v}_i} b^{''} + b^{'''} < 0 \tag{3.57}$$

The solution of Eqn. (3.57) is: $D_{\mathrm{v}_i} < \frac{-b^{''} \pm \sqrt{4b^{'}b^{'''}}}{2b^{'}}$.

The solutions coefficients (b_0, b_1, b_2, b_3, $b^{'}$, $b^{''}$, $b^{'''}$ etc) are provided in the appendix.

3.5.3 DPM with Developed Generalized Droop Controller

The inclusion of improved generalized droop controller in DPM analysis is presented in this sub-section. The characteristic equation of improved GDC-based system with DPM can be expressed by the Eqn. (3.58), which has been derived by solving Eqns. (3.21), (3.22), (3.23), (3.38), and (3.39).

$$c_0 s^3 + c_1 s^2 + c_2 s + c_3 = 0 \tag{3.58}$$

Using Routh's criteria, the conditions that all roots have negative real parts can be obtained by the coefficients of Eqn. (3.58). The conditions are as follows:

$$c_0 c_3 < c_1 c_2; \qquad c_3 > 0 \tag{3.59}$$

Let consider, $c_3 > 0$; from the above mentioned value of c_3, it can be derived as: $k_{f_i} > 0$.

If $c_0 c_3 < c_1 c_2$, the range of D_{v_i} can be written as:

$$D_{\mathrm{v}_i}^2 c^{'} + D_{\mathrm{v}_i} c^{''} + c^{'''} < 0 \tag{3.60}$$

The solution of Eqn. (3.60) is: $D_{\mathrm{v}_i} < \frac{-c^{''} \pm \sqrt{4c^{'} c^{'''}}}{2c^{'}}$.

The solutions coefficients (c_0, c_1, c_2, c_3, $c^{'}$, $c^{''}$, $c^{'''}$ etc) are provided in the appendix.

3.6 Chapter Summary

The gain selection procedures for the proposed controllers are presented in this chapter. In order to choose the control parameters of the designed controllers, microgrid systems (L-type, R-type, and RL-type) are linearized. Firstly, small-signal stability analysis is provided for the purpose of gain selection; in which eigenvalues are determined via successive approximation. However, this method has some inherent disadvantages such as static angular frequency, omitting the dynamics of power

circuit elements, and requirement of more computational analysis in large microgrids. Because of these limitations, this strategy might be inapplicable to predict the stability margin in systems where many parallel inverters are connected. For this reason, extended dynamic phasors modeling (DPM) is developed in this chapter. It has been found that proposed DPM is effective enough to evaluate the suitable stability range of droop gains in inverter-interfaced islanded microgrids.

The following chapter (**Chapter 4**) presents the implementation of DPM-based droop controller (control parameters are selected from the range obtained by the DPM analysis) in photovoltaic systems to verify its robustness.

Chapter 4

Controller Performance Evaluation on Photovoltaic Systems

4.1 Chapter Contributions

This chapter proposes a new type of droop-based controller for Photovoltaic (PV) systems that can share power proportionally during the load change and also can balance power if PV generation varies. Different case studies are considered and a comparison between the designed controller and the existing generalized droop controller is given; from which the effectiveness of the designed controller in PV systems can be verified.

4.2 Literature Review

PV system appears as a promising renewable energy to ensure sustainable electric power supply owing to their small relative size, noiseless and environment-friendly operation [80]. However, atmospheric conditions cause change in the intermittent PV generation [81]. PV system is also affected by the change in connected loads [55], [56]. Therefore, efficient control strategies are essential to attain proper output from PV systems. PV-based low and medium networks have been studied in [82] and droop control for PV systems, to divide the load change based on the capacity of PV units, are discussed in [83]. However, this controller cannot balance power during the change in the PV generation. This shortcoming is overcome in this chapter by implementing the proposed droop-based control scheme in PV systems.

4.3 Chapter Outline

The presentation of rest of the paper is as follows: Section 4.4 describes the modeling of single-phase PV systems. The proposed control algorithm is provided in Section 4.5. The performance of the designed controller, under diverse operating conditions, is evaluated in Section 4.6 and Section 4.7 contains the chapter summary.

4.4 Inverter-connected PV System Model

The mathematical modeling of PV systems is discussed in this section to analyze the control interaction and to design the proposed controller. The block diagram of a PV system is represented in Fig. 4.1. From this figure, it can be noticed that a PV system mainly consists of two parts [84]: 1) solar conversion and 2) power electronic conversion. A PV array is connected to the load by means of a dc-dc boost converter and a dc-ac converter (inverter). The maximum output power transfer, from PV array to the inverter, is ensured by a dc-dc boost converter and an inverter converts that power into ac in order to feed the ac load.

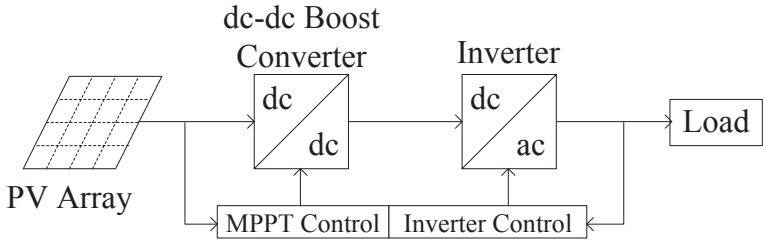

Figure 4.1. Schematic block diagram of a PV system.

This section is organized as follows: Sub-section 4.4.1 contains the mathematical model of the single-phase PV arrays and the inverter model is presented in Sub-section 4.4.2.

4.4.1 PV Cell and Array Modeling

A PV cell is considered as a simple p-n junction, which converts the solar irradiation into the electric energy [81]. Fig. 4.2 illustrates an equivalent circuit diagram of a PV cell which comprises of a current source (I_{L}), a parallel diode, and series and shunt resistances (R_{S}, R_{Sh}) [85].

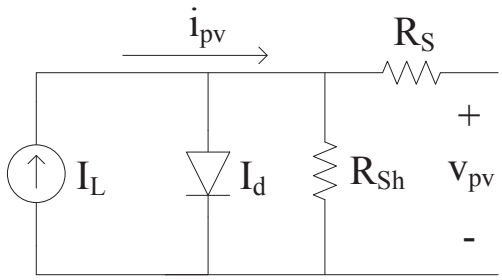

Figure 4.2. Equivalent circuit diagram of a PV cell.

The diode current can be expressed as [81, 86]:

$$I_{\mathrm{d}} = I_{\mathrm{S}}[\exp[\alpha(v_{\mathrm{pv}} + R_{\mathrm{S}} i_{\mathrm{pv}})] - 1] \tag{4.1}$$

where, α is a constant that is equal to q/AkT_{c}, A is the p-n junction ideality factor whose value varies from 1 to 5, $k = 1.3807 \times 110^{-23} JK^{-1}$ represents Boltzmann's constant, $q = 1.6022 \times 10^{-19} C$ indicates the charge of electron, T_{c} is the working temperature of PV cell in kelvin, I_S symbolizes the saturation current, and v_{pv} is the output voltage of PV cell. Using Kirchhoff's current law (KCL) in Fig. 4.2, the output current of a PV cell can be represented as [86]:

$$i_{\mathrm{pv}} = I_{\mathrm{L}} - I_{\mathrm{S}}[\exp[\alpha(v_{\mathrm{pv}} + R_{\mathrm{S}} i_{\mathrm{pv}})] - 1] - \frac{v_{\mathrm{pv}} + R_{\mathrm{S}} i_{\mathrm{pv}}}{R_{\mathrm{Sh}}} \tag{4.2}$$

The light generated current, I_{L}, is dependent on the solar irradiation and their relation can be written by the following Eqn. (4.3) [81].

$$I_{\mathrm{L}} = \frac{S}{1000}[I_{\mathrm{Sc}} + k_{\mathrm{i}}(T_{\mathrm{c}} - T_{\mathrm{ref}})] \tag{4.3}$$

where, S is the solar irradiation, I_{Sc} indicates the short-circuit current, k_{i} denotes the short-circuit current coefficient of PV cell, and T_{ref} is the reference temperature of PV cell.

Since low output voltage is obtained from a PV cell, several cells are connected in series to form a PV module and a number of modules are connected in parallel to construct a PV array [81]. The output current of a PV array is [87, 88]:

$$i_{\mathrm{pv}} = N_{\mathrm{p}} I_{\mathrm{L}} - N_{\mathrm{p}} I_{\mathrm{L}}[\exp[\alpha(\frac{v_{\mathrm{pv}}}{N_{\mathrm{S}}} + \frac{R_{\mathrm{S}} i_{\mathrm{pv}}}{N_{\mathrm{p}}})] - 1] - \frac{N_{\mathrm{p}}}{R_{\mathrm{Sh}}}(\frac{v_{\mathrm{pv}}}{N_{\mathrm{S}}} + \frac{R_{\mathrm{S}} i_{\mathrm{pv}}}{N_{\mathrm{p}}}) \tag{4.4}$$

where, N_{S} and N_{p} are the number of PV cells in series and the number of PV modules in parallel respectively.

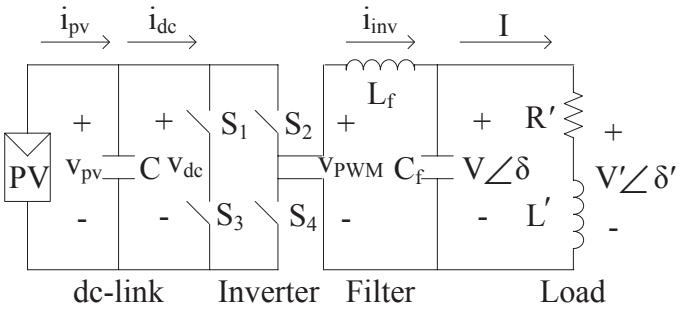

Figure 4.3. A single-phase inverter-connected PV system.

4.4.2 Single-phase Inverter Modeling

The schematic circuit diagram of a single-phase inverter-interfaced PV system is demonstrated in Fig. 4.3. Here, C is the dc-link capacitor and the dc-link voltage across C is denoted by v_{dc}. The value of v_{dc} is adjusted at a level through maximum power point tracking (MPPT) in order to make it suitable for the inverter. According to this figure, v_{dc} is the output voltage of the PV array (v_{pv}). Now, KCL is applied

at the node where the dc-link is connected and Eqn. (4.5) can be written [84].

$$\dot{v}_{\mathrm{dc}} = \frac{1}{C}(i_{\mathrm{pv}} - i_{\mathrm{dc}}) \tag{4.5}$$

Inverter switches are denoted by S_1, S_2, S_3, and S_4 respectively. L_{f} and C_{f} are the inductance and capacitance of the filter. RL load parameters are shown in Fig. 4.3 by $R^{'}$ and $L^{'}$. The complete mathematical model of single-phase inverter can be written as follows by applying KVL and KCL into Fig. 4.3 [86].

$$\dot{i}_{\mathrm{inv}} = \frac{1}{L_{\mathrm{f}}}(mv_{\mathrm{dc}} - V) \tag{4.6}$$

$$\dot{V} = \frac{1}{C_{\mathrm{f}}}(i_{\mathrm{inv}} - I) \tag{4.7}$$

$$\dot{I} = \frac{1}{L^{'}}(R^{'}I + V) \tag{4.8}$$

where, i_{inv} is the current flowing through the inverter, m is the modulation index, V is the magnitude of ac voltage across the filter, and I is the load current.

4.5 Developed Droop-based Algorithm for PV Systems

Let assume, there are multiple PV units and both the PV generation and the RL load in Fig. 4.3 are variable. Therefore, it is essential to distribute these changes among PV units accurately. Let consider, δ_i represents the phase angle of inverter-connected PV units (where, i represents the number of PV units), P_i^0 and Q_i^0 are reference real-reactive powers of inverter-dominated PV units, P_{m_i} and Q_{m_i} are measured powers (subscript m stands for measured values). Besides, R_i, X_i, and Z_i are resistance, inductance, and impedance of the distribution lines. V_i^0 is the initial voltage of PV units and $V^{'}$ is the voltage across the load. k_{fd_i} is the derivative droop gain and other droop gains are represented by k_{f_i} and D_{v_i}, while k_{p_i} is the proportional gain and k_{i_i} indicates the integral gain. Now, based on the whole droop-based analysis, given in **Chapter 2**, the proposed droop-based algorithm for

PV systems can be expressed as:

$$\Delta\dot{\delta}_i = -k_{\mathrm{f}_i}\frac{X_i}{|Z_i|}(P_{\mathrm{m}_i} + P^0_{\mathrm{ft}_i} - P^0_i) - k_{\mathrm{fd}_i}\frac{X_i}{|Z_i|}\frac{d}{dt}(P_{\mathrm{m}_i} + P^0_{\mathrm{ft}_i} - P^0_i) + k_{\mathrm{f}_i}\frac{R_i}{|Z_i|}(Q_{\mathrm{m}_i} - Q^0_i) + k_{\mathrm{fd}_i}\frac{R_i}{|Z_i|}\frac{d}{dt}(Q_{\mathrm{m}_i} - Q^0_i) \tag{4.9}$$

$$P^0_{\mathrm{ft}_i} = k_{\mathrm{dc}_i}\dot{v}_{\mathrm{dc}} = k_{\mathrm{dc}_i}\frac{1}{C}(i_{\mathrm{pv}} - i_{\mathrm{dc}}) \tag{4.10}$$

$$\Delta V_i = k_{\mathrm{p}_i}(V^0_i - D_{\mathrm{v}_i}(P_{\mathrm{m}_i} - P^0_i) - V') + k_{\mathrm{i}_i}\int (V^0_i - D_{\mathrm{v}_i}(P_{\mathrm{m}_i} - P^0_i) - V')\,dt + k_{\mathrm{p}_i}(V^0_i - D_{\mathrm{v}_i}(Q_{\mathrm{m}_i} - Q^0_i) - V') + k_{\mathrm{i}_i}\int (V^0_i - D_{\mathrm{v}_i}(Q_{\mathrm{m}_i} - Q^0_i) - V')\,dt \tag{4.11}$$

where, Δ stands for the change from initial value.

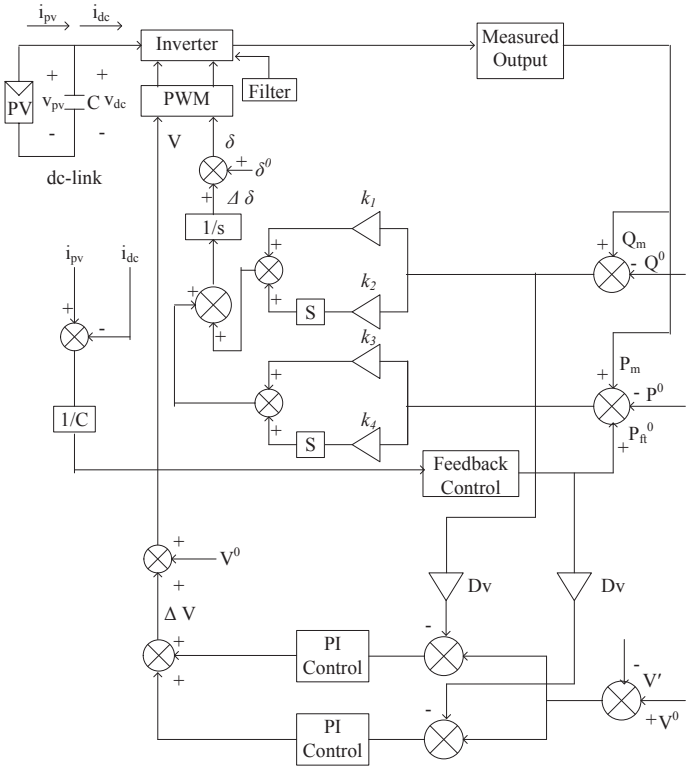

Figure 4.4. Schematic block diagram of designed control scheme for a PV system.

Fig. 4.4 depicts the overall control operation for a PV system. It is observed

that the controller acts as a droop and adjusts the inverter voltage (magnitude and phase angle) when the measured outputs change from their set points. This may happen due to the load change or the variation in the PV generation. In the diagram, the values of control gains are: $k_1 = -k_{\mathrm{f}_i}\frac{R_i}{|Z_i|}$, $k_2 = k_{\mathrm{fd}_i}\frac{R_i}{|Z_i|}$, $k_3 = k_{\mathrm{f}_i}\frac{X_i}{|Z_i|}$, and $k_4 = k_{\mathrm{fd}_i}\frac{X_i}{|Z_i|}$. The feedback control ensures the adjustment of the output power and the proportional-integral (PI) control maintains proportional power sharing.

4.6 Simulation and Results

A single-line diagram of WECC 9-bus test distribution system is demonstrated in Fig. 4.5. The original distribution system [89] is modified by making it islanded microgrid; in which four PV units are connected at buses- 1, 2, 3 and 4. The common load (shared by all PV units) is connected at bus- 9 and buses- 5, 6, 7, and 8 contain the local load of each PV units.

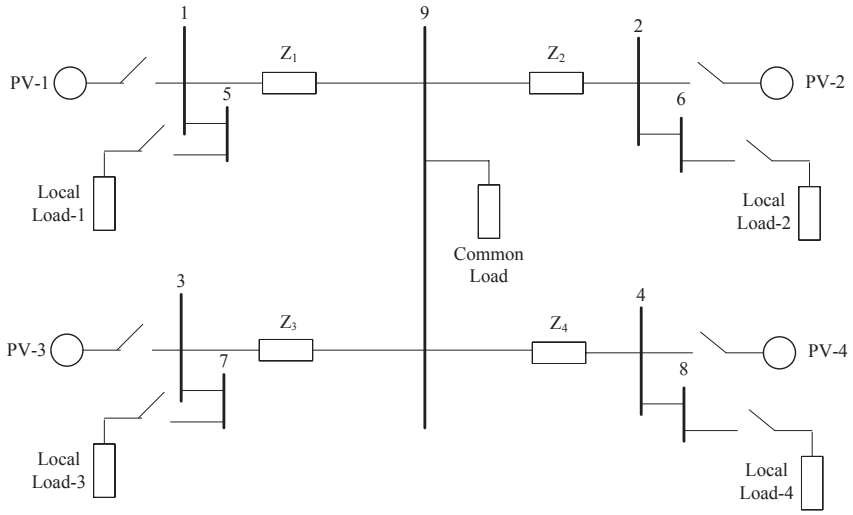

Figure 4.5. Single-line diagram of the test islanded microgrid.

Table 4.1 provides the parameters of a PV system [84]. Each PV units are rated at 1570 kW and 708 kVAr. There are 150 parallel strings in each PV array (array

is rated for 3480 V @ 431 A) and 80 modules in each string (module is rated for 43.5 V @ 2.8735 A). The nominal value of the dc-link voltage is 1582 V with 5000 μF capacitance. The PV units are connected to the distribution side by means of inverters whose nominal power is 1.5 MW. According to the available data of SMA's Medium-Voltage Power Platform Sunny Central Inverters', the output voltage of 1.5 MW inverter is 13.8 kV. Commercially available step down transformer is used to reduce the voltage value to 230 V as the line voltage has been considered as 230 V. The initial values of all reduced output voltages are kept the same (say 1 pu). Each distribution line is indicated by a series lumped Z (RL)-branch (distribution line parameters are given in Table 4.2). The total load of the system is 6 MW, 0.4 MVAr. The rating of the common load is 4 MW, 0.28 MVAr, whereas each local load is rated at 500 kW and 0.03 MVAr.

Table 4.1. PV System Parameters

Parameter	Value
Number of parallel strings in each array	150
Array open circuit voltage	3480 V
Array short circuit current	431 A
Number of modules in each string	80
Module open circuit voltage	43.5 V
Module short circuit current	2.8735 A
Diode ideality factor	1.3
dc-link capacitance	5000 μF
VSC switching frequency	3000 Hz
Inverter nominal power	1.5 MW
Inverter nominal output voltage	13.8 kV (ac)
Filter inductance, capacitance	500 μH, 100 μF

Table 4.2. Line Data

Parameter	Value (pu)
R_1, R_2, R_3, R_4	0.25, 0.2, 0.15, 0.1
X_1, X_2, X_3, X_4	0.25, 0.2, 0.15, 0.1
Z_1, Z_2, Z_3, Z_4	$0.25 + 0.25j$, $0.2 + 0.2j$, $0.15 + 0.15j$, $0.1 + 0.1j$

The values of the control parameters, described in Table 4.3, are selected arbitrarily from the stability range determined by the dynamic phasors analysis.

Table 4.3. Control Parameters

Parameter	Value (pu)
k_{f_1}, k_{f_2}, k_{f_3}, k_{f_4}	1.2, 2.8, 4.4, 6
k_{fd_1}, k_{fd_2}, k_{fd_3}, k_{fd_4}	0.7, 1.8, 2.9, 4
D_{v_1}, D_{v_2}, D_{v_3}, D_{v_4}	0.12, 0.28, 0.44, 0.6
k_{p_1}, k_{p_2}, k_{p_3}, k_{p_4}	0.12, 0.28, 0.44, 0.6
k_{i_1}, k_{i_2}, k_{i_3}, k_{i_4}	1, 5, 1, 5
k_{dc_1}, k_{dc_2}, k_{dc_3}, k_{dc_4}	1, 1, 1, 1
w_f	12 (rad/s)

The performance of the designed controller is tested in this section using industry standard software environment MATLAB. In order to evaluate the effectiveness of the proposed controller, the following different operating conditions have been considered: 1) load change in RL-type distribution line-based system; 2) load change in L-type distribution line-based system; 3) load change in R-type distribution line-based system; and 4) PV generation change in RL-type distribution line-based system. In all these case studies, the designed controller is compared with the traditional generalized droop controller [50] and its robustness is highlighted. The solid lines represent the performance of the proposed controller in Figs. 4.6-4.15, whereas the generalized droop controller is denoted by the dotted lines.

Load Change in RL-type Microgrids

This case study takes both the inductance and resistance of the distribution lines into consideration, and the performance of the controller is tested for the sudden change in connected loads. Let assume, 30 percent change in the connected load is applied at 1 second. The designed controller is implemented to maintain the power balance and the system reaches into stable-state within 2 seconds. Fig. 4.6 shows the angle differences among VSC-interfaced PV units; from which it is seen that

they are of constant values. As a result, the rate-of-change of angles (frequencies) are the same throughout the system, indicating system stability.

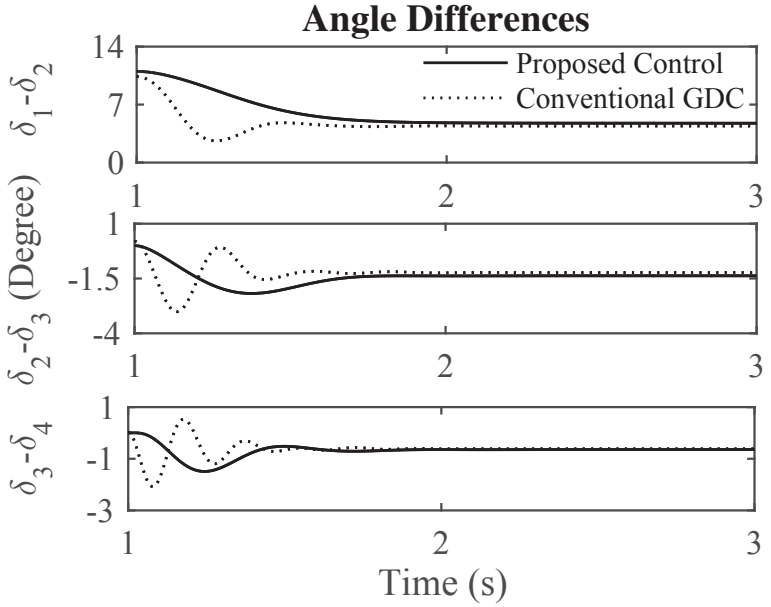

Figure 4.6. Angle differences of RL-type islanded microgrids during the change in the load (solid line-proposed controller, dotted line-droop controller)

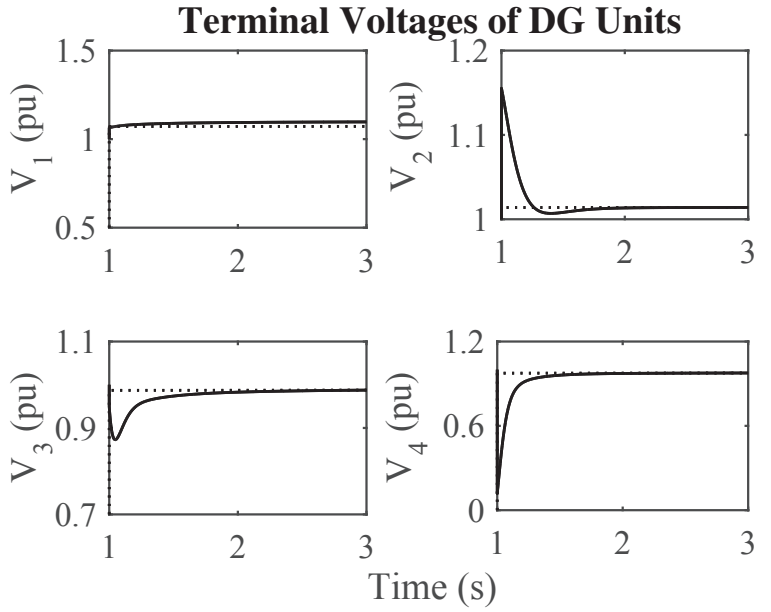

Figure 4.7. Voltages of RL-type islanded microgrids during the change in the load (solid line-proposed controller, dotted line-droop controller)

Fig. 4.7 provides the terminal voltages at buses 1-4, and it is observed that their responses are stable during the sudden change in connected loads.

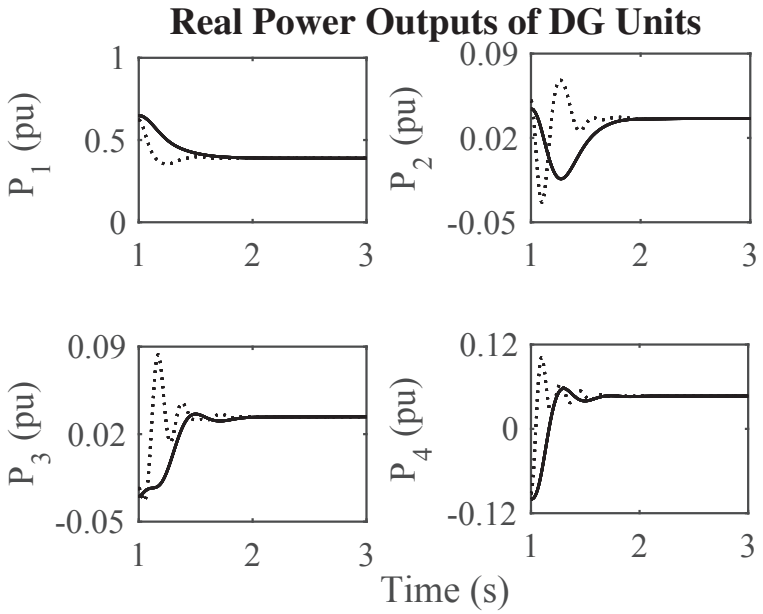

Figure 4.8. Real powers of RL-type islanded microgrids during the change in the load (solid line-proposed controller, dotted line-droop controller)

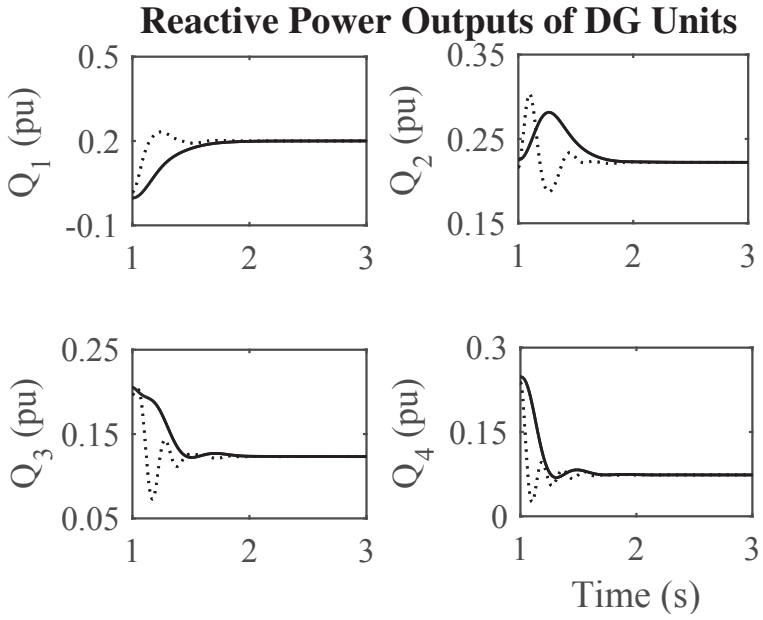

Figure 4.9. Reactive powers of RL-type islanded microgrids during the change in the load (solid line-proposed controller, dotted line-droop controller)

Figs. 4.8 and 4.9 deal with the output powers (real and reactive) of inverter-connected PV units and it is evident that their responses become stable after a bit start-up oscillations. In all these figures, the proposed control scheme (solid line) returns the system into steady-state with less number of oscillations in comparison with the classical GDC (dotted line). The power measurement sensor dynamics cause the system to fluctuate and integral term creates initial oscillations.

Load Change in L-type Microgrids

This case study applies the designed controller on the microgrid test system, operating in highly-inductive mode; in which the line resistances are ignored.

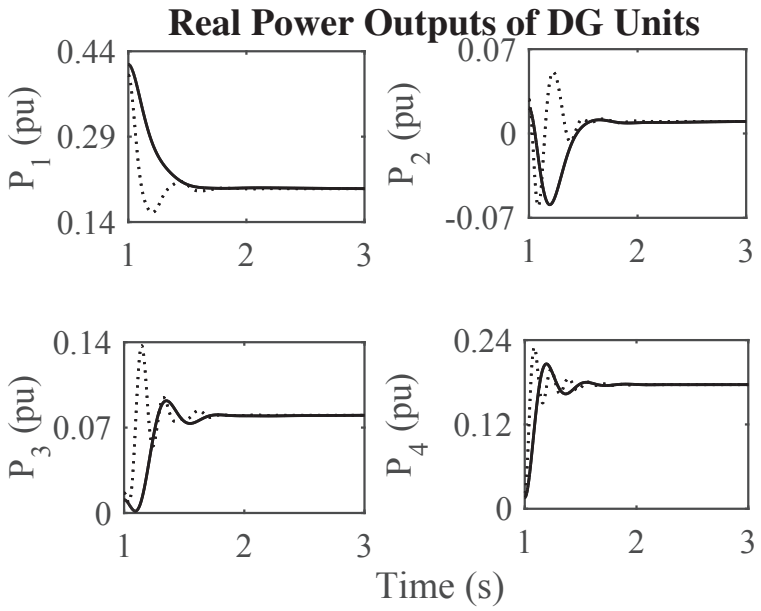

Figure 4.10. Real powers of L-type islanded microgrids during the change in the load (solid line-proposed controller, dotted line-droop controller)

In Fig. 4.10, the real powers of PV units are given while the reactive powers of PV units are illustrated in Fig. 4.11. As is seen from Fig. 4.11 that their responses are decreased initially and then settled to steady-state values within 0.5 second of controller operation. Comparing to GDC-based controller (dotted line),

the proposed controller shows excellent performance in terms of steady-state error, oscillation, overshoot, rise-time, and settling time.

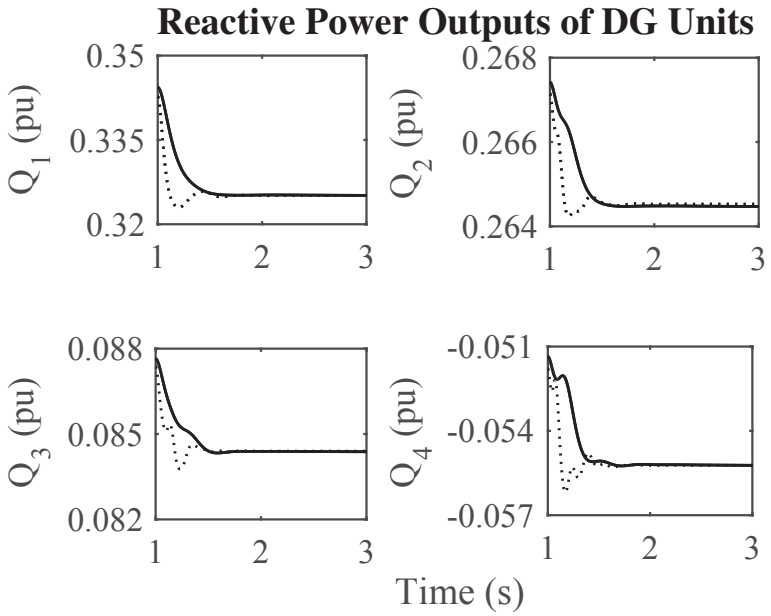

Figure 4.11. Reactive powers of L-type islanded microgrids during the change in the load (solid line-proposed controller, dotted line-droop controller)

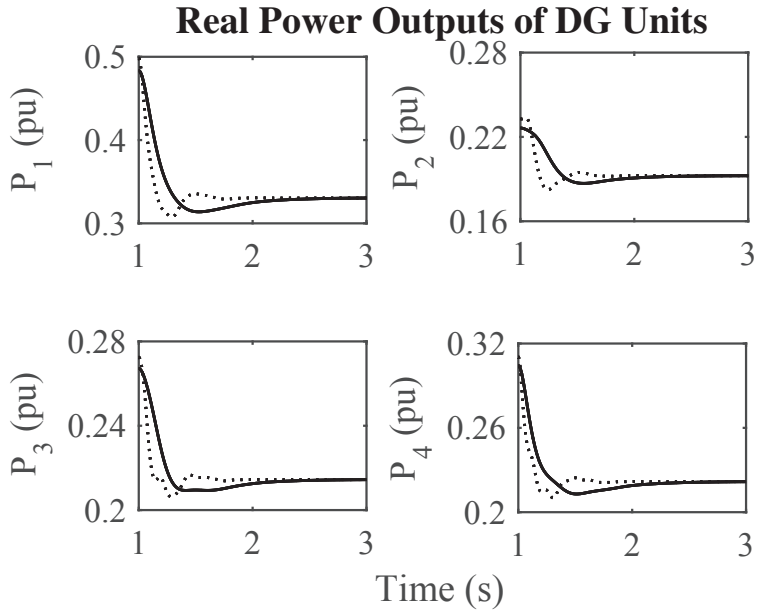

Figure 4.12. Real powers of R-type islanded microgrids during the change in the load (solid line-proposed controller, dotted line-droop controller)

Load Change in R-type Microgrids

In this case study, only resistive nature of the distribution lines within LV islanded test microgrid is considered. Figs. 4.12 and 4.13 depict the real and reactive power sharing with permanent change in connected loads (say 30 percent) in a R-type microgrid system; from which it is observed that the proposed controller (solid line) reacts more promptly than generalized droop controller with a view to ensuring proper damping and settling time within 2 seconds.

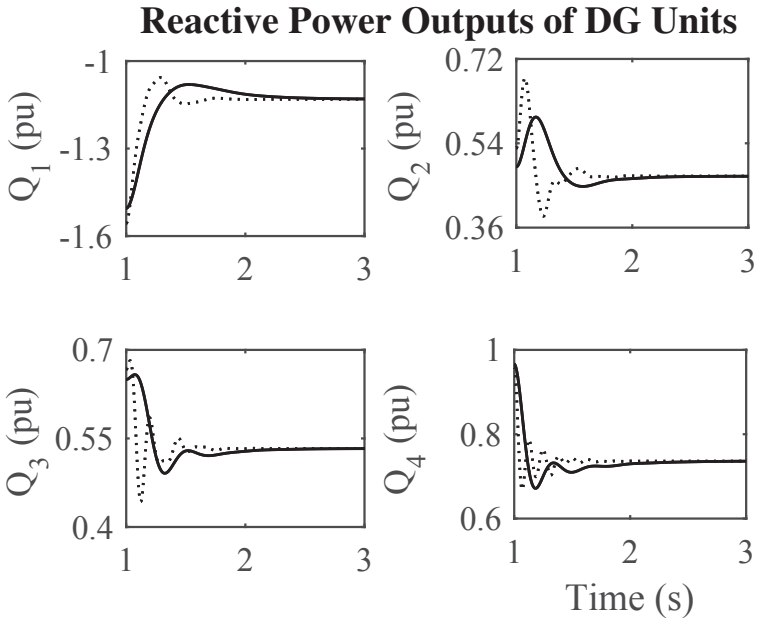

Figure 4.13. Reactive powers of R-type islanded microgrids during the change in the load (solid line-proposed controller, dotted line-droop controller)

Sudden Change in PV Generations

The objective of this case study is to show that the proposed control scheme can maintain frequency within statutory limits and share power among PV units during any variation in the sunlight. Let assume a situation; in which the solar irradiation changes from 1000 Wm^{-2} to 900 Wm^{-2} at 1 second. At this stage, the power delivered to the load is changed and there may be power deficiency. The designed

feedback controller senses it instantly and changes the output power of the microgrid according to the change in the PV generation for balancing the system naturally.

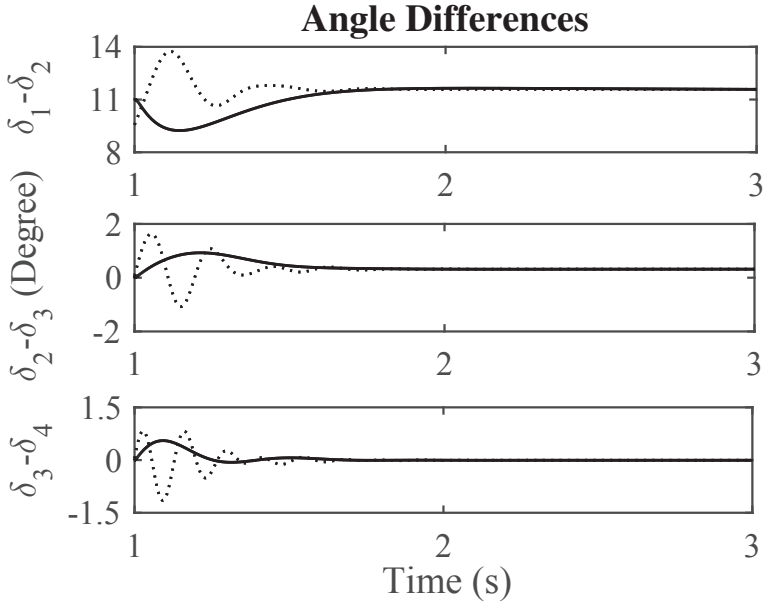

Figure 4.14. Angle differences of RL-type islanded microgrids during the change in the PV generation (solid line-proposed controller, dotted line-droop controller)

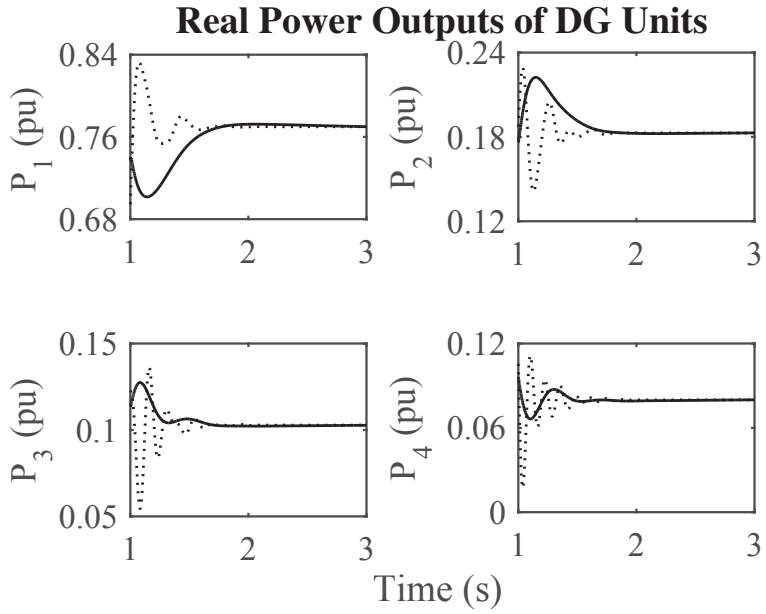

Figure 4.15. Real powers of RL-type islanded microgrids during the change in the PV generation (solid line-proposed controller, dotted line-droop controller)

The constant angle differences and real powers shared among PV units at buses 1-4, with the change in atmospheric conditions, are given in Fig. 4.14 and Fig. 4.15 respectively. In both of the figures, the system stability is ascertained after some start-up transients.

4.7 Chapter Summary

This chapter provides the modeling of a PV-based islanded microgrid in great details. An effective control algorithm is developed to protect the system against the change in connected loads, rapid variation in solar irradiation, and various microgrid structures (L-type, R-type and RL-type). The simulation results justify the viability of the designed controller. In simulated figures, the performance of the proposed controller is compared with that of the traditional GDC-based controller [50], and it is seen that the designed controller shows better performance in ensuring the system stability.

Chapter 5

Conclusions and Future Directions

5.1 Conclusions

Droop-based control algorithms are presented in this dissertation with a view to distributing the change in the load among inverter-interfaced DG units in accordance with droop gains. Diverse islanded microgrid structures are considered and algorithms are given for each microgrid structures (L-type, R-type and RL-type). Modified algorithms are developed in order to reduce the start-up fluctuations and to balance the output power of DG units if the renewable generation varies. For the purpose of sharing the load based on the power ratings of DG units, linearized model-based strategies are proposed initially. However, it is found that linearized model-based power sharing strategies of microgrids depend on the distribution line parameters and proportional power sharing may not be possible without proper optimization during the selection of parameters. Hence, improved droop-based controllers are designed to ensure proportional real-reactive power sharing in islanded microgrids.

The control parameters of the proposed controllers are selected firstly based on the small-signal stability analysis where the eigenvalues are determined by means of successive approximation. However, it is anticipated that on account of the negligence of the dynamics of power circuit elements, this method may fail to calculate the exact stability range in droop-controlled large microgrids. Therefore, this thesis uses an extended dynamic phasors-based analysis to evaluate the accurate stability

margins for the designed controllers.

Finally, the proposed control scheme is applied on a PV-based microgrid test system and it is observed from simulation results that the designed controller is robust against the dependance on communication-based networks, existence of distribution line parameters, component mismatches, disturbances in the load, unpredictability of sunlight, effect of start-up transients, and numerical errors.

The main contributions of the entire thesis can be summarized as:

- Droop-based control algorithms are developed for proportional power sharing during the load change phenomenon in different islanded microgrids.
- A modified droop-based controller is designed to balance the inverter output power in microgrids during both the load change and the renewable generation change phenomena.
- Accurate stability margins are determined for the designed controllers using extended dynamic phasors models.

5.2 Future Directions

The proposed work can further be extended as follows:

- The designed decentralized controllers can share power proportionally in common load-based microgrids. However, in reality it might be difficult to get information about the common load for large test systems. Therefore, cost-effective low-bandwidth communication networks can be utilized.
- Power sharing strategies of microgrids are developed in this dissertation by considering static load. In future, load dynamics can be included to improve the performance of the proposed controllers.
- Practical implementation of the improved droop-based control would be interesting to compare the simulated results with the real-time outputs.

Appendix

The solution coefficients of the extended dynamic phasors models are:

$a_0 = 1 + D_{\mathrm{v}_i} k_{\mathrm{p}_i} k_{\mathrm{qv}_i},$

$a_1 = w_{\mathrm{f}} + w_{\mathrm{f}} D_{\mathrm{v}_i} k_{\mathrm{p}_i} k_{\mathrm{qv}_i} + k_{\mathrm{i}_i} D_{\mathrm{v}_i} k_{\mathrm{qv}_i},$

$a_2 = w_{\mathrm{f}} k_{\mathrm{i}_i} D_{\mathrm{v}_i} k_{\mathrm{qv}_i} + k_{\mathrm{f}_i} w_{\mathrm{f}} k_{\mathrm{p}\delta_i} + k_{\mathrm{f}_i} w_{\mathrm{f}} k_{\mathrm{p}\delta_i} D_{\mathrm{v}_i} k_{\mathrm{p}_i} k_{\mathrm{qv}_i} + k_{\mathrm{f}_i} w_{\mathrm{f}} k_{\mathrm{pv}_i} k_{\mathrm{p}_i} V_i - k_{\mathrm{f}_i} w_{\mathrm{f}} k_{\mathrm{p}_i} k_{\mathrm{pv}_i} D_{\mathrm{v}_i} k_{\mathrm{p}\delta_i}$

$- k_{\mathrm{f}} w_{\mathrm{f}} k_{\mathrm{pv}_i} k_{\mathrm{p}_i} V^{'},$

$a_3 = k_{\mathrm{f}_i} w_{\mathrm{f}} k_{\mathrm{p}\delta_i} k_{\mathrm{i}_i} D_{\mathrm{v}_i} k_{\mathrm{qv}_i} + k_{\mathrm{f}_i} w_{\mathrm{f}} k_{\mathrm{pv}_i} k_{\mathrm{i}_i} V_i - k_{\mathrm{f}_i} w_{\mathrm{f}} k_{\mathrm{pv}_i} D_{\mathrm{v}_i} k_{\mathrm{i}_i} k_{\mathrm{q}\delta_i} - k_{\mathrm{f}_i} w_{\mathrm{f}} k_{\mathrm{pv}_i} k_{\mathrm{i}_i} V^{'},$

$a^{'} = a_6 - a_7 - a_8 - a_9 - a_{10} - a_{11} + a_{12} + a_{13},$

$a^{''} = a_{14} - a_{15} + a_{16} - a_{17} - a_{18} - a_{19} - a_{20} - a_{21} - a_{22} - a_{23} + a_{24} + a_{25} + a_{26},$

$a^{'''} = a_4 - a_5,$

$a_4 = k_{\mathrm{f}_i} w_{\mathrm{f}} k_{\mathrm{pv}_i} k_{\mathrm{i}_i} V_i^0 - k_{\mathrm{f}_i} w_{\mathrm{f}} k_{\mathrm{pv}_i} k_{\mathrm{i}_i} V^{'},$

$a_5 = k_{\mathrm{f}_i} w_{\mathrm{f}}^2 k_{\mathrm{p}\delta_i} + k_{\mathrm{f}_i} w_{\mathrm{f}}^2 k_{\mathrm{pv}_i} k_{\mathrm{p}_i} V_i^0 - k_{\mathrm{f}_i} w_{\mathrm{f}}^2 k_{\mathrm{pv}_i} k_{\mathrm{p}_i} V^{'},$

$a_6 = k_{\mathrm{f}_i} w_{\mathrm{f}} k_{\mathrm{p}\delta_i} k_{\mathrm{i}_i} k_{\mathrm{p}_i} k_{\mathrm{qv}_i}^2,$

$a_7 = -k_{\mathrm{f}_i} w_{\mathrm{f}} k_{\mathrm{pv}_i} k_{\mathrm{i}_i} k_{\mathrm{qv}_i} k_{\mathrm{q}\delta_i} k_{\mathrm{p}_i},$

$a_8 = w_{\mathrm{f}}^2 k_{\mathrm{i}_i} k_{\mathrm{p}_i} k_{\mathrm{qv}_i}^2,$

$a_9 = w_{\mathrm{f}} k_{\mathrm{i}_i}^2 k_{\mathrm{qv}_i}^2,$

$a_{10} = w_{\mathrm{f}}^2 k_{\mathrm{f}_i} k_{\mathrm{p}\delta_i} k_{\mathrm{p}_i}^2 k_{\mathrm{qv}_i}^2,$

$a_{11} = w_{\mathrm{f}} k_{\mathrm{f}_i} k_{\mathrm{p}\delta_i} k_{\mathrm{p}_i} k_{\mathrm{i}_i} k_{\mathrm{qv}_i}^2,$

$a_{12} = -w_{\mathrm{f}}^2 k_{\mathrm{f}_i} k_{\mathrm{p}\delta_i}^2 k_{\mathrm{pv}_i} k_{\mathrm{qv}_i} k_{\mathrm{q}\delta_i},$

$a_{13} = -w_{\mathrm{f}} k_{\mathrm{f}_i} k_{\mathrm{p}_i} k_{\mathrm{pv}_i} k_{\mathrm{q}\delta_i} k_{\mathrm{i}_i} k_{\mathrm{qv}_i},$

$a_{14} = w_{\mathrm{f}} k_{\mathrm{f}_i} k_{\mathrm{p}\delta_i} k_{\mathrm{i}_i} k_{\mathrm{qv}_i},$

$a_{15} = -w_{\mathrm{f}} k_{\mathrm{f}_i} k_{\mathrm{pv}_i} k_{\mathrm{i}_i} k_{\mathrm{q}\delta_i},$

$a_{16} = w_{\mathrm{f}} k_{\mathrm{f}_i} k_{\mathrm{pv}_i} k_{\mathrm{i}_i} V_i k_{\mathrm{p}_i} k_{\mathrm{qv}_i},$

$a_{17} = -w_{\mathrm{f}} k_{\mathrm{f}_i} k_{\mathrm{pv}_i} k_{\mathrm{i}_i} k_{\mathrm{p}_i} k_{\mathrm{qv}_i} V^{'},$

$$a_{18} = w_{\mathrm{f}}^2 k_{\mathrm{i}_i} k_{\mathrm{qv}_i},$$

$$a_{19} = w_{\mathrm{f}}^2 k_{\mathrm{f}_i} k_{\mathrm{p}_i} k_{\mathrm{p}\delta_i} k_{\mathrm{qv}_i},$$

$$a_{20} = w_{\mathrm{f}}^2 k_{\mathrm{f}_i} k_{\mathrm{i}_i} k_{\mathrm{qv}_i} k_{\mathrm{p}\delta_i},$$

$$a_{21} = w_{\mathrm{f}}^2 k_{\mathrm{f}_i} k_{\mathrm{p}\delta_i} k_{\mathrm{p}_i} k_{\mathrm{qv}_i},$$

$$a_{22} = w_{\mathrm{f}}^2 k_{\mathrm{f}_i} k_{\mathrm{pv}_i} k_{\mathrm{p}_i}^2 V_i^0,$$

$$a_{23} = w_{\mathrm{f}} k_{\mathrm{f}_i} k_{\mathrm{pv}_i} k_{\mathrm{p}_i} k_{\mathrm{i}_i} k_{\mathrm{qv}_i} V_i^0,$$

$$a_{24} = -w_{\mathrm{f}}^2 k_{\mathrm{f}_i} k_{\mathrm{p}_i} k_{\mathrm{pv}_i} k_{\mathrm{q}\delta_i},$$

$$a_{25} = -w_{\mathrm{f}}^2 k_{\mathrm{f}_i} k_{\mathrm{pv}_i} k_{\mathrm{p}_i}^2 k_{\mathrm{qv}_i} V^{'},$$

$$a_{26} = -w_{\mathrm{f}} k_{\mathrm{f}_i} k_{\mathrm{i}_i} k_{\mathrm{pv}_i} k_{\mathrm{p}_i} k_{\mathrm{qv}_i} V'.$$

$$b_0 = 1 + D_{\mathrm{v}_i} k_{\mathrm{p}_i} k_{\mathrm{pv}_i},$$

$$b_1 = w_{\mathrm{f}} + w_{\mathrm{f}} D_{\mathrm{v}_i} k_{\mathrm{p}_i} k_{\mathrm{pv}_i} + k_{\mathrm{i}_i} D_{\mathrm{v}_i} k_{\mathrm{pv}_i},$$

$$b_2 = w_{\mathrm{f}} k_{\mathrm{i}_i} D_{\mathrm{v}_i} k_{\mathrm{pv}_i} + k_{\mathrm{f}_i} w_{\mathrm{f}} k_{\mathrm{q}\delta_i} + k_{\mathrm{f}_i} w_{\mathrm{f}} k_{\mathrm{q}\delta_i} D_{\mathrm{v}_i} k_{\mathrm{p}_i} k_{\mathrm{pv}_i} + k_{\mathrm{f}_i} w_{\mathrm{f}} k_{\mathrm{qv}_i} k_{\mathrm{p}_i} V_i - k_{\mathrm{f}_i} w_{\mathrm{f}} k_{\mathrm{p}_i} k_{\mathrm{qv}_i} D_{\mathrm{v}_i} k_{\mathrm{q}\delta_i}$$
$$- k_{\mathrm{f}_i} w_{\mathrm{f}} k_{\mathrm{qv}_i} k_{\mathrm{p}_i} V^{'},$$

$$b_3 = k_{\mathrm{f}_i} w_{\mathrm{f}} k_{\mathrm{q}\delta_i} k_{\mathrm{i}_i} D_{\mathrm{v}_i} k_{\mathrm{pv}_i} + k_{\mathrm{f}_i} w_{\mathrm{f}} k_{\mathrm{qv}_i} k_{\mathrm{i}_i} V_i - k_{\mathrm{f}_i} w_{\mathrm{f}} k_{\mathrm{qv}_i} D_{\mathrm{v}_i} k_{\mathrm{i}_i} k_{\mathrm{p}\delta_i} - k_{\mathrm{f}_i} w_{\mathrm{f}} k_{\mathrm{qv}_i} k_{\mathrm{i}_i} V^{'},$$

$$b^{'} = b_6 - b_7 - b_8 - b_9 - b_{10} - b_{11} + b_{12} + b_{13},$$

$$b^{''} = b_{14} - b_{15} + b_{16} - b_{17} - b_{18} - b_{19} - b_{20} - b_{21} - b_{22} - b_{23} + b_{24} + b_{25} + b_{26},$$

$$b^{'''} = b_4 - b_5,$$

$$b_4 = k_{\mathrm{f}_i} w_{\mathrm{f}} k_{\mathrm{qv}_i} k_{\mathrm{i}_i} V_i^0 - k_{\mathrm{f}_i} w_{\mathrm{f}} k_{\mathrm{qv}_i} k_{\mathrm{i}_i} V^{'},$$

$$b_5 = k_{\mathrm{f}_i} w_{\mathrm{f}}^2 k_{\mathrm{q}\delta_i} + k_{\mathrm{f}_i} w_{\mathrm{f}}^2 k_{\mathrm{qv}_i} k_{\mathrm{p}_i} V_i^0 - k_{\mathrm{f}_i} w_{\mathrm{f}}^2 k_{\mathrm{qv}_i} k_{\mathrm{p}_i} V^{'},$$

$$b_6 = k_{\mathrm{f}_i} w_{\mathrm{f}} k_{\mathrm{q}\delta_i} k_{\mathrm{i}_i} k_{\mathrm{p}_i} k_{\mathrm{pv}_i}^2,$$

$$b_7 = -k_{\mathrm{f}_i} w_{\mathrm{f}} k_{\mathrm{qv}_i} k_{\mathrm{i}_i} k_{\mathrm{pv}_i} k_{\mathrm{p}\delta_i} k_{\mathrm{p}_i},$$

$$b_8 = w_{\mathrm{f}}^2 k_{\mathrm{i}_i} k_{\mathrm{p}_i} k_{\mathrm{pv}_i}^2,$$

$$b_9 = w_{\mathrm{f}} k_{\mathrm{i}_i}^2 k_{\mathrm{pv}_i}^2,$$

$$b_{10} = w_{\mathrm{f}}^2 k_{\mathrm{f}_i} k_{\mathrm{q}\delta_i} k_{\mathrm{p}_i}^2 k_{\mathrm{pv}_i}^2,$$

$$b_{11} = w_{\mathrm{f}} k_{\mathrm{f}_i} k_{\mathrm{q}\delta_i} k_{\mathrm{p}_i} k_{\mathrm{i}_i} k_{\mathrm{pv}_i}^2,$$

$$b_{12} = -w_{\mathrm{f}}^2 k_{\mathrm{f}_i} k_{\mathrm{q}\delta_i}^2 k_{\mathrm{qv}_i} k_{\mathrm{pv}_i} k_{\mathrm{p}\delta_i},$$

$$b_{13} = -w_{\mathrm{f}} k_{\mathrm{f}_i} k_{\mathrm{p}_i} k_{\mathrm{qv}_i} k_{\mathrm{p}\delta_i} k_{\mathrm{i}_i} k_{\mathrm{pv}_i},$$

$$b_{14} = w_{\mathrm{f}} k_{\mathrm{f}_i} k_{\mathrm{q}\delta_i} k_{\mathrm{i}_i} k_{\mathrm{pv}_i},$$

$$b_{15} = -w_{\mathrm{f}} k_{\mathrm{f}_i} k_{\mathrm{qv}_i} k_{\mathrm{i}_i} k_{\mathrm{p}\delta_i},$$

$$b_{16} = w_{\mathrm{f}} k_{\mathrm{f}_i} k_{\mathrm{qv}_i} k_{\mathrm{i}_i} V_i k_{\mathrm{p}_i} k_{\mathrm{pv}_i},$$

$$b_{17} = -w_{\mathrm{f}} k_{\mathrm{f}_i} k_{\mathrm{qv}_i} k_{\mathrm{i}_i} k_{\mathrm{p}_i} k_{\mathrm{pv}_i} V',$$

$$b_{18} = w_{\mathrm{f}}^2 k_{\mathrm{i}_i} k_{\mathrm{pv}_i},$$

$$b_{19} = w_{\mathrm{f}}^2 k_{\mathrm{f}_i} k_{\mathrm{p}_i} k_{\mathrm{q}\delta_i} k_{\mathrm{pv}_i},$$

$$b_{20} = w_{\mathrm{f}}^2 k_{\mathrm{f}_i} k_{\mathrm{i}_i} k_{\mathrm{pv}_i} k_{\mathrm{q}\delta_i},$$

$$b_{21} = w_{\mathrm{f}}^2 k_{\mathrm{f}_i} k_{\mathrm{q}\delta_i} k_{\mathrm{p}_i} k_{\mathrm{pv}_i},$$

$$b_{22} = w_{\mathrm{f}}^2 k_{\mathrm{f}_i} k_{\mathrm{qv}_i} k_{\mathrm{p}_i}^2 V_i^0,$$

$$b_{23} = w_{\mathrm{f}} k_{\mathrm{f}_i} k_{\mathrm{qv}_i} k_{\mathrm{p}_i} k_{\mathrm{i}_i} k_{\mathrm{qv}_i} V_i^0,$$

$$b_{24} = -w_{\mathrm{f}}^2 k_{\mathrm{f}_i} k_{\mathrm{p}_i} k_{\mathrm{pv}_i} k_{\mathrm{p}\delta_i},$$

$$b_{25} = -w_{\mathrm{f}}^2 k_{\mathrm{f}_i} k_{\mathrm{qv}_i} k_{\mathrm{p}_i}^2 k_{\mathrm{pv}_i} V',$$

$$b_{26} = -w_{\mathrm{f}} k_{\mathrm{f}_i} k_{\mathrm{i}_i} k_{\mathrm{qv}_i} k_{\mathrm{p}_i} k_{\mathrm{pv}_i} V'.$$

$$c_0 = |Z_i| + k_{\mathrm{p}_i} D_{\mathrm{v}_i} k_{\mathrm{pv}_i} + |Z_i| + k_{\mathrm{p}_i} D_{\mathrm{v}_i} k_{\mathrm{qv}_i},$$

$$c_1 = |Z_i| k_{\mathrm{i}_i} D_{\mathrm{v}_i} k_{\mathrm{pv}_i} + |Z_i| k_{\mathrm{i}_i} D_{\mathrm{v}_i} k_{\mathrm{qv}_i} + w_{\mathrm{f}} |Z_i| + w_{\mathrm{f}} |Z_i| k_{\mathrm{p}_i} D_{\mathrm{v}_i} k_{\mathrm{pv}_i} + w_{\mathrm{f}} |Z_i| k_{\mathrm{p}_i} D_{\mathrm{v}_i} k_{\mathrm{qv}_i},$$

$$c_2 = w_{\mathrm{f}} |Z_i| k_{\mathrm{i}_i} D_{\mathrm{v}_i} k_{\mathrm{pv}_i} + w_{\mathrm{f}} |Z_i| k_{\mathrm{i}_i} D_{\mathrm{v}_i} k_{\mathrm{qv}_i} - w_{\mathrm{f}} k_{\mathrm{f}_i} X_i k_{\mathrm{pv}_i} 2V_i^0 + w_{\mathrm{f}} k_{\mathrm{f}_i} X_i D_{\mathrm{v}_i} k_{\mathrm{p}\delta_i} k_{\mathrm{pv}_i}$$
$$+ w_{\mathrm{f}} k_{\mathrm{f}_i} X_i D_{\mathrm{v}_i} k_{\mathrm{pv}_i} k_{\mathrm{q}\delta_i} + w_{\mathrm{f}} k_{\mathrm{f}_i} X_i k_{\mathrm{pv}_i} 2V' - w_{\mathrm{f}} k_{\mathrm{f}_i} R_i k_{\mathrm{qv}_i} 2V_i + w_{\mathrm{f}} k_{\mathrm{f}_i} R_i k_{\mathrm{qv}_i} D_{\mathrm{v}_i} k_{\mathrm{p}\delta_i}$$
$$+ w_{\mathrm{f}} k_{\mathrm{f}_i} R_i D_{\mathrm{v}_i} k_{\mathrm{qv}_i} k_{\mathrm{q}\delta_i} + w_{\mathrm{f}} k_{\mathrm{f}_i} R_i k_{\mathrm{pv}_i} 2V',$$

$$c_3 = -w_{\mathrm{f}} k_{\mathrm{f}_i} X_i k_{\mathrm{p}\delta_i} - w_{\mathrm{f}} k_{\mathrm{f}_i} X_i k_{\mathrm{pv}_i} 2V_i^0 + w_{\mathrm{f}} k_{\mathrm{f}_i} X_i D_{\mathrm{v}_i} k_{\mathrm{pv}_i} k_{\mathrm{p}\delta_i} + w_{\mathrm{f}} k_{\mathrm{f}_i} X_i k_{\mathrm{pv}_i} D_{\mathrm{v}_i} k_{\mathrm{q}\delta_i}$$
$$+ w_{\mathrm{f}} k_{\mathrm{f}_i} X_i k_{\mathrm{pv}_i} 2V' - w_{\mathrm{f}} k_{\mathrm{f}_i} R_i k_{\mathrm{q}\delta_i} - w_{\mathrm{f}} k_{\mathrm{f}_i} R_i k_{\mathrm{qv}_i} 2V_i^0 + w_{\mathrm{f}} k_{\mathrm{f}_i} R_i D_{\mathrm{v}_i} k_{\mathrm{p}\delta_i} k_{\mathrm{qv}_i}$$
$$+ w_{\mathrm{f}} k_{\mathrm{f}_i} R_i D_{\mathrm{v}_i} k_{\mathrm{q}\delta_i} k_{\mathrm{qv}_i} + w_{\mathrm{f}} k_{\mathrm{f}_i} R_i k_{\mathrm{qv}_i} 2V',$$

$$c' = c_{15} + c_{16} + c_{17} + c_{18} + c_{19} + c_{20} + c_{21} + c_{22} - c_{23} - c_{24} - c_{25} - c_{26} - c_{27} - c_{28}$$
$$- c_{29} - c_{30} - c_{31} - c_{32} - c_{33} - c_{34} - c_{35} - c_{36} - c_{37} - c_{38} - c_{39} - c_{40} - c_{41} - c_{42}$$

$$- c_{43} - c_{44},$$

$$c^{''} = c_{45} + c_{46} + c_{47} + c_{48} - c_{49} + c_{50} - c_{51} - c_{52} + c_{53} - c_{54} - c_{55} - c_{56} - c_{57} + c_{58}$$

$$+ c_{59} - c_{60} + c_{61} - c_{62} + c_{63} - c_{64} + c_{65} - c_{66} - c_{67} - c_{68} - c_{69} - c_{70} - c_{71} - c_{72}$$

$$+ c_{73} - c_{74} - c_{75} + c_{76} - c_{77} + c_{78} - c_{79} - c_{80} - c_{81} - c_{82},$$

$$c^{'''} = c_4 - c_5 + c_6 - c_7 - c_8 + c_9 + c_{10} + c_{11} - c_{12} + c_{13} - c_{14},$$

$$c_4 = -w_{\mathrm{f}} k_{\mathrm{f}_i} X_i |Z_i| k_{\mathrm{p}\delta_i},$$

$$c_5 = -w_{\mathrm{f}} k_{\mathrm{f}_i} X_i |Z_i| k_{\mathrm{qv}_i} 2V_i^0,$$

$$c_6 = w_{\mathrm{f}} k_{\mathrm{f}_i} X_i |Z_i| k_{\mathrm{pv}_i} 2V^{'},$$

$$c_7 = -w_{\mathrm{f}} k_{\mathrm{f}_i} R_i |Z_i| k_{\mathrm{q}\delta_i},$$

$$c_8 = -w_{\mathrm{f}} k_{\mathrm{f}_i} R_i |Z_i| k_{\mathrm{qv}_i} 2V_i^0,$$

$$c_9 = w_{\mathrm{f}} k_{\mathrm{f}_i} R_i |Z_i| k_{\mathrm{qv}_i} 2V^{'},$$

$$c_{10} = w_{\mathrm{f}} k_{\mathrm{f}_i} X_i |Z_i| k_{\mathrm{p}_i} k_{\mathrm{pv}_i} k_{\mathrm{qv}_i} 2V^{'},$$

$$c_{11} = -w_{\mathrm{f}}^2 k_{\mathrm{f}_i} X_i |Z_i|^2 k_{\mathrm{pv}_i} 2V_i,$$

$$c_{12} = w_{\mathrm{f}}^2 k_{\mathrm{f}_i} X_i |Z_i| k_{\mathrm{pv}_i} 2V^{'},$$

$$c_{13} = w_{\mathrm{f}}^2 k_{\mathrm{f}_i} R_i |Z_i| k_{\mathrm{qv}_i} 2V_i^0,$$

$$c_{14} = w_{\mathrm{f}} k_{\mathrm{f}_i} X_i |Z_i| k_{\mathrm{pv}_i} 2V^{'},$$

$$c_{15} = w_{\mathrm{f}} k_{\mathrm{f}_i} k_{\mathrm{p}_i} k_{\mathrm{pv}_i}^2 k_{\mathrm{p}\delta_i},$$

$$c_{16} = w_{\mathrm{f}} k_{\mathrm{f}_i} X_i k_{\mathrm{p}_i} k_{\mathrm{pv}_i}^2 k_{\mathrm{q}\delta_i},$$

$$c_{17} = w_{\mathrm{f}} k_{\mathrm{f}_i} R_i k_{\mathrm{p}_i} k_{\mathrm{pv}_i} k_{\mathrm{p}\delta_i} k_{\mathrm{qv}_i},$$

$$c_{18} = w_{\mathrm{f}} k_{\mathrm{f}_i} R_i k_{\mathrm{p}_i} k_{\mathrm{pv}_i} k_{\mathrm{qv}_i} k_{\mathrm{q}\delta_i},$$

$$c_{19} = w_{\mathrm{f}} k_{\mathrm{f}_i} |Z_i| k_{\mathrm{p}_i} k_{\mathrm{pv}_i} k_{\mathrm{p}\delta_i} k_{\mathrm{qv}_i},$$

$$c_{20} = w_{\mathrm{f}} k_{\mathrm{f}_i} X_i |Z_i| k_{\mathrm{p}_i} k_{\mathrm{pv}_i} k_{\mathrm{qv}_i} k_{\mathrm{q}\delta_i},$$

$$c_{21} = w_{\mathrm{f}} k_{\mathrm{f}_i} R_i |Z_i| k_{\mathrm{p}_i} k_{\mathrm{p}\delta_i} k_{\mathrm{qv}_i}^2,$$

$$c_{22} = w_{\mathrm{f}} k_{\mathrm{f}_i} R_i |Z_i| k_{\mathrm{p}_i} k_{\mathrm{qv}_i} k_{\mathrm{q}\delta_i},$$

$$c_{23} = w_{\mathrm{f}} |Z_i|^2 k_{\mathrm{i}_i}^2 k_{\mathrm{pv}_i}^2,$$

$$c_{24} = w_{\mathrm{f}} |Z_i|^2 k_{\mathrm{i}_i}^2 k_{\mathrm{pv}_i} k_{\mathrm{qv}_i},$$

$$c_{25} = w_{\mathrm{f}} k_{\mathrm{f}_i} X_i |Z_i| k_{\mathrm{i}_i} k_{\mathrm{pv}_i} k_{\mathrm{p}\delta_i},$$

$$c_{26} = w_{\mathrm{f}} k_{\mathrm{f}_i} X_i |Z_i| k_{\mathrm{i}_i} k_{\mathrm{pv}_i}^2 k_{\mathrm{q}\delta_i},$$

$$c_{27} = w_{\mathrm{f}} k_{\mathrm{f}_i} R_i |Z_i| k_{\mathrm{i}_i} k_{\mathrm{pv}_i} k_{\mathrm{p}\delta_i} k_{\mathrm{qv}_i},$$

$$c_{28} = w_{\mathrm{f}} k_{\mathrm{f}_i} R_i |Z_i| k_{\mathrm{i}_i} k_{\mathrm{pv}_i} k_{\mathrm{q}\delta_i} k_{\mathrm{qv}_i},$$

$$c_{29} = w_{\mathrm{f}} |Z_i|^2 k_{\mathrm{i}_i}^2 k_{\mathrm{pv}_i} k_{\mathrm{qv}_i},$$

$$c_{30} = w_{\mathrm{f}} |Z_i|^2 k_{\mathrm{i}_i}^2 k_{\mathrm{qv}_i}^2,$$

$$c_{31} = w_{\mathrm{f}} k_{\mathrm{f}_i} X_i |Z_i| k_{\mathrm{i}_i} k_{\mathrm{pv}_i} k_{\mathrm{p}\delta_i} k_{\mathrm{qv}_i},$$

$$c_{32} = w_{\mathrm{f}} k_{\mathrm{f}_i} X_i |Z_i| k_{\mathrm{i}_i} k_{\mathrm{p}\delta_i} k_{\mathrm{qv}_i} k_{\mathrm{q}\delta_i},$$

$$c_{33} = w_{\mathrm{f}} k_{\mathrm{f}_i} R_i |Z_i| k_{\mathrm{i}_i} k_{\mathrm{p}\delta_i} k_{\mathrm{qv}_i}^2,$$

$$c_{34} = w_{\mathrm{f}} k_{\mathrm{f}_i} R_i |Z_i| k_{\mathrm{i}_i} k_{\mathrm{q}\delta_i} k_{\mathrm{qv}_i}^2,$$

$$c_{35} = w_{\mathrm{f}}^2 |Z_i|^2 k_{\mathrm{i}_i} k_{\mathrm{p}_i} k_{\mathrm{pv}_i}^2,$$

$$c_{36} = w_{\mathrm{f}}^2 |Z_i|^2 k_{\mathrm{i}_i} k_{\mathrm{p}_i} k_{\mathrm{pv}_i} k_{\mathrm{qv}_i},$$

$$c_{37} = w_{\mathrm{f}}^2 k_{\mathrm{f}_i} X_i |Z_i| k_{\mathrm{p}_i} k_{\mathrm{pv}_i}^2 k_{\mathrm{p}\delta_i},$$

$$c_{38} = w_{\mathrm{f}}^2 k_{\mathrm{f}_i} R_i |Z_i| k_{\mathrm{p}_i} k_{\mathrm{pv}_i} k_{\mathrm{p}\delta_i} k_{\mathrm{qv}_i},$$

$$c_{39} = w_{\mathrm{f}}^2 k_{\mathrm{f}_i} R_i k_{\mathrm{p}_i} k_{\mathrm{pv}_i} k_{\mathrm{q}\delta_i} k_{\mathrm{qv}_i}^2,$$

$$c_{40} = w_{\mathrm{f}}^2 |Z_i| k_{\mathrm{i}_i} k_{\mathrm{p}_i} k_{\mathrm{pv}_i} k_{\mathrm{qv}_i},$$

$$c_{41} = w_{\mathrm{f}}^2 |Z_i|^2 k_{\mathrm{i}_i} k_{\mathrm{qv}_i}^2,$$

$$c_{42} = w_{\mathrm{f}}^2 k_{\mathrm{f}_i} X_i |Z_i| k_{\mathrm{p}_i} k_{\mathrm{pv}_i} k_{\mathrm{p}\delta_i} k_{\mathrm{qv}_i},$$

$$c_{43} = w_{\mathrm{f}}^2 k_{\mathrm{f}_i} R_i |Z_i| k_{\mathrm{p}_i} k_{\mathrm{p}\delta_i} k_{\mathrm{qv}_i}^2,$$

$$c_{44} = w_{\mathrm{f}}^2 k_{\mathrm{f}_i} R_i k_{\mathrm{q}\delta_i} k_{\mathrm{qv}_i}^2,$$

$$c_{45} = w_{\mathrm{f}} k_{\mathrm{f}_i} X_i |Z_i| k_{\mathrm{pv}_i} k_{\mathrm{p}\delta_i},$$

$$c_{46} = w_{\mathrm{f}} k_{\mathrm{f}_i} X_i |Z_i| k_{\mathrm{pv}_i} k_{\mathrm{q}\delta_i},$$

$$c_{47} = w_{\mathrm{f}} k_{\mathrm{f}_i} R_i |Z_i| k_{\mathrm{p}\delta_i} k_{\mathrm{qv}_i},$$

$$c_{48} = w_{\mathrm{f}} k_{\mathrm{f}_i} R_i |Z_i| k_{\mathrm{q}\delta_i} k_{\mathrm{qv}_i},$$

$$c_{49} = -w_{\mathrm{f}} k_{\mathrm{f}_i} X_i k_{\mathrm{p}_i} k_{\mathrm{pv}_i} k_{\mathrm{p}\delta_i},$$

$$c_{50} = w_{\mathrm{f}} k_{\mathrm{f}_i} X_i k_{\mathrm{p}_i} k_{\mathrm{pv}_i}^2 2V',$$

$$c_{51} = w_{\mathrm{f}} k_{\mathrm{f}_i} R_i k_{\mathrm{p}_i} k_{\mathrm{pv}_i} k_{\mathrm{q}\delta_i},$$

$$c_{52} = -w_{\mathrm{f}} k_{\mathrm{f}_i} R_i k_{\mathrm{p}_i} k_{\mathrm{pv}_i} k_{\mathrm{qv}_i} 2V_i^0,$$

$$c_{53} = w_{\mathrm{f}} k_{\mathrm{f}_i} R_i k_{\mathrm{p}_i} k_{\mathrm{pv}_i} k_{\mathrm{qv}_i} 2V^{'},$$

$$c_{54} = -w_{\mathrm{f}} k_{\mathrm{f}_i} X_i |Z_i| k_{\mathrm{p}_i} k_{\mathrm{pv}_i} k_{\mathrm{qv}_i} 2V^{'},$$

$$c_{55} = -w_{\mathrm{f}} k_{\mathrm{f}_i} X_i |Z_i| k_{\mathrm{p}_i} k_{\mathrm{pv}_i} k_{\mathrm{qv}_i} 2V_i^0,$$

$$c_{56} = -w_{\mathrm{f}} k_{\mathrm{f}_i} R_i |Z_i| k_{\mathrm{p}_i} k_{\mathrm{q}\delta_i} k_{\mathrm{qv}_i},$$

$$c_{57} = -w_{\mathrm{f}} k_{\mathrm{f}_i} R_i |Z_i| k_{\mathrm{p}_i} k_{\mathrm{qv}_i}^2 2V_i^0,$$

$$c_{58} = w_{\mathrm{f}} k_{\mathrm{f}_i} R_i |Z_i| k_{\mathrm{p}_i} k_{\mathrm{qv}_i}^2 2V^{'},$$

$$c_{59} = -w_{\mathrm{f}} k_{\mathrm{f}_i} X_i |Z_i| k_{\mathrm{i}_i} k_{\mathrm{pv}_i}^2 2V_i^0,$$

$$c_{60} = w_{\mathrm{f}} k_{\mathrm{f}_i} X_i |Z_i| k_{\mathrm{i}_i} k_{\mathrm{pv}_i}^2 2V^{'},$$

$$c_{61} = -w_{\mathrm{f}} k_{\mathrm{f}_i} R_i |Z_i| k_{\mathrm{i}_i} k_{\mathrm{pv}_i} k_{\mathrm{qv}_i} 2V_i^0,$$

$$c_{62} = w_{\mathrm{f}} k_{\mathrm{f}_i} X_i |Z_i| k_{\mathrm{i}_i} k_{\mathrm{pv}_i}^2 2V^{'},$$

$$c_{63} = -w_{\mathrm{f}} k_{\mathrm{f}_i} X_i |Z_i| k_{\mathrm{pv}_i} k_{\mathrm{qv}_i} 2V_i^0,$$

$$c_{64} = w_{\mathrm{f}} k_{\mathrm{f}_i} X_i |Z_i| k_{\mathrm{i}_i} k_{\mathrm{pv}_i} k_{\mathrm{qv}_i} 2V^{'},$$

$$c_{65} = -w_{\mathrm{f}} k_{\mathrm{f}_i} R_i |Z_i| k_{\mathrm{i}_i} k_{\mathrm{qv}_i}^2 2V_i^0,$$

$$c_{66} = w_{\mathrm{f}} k_{\mathrm{f}_i} X_i |Z_i| k_{\mathrm{i}_i} k_{\mathrm{pv}_i} k_{\mathrm{qv}_i} 2V^{'},$$

$$c_{67} = w_{\mathrm{f}}^2 |Z_i|^2 k_{\mathrm{i}_i} k_{\mathrm{pv}_i},$$

$$c_{68} = w_{\mathrm{f}}^2 |Z_i|^2 k_{\mathrm{i}_i} k_{\mathrm{qv}_i},$$

$$c_{69} = w_{\mathrm{f}}^2 k_{\mathrm{f}_i} X_i |Z_i| k_{\mathrm{pv}_i} k_{\mathrm{p}\delta_i},$$

$$c_{70} = w_{\mathrm{f}}^2 k_{\mathrm{f}_i} X_i |Z_i| k_{\mathrm{pv}_i} k_{\mathrm{q}\delta_i},$$

$$c_{71} = w_{\mathrm{f}}^2 k_{\mathrm{f}_i} R_i |Z_i| k_{\mathrm{p}\delta_i} k_{\mathrm{qv}_i},$$

$$c_{72} = w_{\mathrm{f}}^2 k_{\mathrm{f}_i} R_i |Z_i| k_{\mathrm{q}\delta_i} k_{\mathrm{qv}_i},$$

$$c_{73} = -w_{\mathrm{f}}^2 k_{\mathrm{f}_i} X_i |Z_i| k_{\mathrm{p}_i} k_{\mathrm{pv}_i}^2 2V_i^0,$$

$$c_{74} = w_{\mathrm{f}}^2 k_{\mathrm{f}_i} X_i |Z_i| k_{\mathrm{p}_i} k_{\mathrm{pv}_i}^2 k_{\mathrm{q}\delta_i},$$

$$c_{75} = w_{\mathrm{f}}^2 k_{\mathrm{f}_i} X_i |Z_i| k_{\mathrm{p}_i} k_{\mathrm{pv}_i}^2 2V^{'},$$

$$c_{76} = -w_{\mathrm{f}}^2 k_{\mathrm{f}_i} R_i |Z_i| k_{\mathrm{p}_i} k_{\mathrm{pv}_i} k_{\mathrm{qv}_i} 2V_i^0,$$

$$c_{77} = w_{\mathrm{f}}^2 k_{\mathrm{f}_i} X_i |Z_i| k_{\mathrm{p}_i} k_{\mathrm{pv}_i}^2 2V^{'},$$

$$c_{78} = -w_{\mathrm{f}}^2 k_{\mathrm{f}_i} X_i |Z_i| k_{\mathrm{p}_i} k_{\mathrm{pv}_i} k_{\mathrm{qv}_i} 2V_i^0,$$

$$c_{79} = w_{\mathrm{f}}^2 k_{\mathrm{f}_i} X_i |Z_i| k_{\mathrm{p}_i} k_{\mathrm{pv}_i} k_{\mathrm{qv}_i},$$

$$c_{80} = w_{\mathrm{f}}^2 k_{\mathrm{f}_i} X_i |Z_i| k_{\mathrm{p}_i} k_{\mathrm{pv}_i} k_{\mathrm{qv}_i} 2V^{'},$$

$$c_{81} = -w_{\mathrm{f}}^2 k_{\mathrm{f}_i} R_i |Z_i| k_{\mathrm{p}_i} k_{\mathrm{qv}_i}^2 2V_i^0,$$

$$c_{82} = w_{\mathrm{f}}^2 k_{\mathrm{f}_i} X_i |Z_i| k_{\mathrm{p}_i} k_{\mathrm{pv}_i} k_{\mathrm{qv}_i} 2V^{'}.$$

References

[1] A. F. Zobaa, and C. Cecati, "A comprehensive review on distributed power generation," in *Proc. Int. Symp. on Power Electron., Electr. Drives, Automat. and Motion*, Jun. 11-13, 2008.

[2] F. Blaabjerg, Z. Chen, and S. B. Kjaer, "Power electronics as efficient interface in distributed generation systems," *IEEE Trans. Power Electron.*, vol. 19, no. 5, pp. 1184-1194, Sep. 2004.

[3] E. J. Coster, J. M. A. Myrzik, and B. Kruimer, "Integration issues of distributed generation in distribution grids," in *Proc. of the IEEE*, vol. 99, no. 1, pp. 28-39, Jun. 2011.

[4] F. Z. Peng, "Editorial special issue on distributed power generation," *IEEE Trans. Power Electron.*, vol. 19, no. 5, Sep. 2004.

[5] J. Wang, X. Li, and X. Qiu, "Review on the research of power system containing distributed generation device," *Automat. of Electric Power Syst.*, vol. 24, pp. 90-97, 2005.

[6] F. Blaabjerg, R. Teodorescu, M. liserre, and S. B. Kjaer, "Overview of control and grid synchronization for distributed power generation systems," *IEEE Trans. Ind. Electron.*, vol. 53, no. 5, pp. 1398-1409, Oct. 2006.

[7] M. Dai, M. Marwali, J. Jung, and A. Keyhani, "Power flow control of a single distributed generation unit," *IEEE Trans. Power Electron.*, vol. 23, no. 1, pp. 343-352, Jan. 2008.

[8] X. Zhou, T. Guo, and Y. Ma, "An overview on microgrid technology," in *Proc. IEEE Int. Conf. Mechatron. and Automat.*, pp. 76-81, Aug. 2-5, 2015.

[9] H. Farhangi, "The path of the smart grid," *IEEE Power and Energy Mag.*, vol.

8, pp. 18-28, 2010.

[10] R. Zamora, and A. K. Srivastava, "Controls for microgrids with storage: Review, challenges, and research needs," *Renew. Sustain. Energy Rev.*, vol. 14, no. 7, pp. 2009-2018, 2008.

[11] M. Erol-Kantarci, B. Kantarci, and H. T. Mouftah, "Reliable overlay topology design for the smart microgrid network," *IEEE Network*, vol. 25, no. 5, pp. 38-43, Sep.-Oct. 2011.

[12] R. H. Lasseter, "Microgrids," in *Proc. Power Eng. Soc. Winter Meet.*, vol. 1, pp. 305-308, Jan. 2002.

[13] R. H. Lasseter, "Smart Distribution: Coupled microgrids," in *Proc. of the IEEE*, vol. 99, no. 6, pp. 1074-1082, Jun. 2011.

[14] N. Hatziargyriou, H. Asano, R. Iravani, and C. Marnay, "Microgrids," *IEEE Power Energy Mag.*, vol. 5, no. 4, pp. 78-94, Jul./Aug. 2007.

[15] F. Katiraei, M. R. Iravani, and P. Lehn, "Microgrid autonomous operation during and subsequent to islanding process," *IEEE Trans. Power Del.*, vol. 20, no. 1, pp. 248-257, Jan. 2005.

[16] T. L. Vandoorn, B. Renders, L. Degroote, M. Meersman, and L. Vandevelde, "Power balancing in islanded microgrids by using a dc-bus voltage reference," in *Proc. Int. Symp. on Power Electron., Electr. Drives, Automat. and Motion*, pp. 884-889, Jun. 14-16, 2010.

[17] M. A. Barik, H. R. Pota, and J. Ravishankar, "An automatic load sharing approach for a DFIG based wind generation in a microgrid," in *Proc. IEEE Conf. on Ind. Electron. and Appl.*, pp. 589 - 594, Jun. 19-21, 2013.

[18] I. Wasiak, M. C. Thoma, C. E. T. Foote, R. Mienski, R. Pawelek, P. Gburezyk, and G. M. Burt, "A power-quality management algorithm for low-voltage grids

with distributed resources," *IEEE Trans. Power Del.*, vol. 23, no. 2, pp. 1055-1062, Apr. 2008.

[19] M. J. Hossain, H. R. Pota, M. A. Mahmud, and M. Aldeen, "Robust control for power sharing in microgrids with low-inertia wind and PV generators," *IEEE Trans. Sustain. Energy*, vol. 6, no. 3, pp. 1067-1077, May 2014.

[20] Q. C. Zhong, "Robust droop controller for accurate proportional load sharing among inverters operated in parallel," *IEEE Trans. Power Electron.*, vol. 60, no. 4, pp. 1281-1290, Apr. 2013.

[21] A. G. Tsikalakis, and N. D. Hatziargyriou, "Centralized control for optimizing microgrids operation," in *Proc. IEEE PES Gen. Meet.*, pp. 1-8, Jul 24-26, 2011.

[22] M. J. Hossain, M. A. Mahmud, F. Milano, S. Bacha, and A. Hably, "Design of robust distributed control for interconnected microgrids," *IEEE Trans. Smart Grid*, vol. 7, no. 6, pp. 2724-2735, Nov. 2016.

[23] T. C. Green, and M. Prodanovic, "Control of inverter-based microgrids," *Electric Power Syst. Research*, vol. 77, no. 9, pp. 1204-1213, Jul. 2007.

[24] M. Prodanovic, and T. C. Green, "High-quality power generation through distributed control of a power park microgrid," *IEEE Trans. Ind. Electron.*, vol. 53, no. 5, pp. 1107-1115, Oct. 2006.

[25] M. I. Azim, M. J. Hossain, F. H. M. Rafi, and H. R. Pota, "An improved droop control scheme for islanded microgrids," in *Proc. Australian Control Conf.*, pp. 225-229, Nov. 5-6, 2015.

[26] J. P. Lopes, C. Moreira, and A. Madureira, "Defining control strategies for microgrids islanded operation," *IEEE Trans. Power Syst.*, vol. 21, no. 2, pp. 916-924, May 2006.

[27] A. Tuladhar, H. Jin, T. Unger, and K. Mauch, "Control of parallel inverters in distributed ac power systems with consideration of line impedance effect,"

IEEE Trans. Ind. Appl., vol. 36, no. 1, pp. 131-138, Jan./Feb. 2006.

[28] M. I. Azim, M. A. Hossain, M. J. Hossain, and H. R. Pota, "Effective power sharing approach for islanded microgrids," in *Proc. IEEE PES ISGT Asia*, pp. 1-4, Nov. 4-6, 2015.

[29] J. M. Guerrero, J. C. Vasquez, J. Matas, L. G. de Vicuna, and M. Castilla, "Hierarchical control of droop-controlled AC and DC microgrids," *IEEE Trans. Ind. Electron.*, vol. 58, no. 1, pp. 158-172, Jan. 2011.

[30] T. L. Vandoorn, J. De Kooning, B. Meersman, and L. Vandevelde, "Voltage-based droop control of renewables to avoid on-off oscillations caused by over-voltages," *IEEE Trans. Power Del.*, vol. 28, no. 2, pp. 845-854, Feb. 2013.

[31] T. L. Vandoorn, B. Meersman, J. De Kooning, and L. Vandevelde, "Transition from islanded to grid-connected mode of microgrids with voltage-based droop control," *IEEE Trans. Power Syst.*, vol. 28, no. 3, pp. 2545-2553, Mar. 2013.

[32] J. Guerrero, L. de Vicuna, J. Matas, M. Castilla, and J. Miret, "A wireless controller to enhance dynamic performance of parallel inverters in distributed generation system," *IEEE Trans. Power Electron.*, vol. 19, no. 5, pp. 1205-1213, Sep. 2004.

[33] F. Katiraei, and M. R. Iravani, "Power management strategies for a microgrid with multiple distributed generation units," *IEEE Trans. Power Syst.*, vol. 21, no. 4, pp. 1821-1831, Nov. 2006.

[34] T. L. Vandoorn, J. De Kooning, B. Meersman, J. M. Guerrero, and L. Vandevelde, "Automatic power-sharing modification of P/V droop controllers in low-voltage resistive microgrids," *IEEE Trans. Power Del.*, vol. 27, no. 4, pp. 2318-2324, Oct. 2012.

[35] Y. Tan, K. M. Muttaqi, and L. G. Meegahapola, "A droop control based

load sharing approach for management of renewable and non-renewable energy sources in a remote power system," in *Proc. Australian Univs. Power Eng. Conf.*, pp. 1-6, Sep. 29-Oct. 3, 2013.

[36] H. R. Pota, "Droop control for islanded microgrids," in *Proc. IEEE PES Gen. Meet.*, pp. 1-4, Jul. 21-25, 2013.

[37] M. I. Azim, M. A. Hossain, M. J. Hossain, and H. R. Pota, "Droop control for islanded microgrids with compensating approach," in *Proc. Australasian Univs. Power Eng. Conf.*, pp. 1-6, Sep. 27-30, 2015.

[38] F. Luo, Y. M. Lai, Chi K. Tse, and K. H. Loo, "A triple-droop control scheme for inverter-based microgrids," in *Proc. Annual Conf. IEEE Ind. Electron. Soc.*, pp. 3368-3375, Oct. 25-28, 2012.

[39] F. Luo, Y. M. Lai, K. H. Loo, Chi K. Tse, and X. Ruan, "A generalized droop-control scheme for decentralized control of inverter-interfaced microgrids," in *Proc. IEEE Symp. Inverter-interfaced Microgrids*, pp. 1320-1323, May 19-23, 2013.

[40] Y. Mohamed, and E. El-Saadany, "Adaptive decentralized droop controller to preserve power sharing stability of paralleled inverters in distributed generation microgrids," *IEEE Trans. Power Electron.*, vol. 23, no. 6, pp. 2806-2816, Dec. 2008.

[41] R. Majumder, A. Ghosh, G. Ledwich, and F. Zare, "Power sharing and stability enhancement of an autonomous microgrid with inertial and non-inertial DGs with DSTATCOM," in *Proc. Int. Conf. on Power Syst.*, pp. 1-6, Dec. 27-29, 2009.

[42] R. Majumder, A. Ghosh, G. Ledwich, and F. Zare, "Operation and control of hybrid microgrid with angle droop controller," in *Proc. TENCON- IEEE Region 10 Conf.*, pp. 509-515, Nov. 21-24, 2010.

[43] T. L. Vandoorn, J. D. M. De Kooning, B. Meersman, L. Vandevelde, "Review of primary control strategies for islanded microgrids with power-electronic interfaces," *Renew. and Sustain. Energy Reviews*, vol. 19, pp. 613628, Mar. 2013.

[44] M. I. Azim, M. J. Hossain, and H. R. Pota, "Design of a controller for active power sharing in a highly-resistive microgrid," in *Proc. IFAC Symp. Control of Power and Energy Syst.*, Dec. 9-11, 2015.

[45] Y. W. Li, and C. -N. Kao, "An accurate power control strategy for power electronics-interfaced distributed generation units operating in a low voltage multibus microgrid," *IEEE Trans. Power Electron.*, vol. 24, no. 12, pp. 2977-2988, Aug. 2009.

[46] N. Pogaku, M. Prodanovic, and T. C. Green, "Modelng, analysis and testing of autonomous operation of an inverter-based microgrid," *IEEE Trans. Power Electron.*, vol. 22, no. 2, pp. 613-625, Mar. 2007.

[47] A. Etemadi, E. Davison, and R. Iravani, "A decentralized robust control strategy for multi-der microgrids-part 1: fundamental concepts," *IEEE Trans. Power Del.*, vol. 27, no. 4, pp. 1843-1853, Jul. 2012.

[48] H. Karimi, E. Davison, and R. Iravani, "Multivariable servomechanism controller for autonomous operation of a distributed generation unit: design and performance evaluation," *IEEE Trans. Power Syst.*, vol. 25, no. 2, pp. 853-865, Nov. 2009.

[49] T. L. Vandoorn, B. Meersman, J. D. M. De Kooning, and L. Vandevelde, "Analogy between conventional grid control and islanded microgrid control based on a global dc-link voltage droop," *IEEE Trans. on Power Del.*, vol. 27, no. 3, pp. 1405-1414, May 2012.

[50] M. I. Azim, M. J. Hossain, and H. R. Pota, "Design of a general droop controller for islanded microgrids," in *Proc. Australasian Univs. Power Eng. Conf.*, pp.

1-5, Sep. 27-30, 2015.

[51] K. De Brabandere, B. Bolsens, J. Van den Keybus, A. Woyte, J. Driesen, and R. Belmans, "A voltage and frequency droop control method for parallel inverters," *IEEE Trans. Power Electron.*, vol. 22, no. 4, pp. 1107-1115, Jul. 2007.

[52] H. Bevrani, S. Shokoohi, "An intelligent droop control for simultaneous voltage and frequency regulation in islanded microgrids," *IEEE Trans. Smart Grid*, vol. 4, no. 3, pp. 1505-1513, Sep. 2013.

[53] Y. Wang, H. Nazaripouya, C. Chu, R. Gadh, and H. R. Pota, "Vehicle-to-grid automatic load sharing with driver preferences in microgrids," in *Proc. IEEE PES ISGT Europe*, pp. 1-6, Oct. 12-15, 2014.

[54] B. Johnson, A. Davoudi, P. Chapman, and P. Sauer, "A unified dynamic characterization framework for microgrid systems," *Electric power Components and Syst.*, vol. 40, no. 1, pp. 93-111, Nov. 2011.

[55] H. R. Pota, M. J. Hossain, M. A. Mahmud, and R. Gadh, "Control for microgrids with inverter connected renewable energy resources," in *Proc. IEEE PES Gen. Meet.*, pp. 1-5, Jul. 27-31, 2014.

[56] H. R. Pota, M. J. Hossain, M. A. Mahmud, R. Gadh, and R. C. Bansal, "Islanded Operation of microgrids with inverter connected renewable energy sources," in *Proc. IFAC World Congress*, Aug. 24-29, 2014.

[57] H. Han, Y. Liu, Y. Sun, M. Su, and J. M. Guerrero, "An improved droop control stratgy for reactive power sharing in islanded microgrid," *IEEE Trans. Power Electron.*, vol. 30, no. 6, pp. 3133-3141, Jun. 2015.

[58] A. Milczarek, M. Malinowski, and J. M. Guerrero, "Reactive power management in islanded microgrid-proportional power sharing in hierarchical droop control," *IEEE Trans. Smart Grid*, vol. 6, no. 4, pp. 1631-1638, Jul. 2015.

[59] F. Katiraei, M. R. Iravani, and P. W. Lehn, "Small-signal dynamic model of a microgrid including conventional and electronically interfaced distributed resources," *IET Gen. Transmiss. Distrib.*, vol. 1, no. 3, pp. 369-378, May 2007.

[60] E. Barklund, N. Pogaku, M. Prodanovic, C. Hernandez-Aramburo, and T. C. Green, "Energy management in autonomous microgrid using stability-constrained droop control of inverters," *IEEE Trans. Power Electron.*, vol. 23, no. 5, pp. 2346-2352, Sep. 2008.

[61] R. Majumder, B. Chaudhuri, and A. Ghosh, "Improvement of stability and load sharing in an autonomous microgrid using supplementary droop control loop," *IEEE Trans. Power Syst.*, vol. 25, no. 2, pp. 796-808, May 2010.

[62] R. Majumder, "Some aspects of stability in microgrids," *IEEE Trans. Power Syst.*, vol. 28, no. 3, pp. 3243-3252, Aug. 2013.

[63] G. Diaz, C. G. -Moran, J. G. -Alxeixandre, "Complex-valued state matrices for simple representation of large autonomous microgrids supplied by PQ and Vf generation," *IEEE Trans. Power Electron.*, vol. 24, no. 4, pp. 1720-1730, Nov. 2009.

[64] F. Gao, Z. Li, Y. Li, P. Wang, and H. Zhu, "Small-signal stability analysis of parallel-connected inverters based on time-varying phasor," in *Proc. IEEE Conf. Ind. Electron. and Appl.*, pp. 1239-1244, Jun. 21-23, 2011.

[65] J. Zhang, J. Chen, X. Chen, and C. Gong, "Modelling, analysis and design of droop-controlled parallel three phase voltgae source inverter using dynamic phasors method," in *Proc. ITEC Asia-Pacific*, pp. 1-6, Aug. 31-Sep. 3, 2014.

[66] K. De Brabandere, B. Bolsens, and J. Van den Keybus, "Small-signal stability of grids with distributed low-inertia generators taking into account line phasor dynamics," in *Proc. Int. Conf. Electricity Distrib.*, pp. 1-5, Jun. 6-9, 2005.

[67] X. Guo, Z. Lu, B. Wang, X. Sun, L. Wang, and J. M. Guerrero, "Dynamic

phasors-based modeling and stability analysis of droop-controlled inverters for microgrid applications," *IEEE Trans. Smart Grid*, vol. 5, no. 6, pp. 2980-2987, Nov. 2014.

[68] T. Yang, S. Bozhko, J. Le-Peuvedic, G. Asher, and C. I. Hill, "Dynamic phasor modeling of multi-generator variable frequency electrical power systems," *IEEE Trans. Power Syst.*, vol. 31, no. 1, pp. 563-571, Jan. 2016.

[69] E. A. A. Coelho, P. C. Cortizo, and P. F. D. Garcia, "Small-signal stability for parallel-connected inverters in stand-alone ac supply systems," *IEEE Trans. Ind. Appl.*, vol. 38, no. 2, pp. 533-542, Mar./Apr. 2002.

[70] J. W. Simpson-Porco, F. Dorfler, and F. Bullo, "Voltage stabilization in microgrids via quadratic droop control," in *Proc. IEEE Annual Conf. on Decision and Control*, pp. 7582-7589, Dec. 10-13, 2013.

[71] M. I. Azim, M. A. Hossain, S. M. Mohiuddin, M. J. Hossain, and H. R. Pota, "Proportional Reactive Power Sharing for Islanded Microgrids," in *Proc. IEEE Conf. Ind. Electron. and Appl.*, pp. 1-6, Jul. 5-7, 2016.

[72] N. Martins, "Efficient eigenvalue and frequency response methods applied to power system small-signal stability studies," *IEEE Trans. Power Syst.*, vol. 1, no. 1, pp. 217-224, Feb. 1986.

[73] J. J. Sanchez-Gasca, V. Vittal, M. J. Gibbard, A. R. Messina, D. J. Vowles, S. Liu, and U. D. Annakkage, "Inclusion of higher order terms for small-signal (modal) analysis: committe report-task force on assessing the need to include higher order terms for small-signal (modal) analysis," *IEEE Trans. Power Syst.*, vol. 20, no. 4, pp. 1886-1904, Nov. 2005.

[74] R. T. Byerly, R. J. Bennon, and D. E. Sherman, "Eigenvalue analysis of synchronizing power-flow oscillations in large electric power systems," *IEEE Trans. Power Apparatus and Syst.*, vol. PAS-101, no. 1, pp. 235-243, Jan. 1982.

[75] P. Mattavelli, A. M. Stankovic, and G. C. Verghese, "SSR analysis with dynamic phasor model of thyristor-controlled series capacitor," *IEEE Trans. Power Syst.*, vol. 14, no. 1, pp. 200-208, Feb. 1999.

[76] H. Ruiwen, and C. Zexiang, "Modeling and harmonic analysis of TCSC with dynamic phasors," in *Proc. IEEE/PES Tranmiss. Distrib. Conf. Exhib.*, pp. 1-5, 2005.

[77] P. C. Stefanov, and A. M. Stankovic, "Modeling of UPFC operation under unbalanced conditions with dynamic phasors," *IEEE Trans. Power Syst.*, vol. 17, no. 2, pp. 395-403, May 2002.

[78] E. Zhijun, K. Chan, and D. Fang, "Dynamic phasor modeling of TCR based FACTS devices for high speed power system fast transients simulation," *Asian Power Electron. J.*, vol. 1, no. 1, pp. 42-48, Aug. 2007.

[79] D. Maksimovic, A. M. Stankovic, V. J. Thottuvelil, and G. C. Verghese, "Modeling and simulation of power electronic converters," in *Proc. IEEE*, vol. 89, no. 6, pp. 898-912, Jan. 2001.

[80] A. Zahedi, "Development of an economical model to determine an appropriate feed-in-tariff for grid-connected solar PV electricity in all states of Australia," *Renew. and Sustain. Energy Reviews*, vol. 13, no. 4, pp. 871-878, May 2009.

[81] M. A. Mahmud, H. R. Pota, and M. J. Hossain, "Nonlinear current control scheme for a single-phase grid-connected photovoltaic system," *IEEE Trans. Sustain. Energy*, vol. 5, no. 1, pp. 218-227, Jan. 2014.

[82] M. Liserre, T. Sauter, and J. Y. Hung, "Future energy systems: Integrating renewable energy sources into smart power grids through industrial electronics," *IEEE Ind. Electron. Mag.*, vol. 4, no. 1, pp. 18-37, Mar. 2010.

[83] M. W. Hadi, N. Hariyanto, and J. Choi, "Stability enhancement of hybrid diesel generator and photovoltaic generator based on droop control," in *Proc. IEEE*

PES ISGT Asia, pp. 1-6, Nov. 4-6, 2015.

[84] M. J. Hossain, M. A. Mahmud, H. R. Pota, and N. Mithulananthan, "Design of non-interating controllers for PV systems in distribution networks," *IEEE Trans. Power Systems*, vol. 29, no. 6, pp. 2763-2774, Nov. 2014.

[85] I. Kim, "Robust maximum power point tracker using sliding mode controller for the three-phase grid-connected photovoltaic system," *Solar Energy*, vol. 81, no. 3, pp. 405-414, Mar. 2007.

[86] M. S. Rahman, M. A. Mahmud, A. M. T. Oo, and T. F. Orchi, "Distributed agent-based control scheme for single-phase parallel inverters in microgrids with photovoltaic systems," in *Proc. Australasian Univs. Power Eng. Conf.*, pp. 1-6, Sep. 27-30, 2015.

[87] M. A. Mahmud, H. R. Pota, and M. J. Hossain, "Dynamic stability of three-phase grid-connected photovoltaic system using zero dynamic design approach," *IEEE J. Photovoltaics*, vol. 2, no. 4, pp. 564-571, Oct. 2012.

[88] A. Yazdani, A. R. Di Fazio, H. Ghoddami, M. Russo, M. Kazerani, J. Jatskevich, K. Strunz, S. Leva, and J. A. Martinez, "Modeling guidelines and a bechmark for power system simulation studies of three-phase single-stage photovoltaic systems," *IEEE Trans. Power Del.* , vol. 26, no. 4, pp. 748-755, Dec. 2004.

[89] N. Mithulananthan, "Hopf Bifurcation Control and Indices for Power System with Interacting Generator and FACTS Controllers," PhD dissertation, Department of Electrical and Computer Engineering,University of Waterloo, Canada, 2002.